0-315-01174-2

National Library of Canada | Bibliothèque nationale du Canada

Canadian Theses Division | Division des thèses canadiennes

Ottawa, Canada
K1A 0N4

49032

PERMISSION TO MICROFILM — AUTORISATION DE MICROFILMER

• Please print or type — Écrire en lettres moulées ou dactylographier

Full Name of Author — Nom complet de l'auteur

Larry Wayne Marks

Date of Birth — Date de naissance

March 20, 1953

Country of Birth — Lieu de naissance

Canada

Permanent Address — Résidence fixe

Box 606 Westlock Alberta T0G 2L0

Title of Thesis — Titre de la thèse

Computational Topics in Ray Seismology

University — Université

Alberta.

Degree for which thesis was presented — Grade pour lequel cette thèse fut présentée

Doctor of Philosophy

Year this degree conferred — Année d'obtention de ce grade

1980

Name of Supervisor — Nom du directeur de thèse

Dr. F. Hron, Physics Dept

Permission is hereby granted to the NATIONAL LIBRARY OF CANADA to microfilm this thesis and to lend or sell copies of the film.

The author reserves other publication rights, and neither the thesis nor extensive extracts from it may be printed or otherwise reproduced without the author's written permission.

L'autorisation est, par la présente, accordée à la BIBLIOTHÈQUE NATIONALE DU CANADA de microfilmer cette thèse et de prêter ou de vendre des exemplaires du film.

L'auteur se réserve les autres droits de publication; ni la thèse ni de longs extraits de celle-ci ne doivent être imprimés ou autrement reproduits sans l'autorisation écrite de l'auteur.

Date

April 11/80

Signature

Larry W Marks

NL-91 (4/77)

National Library of Canada
Collections Development Branch

Canadian Theses on
Microfiche Service

Bibliothèque nationale du Canada
Direction du développement des collections

Service des thèses canadiennes
sur microfiche

NOTICE

The quality of this microfiche is heavily dependent upon the quality of the original thesis submitted for microfilming. Every effort has been made to ensure the highest quality of reproduction possible.

If pages are missing, contact the university which granted the degree.

Some pages may have indistinct print especially if the original pages were typed with a poor typewriter ribbon or if the university sent us a poor photocopy.

Previously copyrighted materials (journal articles, published tests, etc.) are not filmed.

Reproduction in full or in part of this film is governed by the Canadian Copyright Act, R.S.C. 1970, c. C-30. Please read the authorization forms which accompany this thesis.

THIS DISSERTATION
HAS BEEN MICROFILMED
EXACTLY AS RECEIVED

AVIS

La qualité de cette microfiche dépend grandement de la qualité de la thèse soumise au microfilmage. Nous avons tout fait pour assurer une qualité supérieure de reproduction.

S'il manque des pages, veuillez communiquer avec l'université qui a conféré le grade.

La qualité d'impression de certaines pages peut laisser à désirer, surtout si les pages originales ont été dactylographiées à l'aide d'un ruban usé ou si l'université nous a fait parvenir une photocopie de mauvaise qualité.

Les documents qui font déjà l'objet d'un droit d'auteur (articles de revue, examens publiés, etc.) ne sont pas microfilmés.

La reproduction, même partielle, de ce microfilm est soumise à la Loi canadienne sur le droit d'auteur, SRC 1970, c. C-30. Veuillez prendre connaissance des formules d'autorisation qui accompagnent cette thèse.

LA THÈSE A ÉTÉ
MICROFILMÉE TELLE QUE
NOUS L'AVONS REÇUE

Ottawa, Canada
K1A 0N4

NL-339 (Rev. 8/80)

THE UNIVERSITY OF ALBERTA

COMPUTATIONAL TOPICS IN RAY SEISMOLOGY

by

© LARRY WAYNE MARKS

A THESIS

SUBMITTED TO THE FACULTY OF GRADUATE STUDIES AND RESEARCH

IN PARTIAL FULFILMENT OF THE REQUIREMENTS FOR THE DEGREE

OF DOCTOR OF PHILOSOPHY

IN

GEOPHYSICS

DEPARTMENT OF PHYSICS

EDMONTON, ALBERTA

SPRING 1980

THE UNIVERSITY OF ALBERTA

FACULTY OF GRADUATE STUDIES AND RESEARCH

The undersigned certify that they have read, and recommend to the Faculty of Graduate Studies and Research, for acceptance, a thesis entitled COMPUTATIONAL TOPICS IN RAY SEISMOLOGY submitted by LARRY WAYNE MARKS in partial fulfilment of the requirements for the degree of DOCTOR OF PHILOSOPHY in GEOPHYSICS.

.....

Supervisor

.....

.....

.....

.....

.....

External Examiner

Date... January 18, 1980...

DEDICATION

TO MARIA

WHO WAS HAPPY WHEN I STARTED THIS PROJECT,

AND EVEN HAPPIER WHEN I COMPLETED IT.

ABSTRACT

Studying seismic wave propagation by ray techniques has been popular in the geophysical community for some time. Due to the low cost of computation and the ability to associate individual events on synthetic seismograms with particular paths of energy propagation (ray paths), asymptotic ray theory is one of the most practical of the ray methods. Although the theoretical aspects of this theory have been well documented, much greater difficulties of a computational nature must be overcome to truly establish this theory. This thesis addresses itself to three of these topics. First, the role of the non-leading term in the ray series in inhomogeneous media is examined. Second, the accuracy of the ray method for reflected and head waves is checked by comparison with direct numerical integration of the displacement potentials. Finally, several chapters are devoted to the development and testing of computational methods applicable to numerical modelling of seismic body waves in laterally inhomogeneous media with curved interfaces. Travel times, amplitude-distance curves and synthetic seismograms are computed for several models.

ACKNOWLEDGEMENTS

I wish to express my many thanks to Dr. F. Hron for the suggestion of these topics and for his assistance in the completion of the study. I appreciate the fact that he allowed me to use and modify some of his computer programs which aided my research greatly.

I am grateful to Dr. Pat Daley and Mr. Albert Choi for helpful discussions and for providing some computer programs.

Muriel Tait is to be thanked for her excellent stenographic assistance.

Over all, this scientific work could not have been completed without the loving support of my wife, Maria.

During the course of this study, I received financial support from the National Science and Engineering Research Council as well as the University of Alberta.

List of Tables

Table | Page

3.1 The Alberta model.....63

6.1 Comparison of ray paths in the Bohemian Massif.113

List of Figures

Figure		Page
2.1	Unit vectors for P waves	13
2.2	Evaluation of the t_3 derivatives	32
2.3	Evaluation of the t_1 derivatives	33
2.4	Displacements for P waves in a homogeneous layer reflected from a homogeneous halfspace	39
2.5	Displacements for P waves in a vertically inhomogeneous layer reflected from a homogeneous halfspace	41
2.6	Displacements for P waves refracted through a vertically inhomogeneous halfspace	43
2.7	Displacements for P waves in a homogeneous layer reflected from a vertically inhomogeneous halfspace	45
2.8	Solutions to the k=0,1 boundary conditions corresponding to the results in Figure 2.7	46
2.9	Displacements for P waves in a homogeneous layer reflected from a vertically inhomogeneous halfspace	48
2.10	Solutions to the k=0,1 boundary conditions corresponding to the results in Figure 2.9	50

3.1 Contours of integration.....58

3.2 Reflected unconverted wave displacement computed by different techniques.....64

3.3 Reflected converted wave displacement computed by different techniques.....66

3.4 SSS head wave displacement computed by different techniques.....67

3.5 Frequency dependence of head waves.....68

3.6 Comparison of Weber function approach with numerical integration.....70

4.1 The bending method of seismic ray tracing.....74

5.1 Symbols and geometry used to trace rays by circular approximation.....83

6.1 Geometry of the ray tube.....101

6.2 P1P2P2P1 in an inhomogeneous medium with curved boundaries.....105

6.3 The effect of the curvature and inhomogeneity terms in dynamic ray tracing.....106

6.4 P1S2S2P1 in an inhomogeneous medium with plane boundaries.....107

6.5 P wave isovelocity contours for the Bohemian Massif.....108

6.6 Transect plot of P wave velocity for the Bohemian Massif.....110

6.7 Comparison of ray paths for the reflected and refracted branches of P1P1 propagating through the Bohemian Massif.....111

6.8 Comparison of travel time for the reflected branch of P1P1 propagating through the Bohemian Massif.....114

6.9 Comparison of amplitudes for the reflected branch of P1P1 propagating through the Bohemian Massif.....115

7.1 Take off angle, epicentral distance, travel time and amplitude in a complex medium....118

7.2 General modelling procedure for laterally inhomogeneous media.....121

7.3 Rays, travel times and amplitudes in the Cerveny model.....124

7.4 Synthetic seismograms for the Cerveny model...126

7.5 Reflected and refracted primary P rays in the Bohemian Massif.....127

7.6 Travel times and amplitude in the Bohemian Massif.....129

7.7 Synthetic seismograms for the Bohemian Massif.130

A.1 Geometry employed to find ray intersection points.....140

Table of Contents

Chapter Page

1. GENERAL INTRODUCTION.....1

2. ACCURACY OF GEOMETRICAL RAY THEORY IN SEISMOLOGY.....5

2.1 Introduction.....5

2.2 Basic equations of asymptotic ray theory.....9

2.2.1 A medium with continuous elastic parameters.....10

2.2.2 The effect of an interface.....19

2.3 Numerical evaluation of the term k=1 for P waves in media with linear velocity gradients.....26

2.3.1 Selection of a medium.....27

2.3.2 The vector operators.....28

2.3.3 Evaluation of boundary conditions.....34

2.4 Numerical results.....37

2.5 Conclusions.....49

3. NUMERICAL CONFIRMATION OF METHODS OF COMPUTING SEISMIC WAVE AMPLITUDE.....53

3.1 Introduction.....53

3.2 Theory for numerical integrations.....54

3.3 Numerical results.....61

3.4 Conclusions.....69

4. RAY TRACING BY CLASSICAL METHODS.....72

4.1 Introduction.....72

4.2 The bending method for ray tracing.....72

4.3 Complex analysis.....76

4.4 Differential equations for ray tracing.....76

5. RAY TRACING BY CIRCULAR APPROXIMATION.....80

5.1 Introduction.....80

5.2 Circular approximation ray tracing without interfaces.....81

5.3 Determining the ray as a function of time.....86

5.4 The effect of an interface.....86

6. GEOMETRICAL SPREADING OF WAVEFRONTS IN LATERALLY INHOMOGENEOUS MEDIA.....89

6.1 Introduction.....89

6.2 Differential equation solution for ray amplitude...89

6.3 The effect of an interface.....92

6.4 Ray amplitude by dynamic ray tracing.....95

6.5 Ray amplitude by circular approximation.....99

6.6 Numerical tests.....104

7. NUMERICAL MODELLING OF SEISMIC BODY WAVES IN LATERALLY INHOMOGENEOUS MEDIA.....116

7.1 Introduction.....116

7.2 The relationship between take off angle, epicentral distance, travel time and amplitude in a complex medium.....116

7.3 General modelling procedure for laterally inhomogeneous media.....120

7.4 Cerveny model.....123

7.5 Bohemian Massif.....125

7.6 Conclusions.....131

REFERENCES.....132

APPENDIX A
EQUATIONS FOR RAY INTERSECTION POINTS.....139

APPENDIX B
THE WEBER FUNCTION APPROACH FOR AMPLITUDE COMPUTATION.....144

APPENDIX C
APPROXIMATION OF INTERFACES BY PIECEWISE CONTINUOUS

PARABOLAE.....150

APPENDIX D
RAY AMPLITUDE IN THE VICINITY OF A CAUSTIC.....154

1. GENERAL INTRODUCTION

Elastic wave propagation problems are of paramount importance in all branches of seismology. For complex media, analytical solutions to the equations of motion are unknown and seismologists must turn to numerical techniques to investigate wave fields. One common approach is a direct computational solution to the elastodynamic equation. This technique generally has some variation of the finite difference algorithm at its hub. If properly applied, this method will give a total solution including refracted and reflected waves, surface waves, and diffracted waves. Unfortunately, on the resulting synthetic seismograms no identification of particular phases can be made. For this purpose, one can use ray methods. This thesis will be devoted to various computational topics related to one of these methods, namely asymptotic ray theory, often termed the ray series method in European literature.

The basic tenets of asymptotic ray theory were developed simultaneously and independently by Babich and Alekseev (1958) in the Soviet Union and Karal and Keller (1959) in America. This ray theory is powerful in that it can be applied to the elastodynamic equation in general inhomogeneous media. However, in order to fully employ asymptotic ray theory, some very lengthy computations related to the seismic body wave field must be performed.

This thesis presents techniques and numerical results for three computational topics related to asymptotic ray theory. The basic principles of the theory are presented in Chapter 2. For a particular choice of inhomogeneous media, the second term in the ray series (which is inversely proportional to frequency) is evaluated numerically and compared with the leading term which coincides with geometrical ray theory. The most interesting feature of the non-leading term is that for P waves, it has components both parallel to and perpendicular to the ray. Due to the frequency dependence of this term, it will be shown that it is of little significance relative to the leading term for source-receiver distances less than the critical distance and for small degrees of inhomogeneity in the earth.

In Chapter 3, the leading term of the ray series is compared with direct numerical integration of the expression representing displacement. In the neighborhood of a critical point, where ray theory is not valid, the computations are compared with a more exact wave method. Some results of this work have been published by Marks and Hron (1978).

The last topic, numerical modelling of seismic body waves in laterally inhomogeneous media with curved interfaces, is discussed in Chapters 4-7. Chapter 4 deals with methods of ray tracing which are currently in existence. These techniques involve either the solution of a

set of differential equations at many points along the ray or the inversion of a large matrix. Due to the lack of sufficient computer time to properly utilize these approaches, an approximation is presented in Chapter 5 and compared with the other techniques. Termed the circular approximation, it concerns itself only with the inhomogeneities of the medium in the vicinity of the raypath. With a transformation of coordinate systems, one is allowed to write compact analytical expressions for the ray paths. This produces a tremendous saving in computing time and allows one to calculate economically, yet accurately values of travel times, amplitudes and finally synthetic seismograms.

The works in Chapters 4-5 are in essence, a paper which was read to the European Seismological Commission (Marks and Hron 1978a).

One prerequisite for computing ray amplitude is to calculate the geometrical spreading of the wave front. Analytic techniques which perform this task are generally cast as sets of differential equations or time integration approaches. These, however, consume vast amounts of computer time and are better replaced by a modification of the circular approximation technique. Chapter 6 describes this alteration as well as two of the analytic means of determining wave front spreading. A number of computational

examples and comparisons are presented which indicate the expediency of this approximation.

Chapter 7 concerns itself with a general procedure linking together the seismic ray tracing techniques and geometrical spreading of wave fronts to produce synthetic seismograms for laterally varying media. The circular approximation method is the basis for most work performed in Chapter 7. The work presented in Chapter 7 is the basis for a paper presented to the Society of Exploration Geophysicists (Marks and Hron 1979b).

2. ACCURACY OF GEOMETRICAL RAY THEORY IN SEISMOLOGY

2.1 Introduction

Applied seismology is concerned with locating and geologically interpreting structures within the earth. Rays are often used as a means of following the path that seismic wave energy takes in propagating from source to receiver. In short, the laws of geometrical ray theory provide the groundwork for many of the existing seismic interpretation methods. It is rather surprising to notice how uncritically the approximation is accepted. In this chapter we shall show results of a test of the accuracy of geometrical ray theory.

What is meant by geometrical ray theory in seismology? Basically, it is the concept that seismic energy travels through an elastic medium along well-defined paths termed rays. The geometry of these paths is governed by the well known Snell's law. This definition, however, gives no information on energy properties (amplitudes). For this, it is necessary to turn to the law of conservation of energy. This states that the energy flux across the wave front must be equal at all times as long as the elastic parameters of the medium are continuous. Thus, if a value for the displacement is known at some reference point on the ray, it is a simple matter to compute displacement at any other point along the ray by comparing surface areas of the wave

fronts, velocities and densities at these two points plus the effect of energy partitioning at interfaces. These concepts will be discussed in more detail later on. For the remainder of this chapter the term "geometrical ray theory" will imply both the energy conservation law and Snell's Law.

Asymptotic ray theory will be applied to the propagation of elastic waves through an inhomogeneous, perfectly elastic and isotropic medium. The density of the medium is denoted ρ and its Lamé parameters μ and λ. The elastodynamic equation for particle displacement, $\vec{W}$, is given by

$$\rho \frac{\partial^2 \vec{W}}{\partial t^2} = (\lambda+\mu)\nabla(\nabla\cdot\vec{W}) + \mu \nabla^2\vec{W} + \nabla\lambda(\nabla\cdot\vec{W}) + \nabla\mu\times(\nabla\times\vec{W}) + 2(\nabla\cdot\nabla)\vec{W} \qquad (2.1)$$

where t is time. Using the basic tenets as set forth by Hron and Kanasewich (1971) or Cerveny and Ravindra (1971) a time harmonic solution to 2.1 is assumed to be given by a series in inverse powers of frequency, ω,

$$\vec{W} = \exp(i\omega(t-\tau(x,y,z)) \sum_{k=0}^{\infty} \frac{\vec{W}_k(x,y,z)}{(i\omega)^k} \qquad (2.2)$$

This expansion is termed a ray series with τ the phase function and

$\vec{W}_k$, (k=0,1,2,...) the amplitude coefficients of the series.

In this chapter we attempt quantitively to describe the frequency dependent connections between the magnitudes of the first two terms in 2.2 and the degree of inhomogeneity of the medium. These results will also illustrate the error which arises when only the leading term

$$\vec{W} = \exp(i\omega(t-\tau))\vec{W}_0 \tag{2.3}$$

is taken. This expression, termed the zeroth order approximation, is that which can be derived through the laws of geometrical ray theory. On the other hand we term

$$\vec{W} = \exp(i\omega(t-\tau))(\vec{W}_0+\vec{W}_1/i\omega) \tag{2.4}$$

to be the first order approximation which essentially serves as a correction represented by

$$\vec{W}_1 \, e^{i\omega(t-\tau)}/i\omega$$

Let us briefly mention two properties of the first order approximation as opposed to the zeroth order. The first of these is the loss of polarization of particle displacement. $\vec{W}_1$, in general has components normal to the wave front, corresponding to compressional wave motion, and tangent to the wave front, corresponding to shear wave motion. For P waves, the component normal to the wave front

is termed the principal component while the component tangent to the wave front is called the additional component. Analogous definitions exist for S waves. Secondly, the correction term in 2.4 is frequency dependent implying justification of the zeroth order approximation for high frequency sources.

A perusal of seismological literature demonstrates that little work has been performed on determining the magnitude of any term in the ray series other than the zeroth order approximation. Brekhovskikh (1960) carried out an analysis of the field of a reflected spherical electromagnetic wave as well as an acoustic wave. However, the approach used in that book is inappropriate for solving the more intricate elastodynamic equation. Pod''yapol'skiy (1966) calculated formulae for the first order approximation by comparing the terms of the ray series with exact formulae for displacement for reflected and refracted waves in a homogeneous plane parallel layered medium. Unfortunately, for inhomogeneous media, such expressions are not available and one must resort to numerical techniques. However, Pod''yapol'skiy did demonstrate that the zeroth order approximation may not be adequate for two special conditions. One of these is for rays which have only travelled a few wavelengths from the source. The other is for rays reflected at angles approaching

$\pi/2$ with the interface normal, commonly called grazing rays. Woodhouse (1974), in his doctoral dissertation, computed the magnitude of the transverse component of compressional waves propagating in a radially symmetric earth. This work provides a lucid mathematical account of the ray series method although extensive numerical results were absent. Woodhouse paid attention to the additional component of P waves, which is a rather striking feature of asymptotic ray theory. From the practical point of view, however, the principal component is more significant as it carries more energy. Its evaluation must be carried out numerically. To simplify the task, the results will be computed for plane layered media with linear velocity gradients within the layers. This reduction leads to simple ray geometries (circular arcs) and allows considerable use of analytic expressions.

2.2 Basic equations of asymptotic ray theory

The basics equations of asymptotic ray theory have been discussed in numerous works. For details, interested readers are referred to Babich and Alexseev (1958), Alexseev and Gel'chinskiy (1959), Alexseev et al (1961), Kline and Kay (1965), Cerveny and Ravindra (1971), Hron and Kanasewich (1971), Woodhouse (1974), Cerveny et al (1977) and Cerveny and Hron (1979) among others. We shall briefly derive the equations for the case where

λ, μ, ρ and all their derivatives are continuous functions of coordinates. The case where interfaces are present will be discussed later on.

2.2.1 A medium with continuous elastic parameters

Substitution of equation 2.2 into 2.1 yields

$$\sum_{k=0}^{\infty} (i\omega)^{-k} (i\omega)^2 \vec{N}(\vec{W}_k) - i\omega \vec{M}(\vec{W}_k) + \vec{L}(\vec{W}_k) = 0 \tag{2.5}$$

where

$$\begin{aligned}
\vec{N}(\vec{W}_k) &= -\rho \vec{W}_k + (\lambda+\mu)(\vec{W}_k \cdot \nabla\tau)\nabla\tau + \mu(\nabla\tau)^2 \vec{W}_k \\
\vec{M}(\vec{W}_k) &= (\lambda+\mu)(\nabla(\vec{W}_k \cdot \nabla\tau) + \nabla\tau(\nabla \cdot \vec{W}_k)) \\
&\quad + \mu(2(\nabla\tau \cdot \nabla)\vec{W}_k + (\nabla^2\tau)\vec{W}_k) + \nabla\lambda(\vec{W}_k \cdot \nabla\tau) \\
&\quad + \nabla\mu \times (\nabla\tau \times \vec{W}_k) + 2(\nabla\mu \cdot \nabla\tau)\vec{W}_k \\
\vec{L}(\vec{W}_k) &= (\lambda+\mu)\nabla(\nabla \cdot \vec{W}_k) + \mu\nabla^2 \vec{W}_k + \nabla\lambda(\nabla \cdot \vec{W}_k) \\
&\quad + \nabla\mu \times (\nabla \times \vec{W}_k) + 2(\nabla\mu \cdot \nabla)\vec{W}_k
\end{aligned} \tag{2.6}$$

Since 2.5 must be true for all ω, the coefficient of any power of ω must be zero, implying

$$\begin{aligned}
&\vec{N}(\vec{W}_1) - \vec{M}(\vec{W}_0) = 0 \qquad \vec{N}(\vec{W}_0) = 0 \\
&\vec{N}(\vec{W}_k) - \vec{M}(\vec{W}_{k-1}) + \vec{L}(\vec{W}_{k-2}) = 0 \qquad (k \geq 2)
\end{aligned} \tag{2.7}$$

This is a recurrent system of partial differential equations

which allows us to determine τ (which is invariant for all terms in the series) and all $\vec{W}_k$. If we introduce $\vec{W}_{-1} = \vec{W}_{-2} = 0$ we may write

$$\vec{N}(\vec{W}_k) - \vec{M}(\vec{W}_{k-1}) + \vec{L}(\vec{W}_{k-2}) = 0 \qquad (k \geq 0) \qquad (2.8)$$

Eikonal equations for compressional or shear waves can be obtained as necessary conditions for the non-zero solution of the system for k=0. These are

$$(\nabla\tau)\cdot(\nabla\tau) = \alpha^{-2}, \qquad \alpha^2 = (\lambda+2\mu)/\rho \qquad (2.9)$$

or

$$(\nabla\tau)\cdot(\nabla\tau) = \beta^{-2}, \qquad \beta^2 = \mu/\rho \qquad (2.10)$$

α is the velocity of propagation of compressional waves, sometimes termed P, longitudinal, irrotational or dilatational waves, while β is the velocity of propagation of shear waves, sometimes known as S, transverse, equivoluminal or distortional waves.

In inhomogeneous media the elastodynamic equation cannot be decoupled into two wave equations, each describing the propagation of compressional and shear waves (Grant and West 1965, p. 43-47). In the high frequency limit, however,

two independent waves exist as long as the elastic parameters and all their derivatives are continuous. It should not be inferred that all particle motion associated with the compressional wave is purely longitudinal or parallel to the ray. The results of this chapter will demonstrate that for the term k=1 an albeit small transverse component normal to the ray is present.

The eikonal equations, 2.9 and 2.10 plus Snell's Law at boundaries, provide us with all the information necessary to determine the kinematic properties of the waves, such as wave front geometry, ray paths and travel times. Various schemes have been designed to solve these equations. Wesson (1970,1971), Cerveny et al (1974), Popov and Psencik (1978), Sorrells et al (1971), and Cerveny and Hron (1979) are only a few of the major contributors.

For evaluation of the coefficients of the ray series, 2.2, we introduce three orthogonal right-handed unit vectors $\hat{t}_i$, (i=1,2,3) which correspond to the tangent, binormal and normal to the ray (see Figure 2.1). All calculations performed in this chapter will assume that the ray is a plane curve confined to the $\hat{t}_1$-$\hat{t}_3$ plane and that the vector $\hat{t}_2$ points out of the plane of propagation. It is also assumed that the z-coordinate points downward into the earth and that

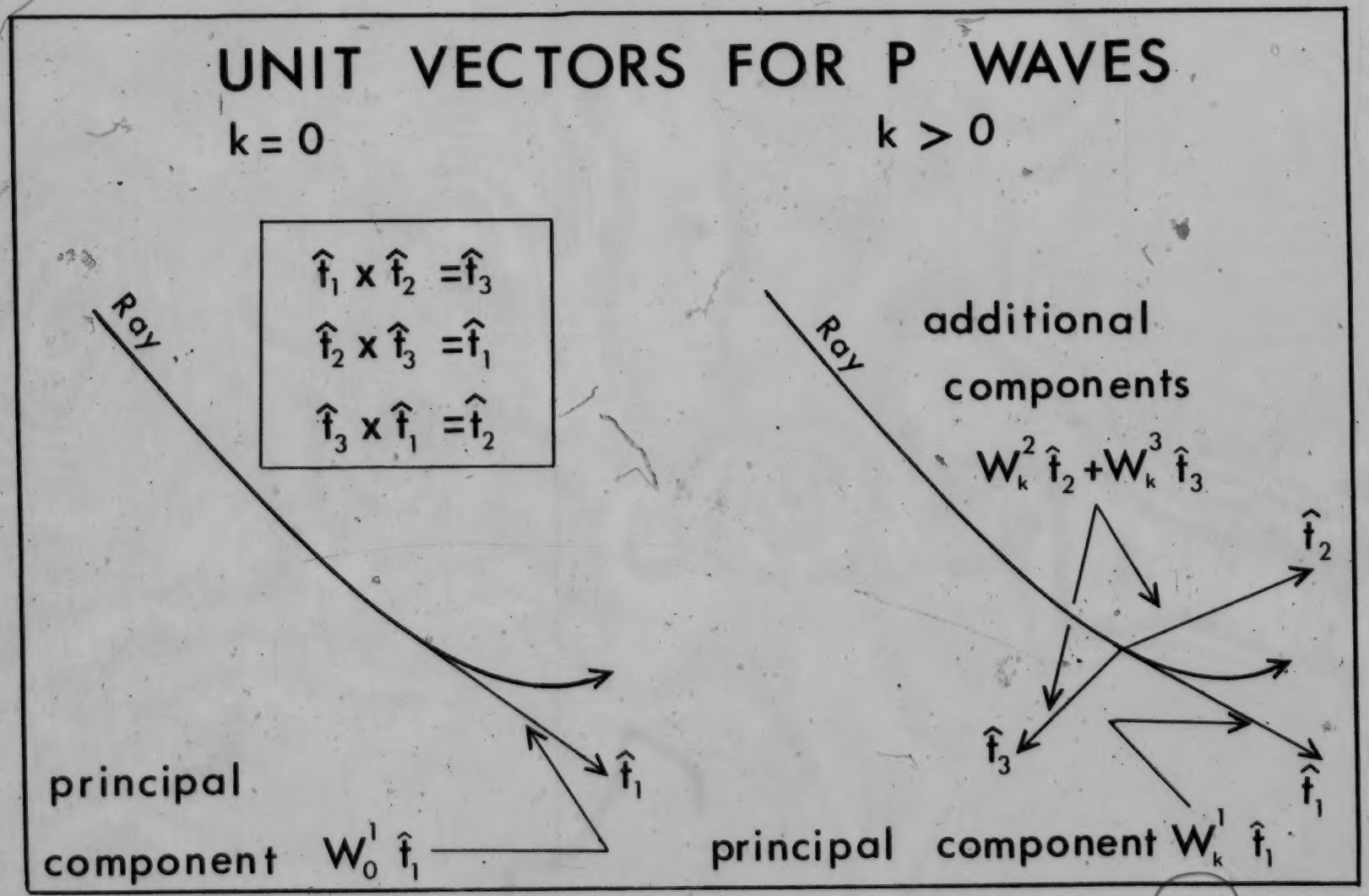

Figure 2.1 Unit vectors for P waves.

$\hat{t}_3$ is oriented such that its projection onto the z axis is always positive. In this fashion all ambiguity regarding unit vector orientation is removed. We shall employ one property of an isotropic medium, namely that is parallel to $\hat{t}_1$.

We can write $\vec{W}_k$ in component form as

$$\vec{W}_k = \sum_{L=1}^{3} W_k^L \hat{t}_L \tag{2.11}$$

For compressional waves, the component $W_k^1 \hat{t}_1$ is termed the principal component while $W_k^2 \hat{t}_2 + W_k^3 \hat{t}_3$ is termed the additional component.

From 2.6, 2.9, and 2.11 we obtain

$$\begin{aligned} \vec{N}(W_k)\cdot\hat{t}_2 &= (-\rho+\mu\alpha^{-2})W_k^2 \\ \vec{N}(W_k)\cdot\hat{t}_3 &= (-\rho+\mu\alpha^{-2})W_k^3 \end{aligned} \tag{2.12}$$

Substituting from 2.8 for $\vec{N}(\vec{W}_k)$ yields

$$\begin{aligned} W_k^2 &= -\alpha^2/(\lambda+\mu)\cdot(\vec{M}(\vec{W}_{k-1}) - \vec{L}(\vec{W}_{k-2}))\cdot\hat{t}_2 \\ W_k^3 &= -\alpha^2/(\lambda+\mu)\cdot(\vec{M}(\vec{W}_{k-1}) - \vec{L}(\vec{W}_{k-2}))\cdot\hat{t}_3 \end{aligned} \tag{2.13}$$

With the geometry we have chosen,

$W_k^2 = 0$. Thus the additional component of P waves is given by $W_k^3 \hat{t}_3$.

The evaluation of the principal component $W_k^1 \hat{t}_1$ is somewhat more involved. Taking the scalar product of equation 2.7 with $\nabla\tau$ yields

$$\vec{M}(\alpha W_k^1 \nabla\tau)\cdot\nabla\tau = (\vec{L}(\vec{W}_{k-1}) - \vec{M}(W_k^3 t_3))\cdot\nabla\tau \qquad (2.14)$$

The left hand side of this equation can be recast by using some vector identities as

$$\vec{M}(\alpha W_k^1 \nabla\tau)\cdot\nabla\tau = 2\rho(\nabla\tau\cdot\nabla)\alpha W_k^1 + \alpha W_k^1(\rho\nabla^2\tau + (\nabla\tau\cdot\nabla)\rho)$$

Introducing the variable t as time along the ray,

$$(\nabla\tau\cdot\nabla)\alpha W_k^1 = \frac{1}{\alpha^2}\frac{d(\alpha W_k^1)}{dt}$$

$$(\nabla\tau\cdot\nabla)\rho = \frac{1}{\alpha^2}\frac{d\rho}{dt}$$

and hence

$$\vec{M}(\alpha W_k^1 \nabla\tau)\cdot\nabla\tau = \frac{2\rho}{\alpha^2}\frac{d(\alpha W_k^1)}{dt} + \alpha W_k^1\left(\rho\nabla^2\tau + \frac{1}{\alpha^2}\frac{d\rho}{dt}\right)$$

Substituting this expression into 2.14 gives a linear ordinary differential equation for αW_k^1

$$\frac{d(\alpha W_k^1)}{dt} + \alpha W_k^1 \frac{\alpha^2}{2}\nabla^2\tau + \frac{1}{2\rho}\frac{d\rho}{dt} =$$

$$\frac{\alpha^2}{2\rho}(\vec{L}(\vec{W}_{k-1}) - \vec{M}(W_k^3 \hat{t}_3))\cdot\nabla\tau \qquad (2.15)$$

This is one form of the higher order transport equation. Equation 2.15 enables us to find recursively all values of W_k^1 given $\vec{W}_j$, $j=0,1,\ldots,k-1$ and τ .

An explicit solution of 2.15 can be found by standard techniques (Simmons 1973). Denoting t_0 as some arbitrary initial point along the ray,

$$W_k^1(t) = W_k^1(t_0) \left(\frac{\rho(t_0)}{\rho(t)}\right)^{\frac{1}{2}} \frac{\alpha(t_0)}{\alpha(t)} S(t_0) + \frac{1}{2\alpha(t)} \cdot$$

$$\cdot \int_{t_0}^{t} \frac{\alpha^2(\xi)}{\rho(\xi)} \left((\vec{L}(\vec{W}_{k-1}) - \vec{M}(W_k^3\, \hat{t}_3))\cdot\nabla\tau\right) S(\xi) \left(\frac{\rho(\xi)}{\rho(t)}\right)^{\frac{1}{2}} d\xi \qquad (2.16)$$

where

$$S(t') = \exp\left(-\frac{1}{2}\int_{t'}^{t} \alpha^2(\xi)\nabla^2\tau \, d\xi\right)$$

Let us discuss the term S. For this purpose we introduce ray coordinates (q_1,q_2,t) where q_1,q_2 specify the ray under consideration and t gives the travel time to any point on the ray. For a point source, q_1,q_2 can be regarded as take-off angles at the source. For given ray coordinates, we can write the location of any point along the ray as $\vec{x} = \vec{x}(q_1,q_2,t)$. Then for a fixed t, variation of

q_1, q_2 gives the equation of a wave front. A useful concept to introduce now is that of the ray tube, i.e. the family of rays, the parameters of which are within the limits $q_1, q_1 + dq_1$; $q_2, q_2 + dq_2$. The infinitesimal cross sectional area of the ray tube can be evaluated as $d\sigma(t) = |J(t)|\, dq_1 dq_2$ where

$$J(t) = \left| \frac{\partial \vec{x}}{\partial q_1} \times \frac{\partial \vec{x}}{\partial q_2} \right|$$

and

$$\nabla^2 \tau = \frac{1}{J\alpha} \frac{d(J/\alpha)}{dt}$$

so that

$$S(t') = \frac{\alpha(t)}{\alpha(t')} \frac{d\sigma(t')}{d\sigma(t)}^{\frac{1}{2}}$$

An expression for the principal component of P waves from equation 2.16 is

$$W_k^1(t) = W_k^1(t_0) \frac{\alpha(t_0)}{\alpha(t)} \frac{\rho(t_0)}{\rho(t)} \frac{d\sigma(t_0)}{d\sigma(t)}^{\frac{1}{2}} + \frac{1}{2(\rho(t)\alpha(t))^{\frac{1}{2}}} \int_{t_0}^{t} \frac{d\sigma(\xi)}{d\sigma(t)}^{\frac{1}{2}} \frac{\alpha^3(\xi)}{\rho(\xi)}^{\frac{1}{2}} \cdot ((\vec{L}(\vec{W}_{k-1}) - \vec{M}(W_k^3\, \hat{t}_3)) \cdot \nabla\tau)\, d\xi \qquad (2.17)$$

On the basis of equation 2.17 we can compute the principal component W_k^1 at any point t of the ray if we know its value at an earlier time t_0. Thus according to asymptotic ray theory, the principal components of displacement at any point along the ray are expressed as relative displacements; i.e. relative to some initial value. For our purposes, we

will give all displacements relative to a displacement of 1.0 as measured on the unit sphere surrounding the seismic source. Due to the difficulty of studying sources in inhomogeneous media, we further assume the medium contained within this sphere to be homogeneous. To be completely rigorous, a function describing the directivity or radiation pattern of the source should be included in all expressions for displacement. However, the directivity will be taken as equal in all directions outward from the source.

For the leading term of the ray series, W_0^1, the integral in 2.17 vanishes as does W_0^3. This means that

$$\vec{W}_0 = W_0^1 \hat{t}_1 = W_0^1(t_0) \left[\frac{\alpha(t_0)}{\alpha(t)} \frac{\rho(t_0)}{\rho(t)} \frac{d\sigma(t_0)}{d\sigma(t)} \right]^{\frac{1}{2}} \hat{t}_1$$

This zeroth order solution is exactly that obtained by application of geometrical ray theory. If it is assumed that energy propagates only along rays (the validity of this assumption is an entirely different topic), then, in the zeroth order approximation, no energy flows through the side walls of the ray tube. This confinement of energy flux does not hold in general for any k, but only for k=0.

Similar expressions can be derived for principal and additional components of S waves. The additional component of an S wave is

$$W_k^1 = \frac{\beta^2}{(\lambda+u)} \left(\vec{M}(\vec{W}_{k-1}) - \vec{L}(\vec{W}_{k-2}) \right) \cdot \hat{t}_1 \qquad (2.18)$$

while the principal component of SV-polarized waves is

$$W_k^3(t) = W_k^3(t_0) \left[\frac{\beta(t_0)}{\beta(t)} \frac{\rho(t_0)}{\rho(t)} \frac{d\sigma(t_0)}{d\sigma(t)}\right]^{\frac{1}{2}} + \\ + \frac{1}{2(\rho(t)\beta(t))^{\frac{1}{2}}} \int_{t_0}^{t} \left[\frac{\beta(\xi)}{\rho(\xi)}\right]^{\frac{1}{2}} \left[\frac{d\sigma(\xi)}{d\sigma(t)}\right]^{\frac{1}{2}} \\ (\vec{L}(\vec{W}_{k-1}) - \vec{M}(\vec{W}_k^1)) \cdot \hat{t}_1 \, d\xi \qquad (2.19)$$

It should be pointed out that this expression for the principal component of shear waves is valid only for the specific two-dimensional geometry employed herein. In general, the principal component has two vector components and the coupling between them may be problematic (Cerveny and Hron 1979).

2.2.2 The effect of an interface

The formulae derived in section 2.2.1 can only be used when λ, μ and ρ and all their derivatives are continuous along the ray. When the ray strikes a surface where the k-th derivatives of the elastic parameters become discontinuous, $\vec{W}_k$ also becomes discontinuous. It is assumed that the media on either side of the interface are in welded contact. Reflected and refracted compressional and shear waves must be introduced in order to satisfy the condition of welded contact. The properties of these waves can be determined from the natures of the media, interface and incident wave. We say that an interface is of order n+1 when at least one elastic parameter and its derivatives of order less than n

are continuous across the interface, but the n-th derivative is discontinuous ($n \geq 0$).

The problem of reflection and refraction of elastic waves at an interface is a fundamental one in seismology. A host of workers have devoted much time to this problem. Several good sources of information include Knott (1899), Zoeppritz (1919) and Ewing et al (1957).

For P-SV waves propagating along plane rays, there are four boundary conditions expressing continuity of displacement and stress across the interface. It turns out that for the type of medium we have chosen, that upon solving the boundary conditions, the case for SH waves can be treated independently. We shall employ this result a priori and omit further mention of SH waves. The incident wave plus the four waves arising at the boundary, reflected and refracted compressional and shear waves, must satisfy these conditions. We shall designate these waves by an index n, where n=1 and 2 refer to compressional and shear waves in the upper medium while n=3 and 4 refer to compressional and shear waves in the lower medium. The incident wave is labelled n=0. Furthermore, we assume that displacement for each of these waves can be expressed in terms of a ray series expansion,

$$\vec{W}^n = \exp(i\omega(t - \tau_n)) \sum_{k=0}^{\infty} W_k^n \, (i\omega)^{-k} \qquad (2.20)$$

where the superscript value n refers to wave type, not component. V_n shall be used to denote the velocity of the n-th wave:

$$V_1=\alpha_1 \qquad V_2=\beta_1 \qquad V_3=\alpha_2 \qquad V_4=\beta_2$$

The phase functions τ_n are given by solutions to the eikonal equations 2.9 and 2.10

$$(\nabla\tau_n)\cdot(\nabla\tau_n) = V_n^{-2}, \qquad n=1,2,3,4 \tag{2.21}$$

with initial conditions on the interface $\tau_n=\tau_0$. We employ local Cartesian coordinates (x,z) with positive x pointing to the right and positive z pointing into the earth. The point 0, where (x,z)=(0,0), is the point where the incident ray intersects the interface. Then

$$\frac{\partial\tau_n}{\partial x} = \frac{\partial\tau_0}{\partial x} = \frac{\sin\theta_n}{V_n} \tag{2.22}$$

where θ_n is the acute angle between the z axis and the ray of the n-th wave. Equation 2.22 is merely Snell's Law.

For waves leaving the interface into the first medium, $\partial\tau_n/\partial z<0$ for n=1,2 at 0. Similarly, $\partial\tau_n/\partial z>0$ for n=3,4 at 0. Then at point 0,

$$\frac{\partial\tau_n}{\partial z} = (-1)^{e_n}\frac{\cos\theta_n}{V_n} \tag{2.23}$$

where

$$e_n = 1 \quad \text{for} \quad n=1,2$$

$$e_n = 2 \quad \text{for} \quad n=3,4$$

If $\partial\tau_0/\partial x > V_n^{-1}$, then $\sin\theta_n > 1$ and the radiation condition decrees that $\cos\theta_n = -i(\sin^2\theta_n - 1)^{\frac{1}{2}}$. We shall also introduce where $e_0 = 1$ or 2 depending on whether the incident wave impinges the interface from below or above, respectively. Then,

$$\frac{\partial\tau_0}{\partial z} = (-1)^{e_0} \frac{\cos\theta_0}{V_0}$$

At the point 0, we introduce two perpendicular unit vectors $\hat{m}_P^n$ and $\hat{m}_{SV}^n$ for each n connected with the rays of the waves under consideration. $\hat{m}_P^n$ is the unit vector parallel to the ray and pointing in the direction of propagation. $\hat{m}_{SV}^n$ is perpendicular to $\hat{m}_P^n$ and is oriented so that its z component is always positive. $\hat{m}_P^n$ and $\hat{m}_{SV}^n$ correspond to the vectors $\hat{t}_1$ and $\hat{t}_3$ respectively. Thus,

$$\vec{W}_k^n = W_{k,P}^n \hat{m}_P^n + W_{k,SV}^n \hat{m}_{SV}^n \qquad (2.24)$$

Eight components now exist for the four waves generated at the boundary. Four are principal components,

$$(W_{k,P}^1 \quad W_{k,SV}^2 \quad W_{k,P}^3 \quad W_{k,SV}^4)$$

and four are additional components,

$$(W_{k,SV}^1 \quad W_{k,P}^2 \quad W_{k,SV}^3 \quad W_{k,P}^4)$$

Provided all lower terms in the series are known, the additional components can be computed at any point along the ray without knowledge of initial values (see 2.13 and 2.18).

It follows then that the only undetermined quantities are the four principal components. These values will serve as initial values in equations 2.17 and 2.19.

The projections of $\vec{W}^n$ and $\vec{W}^n_k$ on the x and z axes will be required for n=0,1,2,3,4. We ascribe the variables W^n_x, W^n_z and W^n_{kx}, W^n_{kz} to these quantities. After some geometrical considerations we may write

$$W^n_{kx} = W^n_{k,P}\sin\theta_n + (-1)^{e_n+1} W^n_{k,SV}\cos\theta_n$$

$$W^n_{kz} = (-1)^{e_n} W^n_{k,P}\cos\theta_n + W^n_{k,SV}\sin\theta_n \qquad (2.25)$$

The assumption that the two solid elastic media are in welded contact at the boundary implies that stress (η_{xz}, η_{zz}) and displacement components (W_x, W_z) be continuous across the interface. The relationships between stresses and displacements are

$$\eta_{xz} = \mu \left(\frac{\partial W_x}{\partial z} + \frac{\partial W_z}{\partial x} \right)$$

$$\eta_{zz} = (\lambda+2\mu) \frac{\partial W_z}{\partial z} + \frac{\lambda \partial W_x}{\partial x}$$

The four interface conditions can be written as

$$\sum_{n=1}^{4} (-1)^{e_n} W^n_x = (-1)^{e_0} W^0_x$$

$$\sum_{n=1}^{4} (-1)^{e_n} W^n_z = (-1)^{e_0} W^0_z$$

$$\sum_{n=1}^{4} (-1)^{e_n} \eta_{zz}(\vec{W}^n) = (-1)^{e_0} \eta_{zz}(\vec{W}^0)$$

$$\sum_{n=1}^{4} (-1)^{e_n} \eta_{xz}(\vec{W}^n) = (-1)^{e_0} \eta_{xz}(\vec{W}^0) \tag{2.26}$$

We substitute in the values of the principal and additional components from 2.20 and 2.25. After a voluminuous amount of tedious algebra, we arrive at a set of four simultaneous linear equations for the four principal components, expressible as

$$\bar{\bar{A}} \; \bar{W} = \bar{F} \tag{2.27}$$

with

A =

$$\begin{bmatrix} \sin\theta_1 & \cos\theta_2 & -\sin\theta_3 & \cos\theta_4 \\ -\cos\theta_1 & \sin\theta_2 & -\cos\theta_3 & -\sin\theta_4 \\ -\rho_1\alpha_1\cos2\theta_2 & \rho_1\beta_1\sin2\theta_2 & \rho_2\alpha_2\cos2\theta_4 & \rho_2\beta_2\sin2\theta_4 \\ \gamma_1\rho_1\beta_1\sin2\theta_1 & \rho_1\beta_1\cos2\theta_2 & \gamma_2\rho_2\beta_2\sin2\theta_3 & -\rho_2\beta_2\cos2\theta_4 \end{bmatrix}$$

and

$$\bar{W} = \begin{bmatrix} W^1_{k,P} \\ W^2_{k,SV} \\ W^3_{k,P} \\ W^4_{k,SV} \end{bmatrix}$$

and

$$\bar{F} = \begin{bmatrix} F_1 \\ F_2 \\ F_3 \\ F_4 \end{bmatrix}$$

where

$$F_1 = (-1)^{e_0+1} W^0_{kx} - W^1_{k,SV}\cos\theta_1 - W^2_{k,P}\sin\theta_2$$

$$-W^3_{k,SV}\cos\theta_3 + W^4_{k,P}\sin\theta_4$$

$$F_2 = (-1)^{e_0+1} W^0_{kz} - W^1_{k,SV}\sin\theta_1 + W^2_{k,P}\cos\theta_2$$

$$+ W^3_{k,SV}\sin\theta_3 + W^4_{k,P}\cos\theta_4$$

$$F_3 = (-1)^{e_0}\left(\lambda_{3-e_0}\frac{\partial\tau_0}{\partial x} W^0_{kx} + \left(\lambda_{3-e_0}+2\mu_{3-e_0}\right) W^0_{kz}\frac{\partial\tau_0}{\partial z}\right)$$

$$+ (-1)^{e_0}\left(\lambda_{3-e_0}\frac{\partial W^0_{k-1,x}}{\partial x} + \left(\lambda_{3-e_0}+2\mu_{3-e_0}\right)\frac{\partial W^0_{k-1,z}}{\partial z}\right.$$

$$-\rho_1\gamma_1\beta_1 W^1_{k,SV}\sin 2\theta_1 + \frac{\rho_1}{\beta_1}\left(\alpha_1^2 - 2\beta_1^2\sin^2\theta_2\right) W^2_{k,P}$$

$$-\rho_2\gamma_2\beta_2 W^3_{k,SV}\sin 2\theta_3 - \frac{\rho_2}{\beta_2}\left(\alpha_2^2 - 2\beta_2^2\sin^2\theta_4\right) W^4_{k,P}$$

$$\left.+\sum_{n=1}^{4}(-1)^{e_n+1}\left(\lambda_{e_n}\frac{\partial W^n_{k-1,x}}{\partial x} + \lambda_{e_n}+2\mu_{e_n}\right)\frac{\partial W^n_{k-1,z}}{\partial z}\right)$$

$$F_4 = (-1^{e_0}\mu_{3-e_0}\left(W^0_{kx}\frac{\partial\tau_0}{\partial z} + W^0_{kz}\frac{\partial\tau_0}{\partial x}\right)$$

$$+ (-1)^{e_0}\mu_{3-e_0}\left(\frac{\partial W^0_{k-1,x}}{\partial z} + \frac{\partial W^0_{k-1,z}}{\partial x}\right) -$$

$$-\rho_1\gamma_1\beta_1 W^1_{k,SV}\cos 2\theta_1 - \rho_1\beta_1 W^2_{k,P}\sin 2\theta_2$$

$$+\rho_2\gamma_2\beta_2 W^3_{k,SV}\cos 2\theta_3 - \rho_2\beta_2 W^4_{k,P}\sin 2\theta_4$$

$$+ \sum_{n=1}^{4} (-1)^{e_n+1} \mu_{e_n} \left(\frac{\partial W^n_{k-1,x}}{\partial z} + \frac{\partial W^n_{k-1,z}}{\partial x} \right)$$

$$\gamma_L = \beta_L/\alpha_L$$

Note that the matrix $\bar{\bar{A}}$ is independent of the value of k. In general to solve 2.27 for any k=j, it must have been previously solved for all values k=0,1,...,j-1. Only then can the variables F_i be computed. It should be stated that for k=0, equation 2.27 degenerates to the usual set of plane wave reflection and refraction coefficients as discussed and employed by numerous researchers.

2.3 Numerical evaluation of the term k=1 for P waves in media with linear velocity gradients

In this section we shall discuss techniques of numerical evaluation of the equations for principal and additional components of seismic waves (2.13, 2.17-2.19) as well as evaluation of the boundary conditions (2.27). This analysis will only be performed for compressional waves. More involved relationships can be developed for shear waves and shall thus be omitted. The key points in need of inquiry

are selection of a medium, rewriting of the vector operators into a form better suited to numerical computation and evaluation of terms appearing in the boundary conditions.

2.3.1 Selection of a medium

One model which lends itself to easy calculation is a vertically inhomogeneous medium. If we specify that the velocity of P waves be given by

$$\alpha(z) = \alpha_0 + \nabla\alpha \cdot \hat{z}, \quad \alpha_0 = \text{constant}, \quad \nabla\alpha = \text{constant}$$

where $\hat{z}$ is a unit vector in the positive z direction, then ray paths are circular arcs (Nettleton 1940). This approximation produces a sizeable reduction in the numerical calculations since many of the analytical and geometrical properties of circular ray paths can be utilized. One such saving is the abridged determination of the ray take-off angle at the source which causes the ray to arrive at a prescribed epicentral distance. We shall also impose the condition that all geological interfaces be plane and parallel to one another.

We shall utilize common relations for the other elastic parameters as discussed by Gardner et al (1974), viz.,

$$\beta(x) = \alpha(z)/3^{\frac{1}{2}}$$

$$\rho(z) = \alpha^{\frac{1}{4}}(z)3^{\frac{1}{2}}$$

$$\lambda(z) = \mu(z) = \alpha^{9/4}(z)/3^{\frac{1}{2}}$$

The use of compact analytic expressions for the elastic parameters allows very easy differentiation which is essential in evaluating the vector operators $\vec{L}$ and $\vec{M}$.

The choice of such models also makes it possible to write simple analytic expressions for the geometrical spreading of the wave front $d\sigma(t_0)/d\sigma(t)$ (Cerveny and Ravindra 1971, pp. 86-88).

2.3.2 The vector operators

For k=1 the vector operators in equations 2.13 and 2.17 must be in a computationally viable form. Consider first of all 2.13, the additional component of the P wave

$$W_1^3 = -(\vec{M}(\vec{W}_0)\cdot\hat{t}_3)\alpha^2/(\lambda+u)$$

The t_3 component of $\vec{M}(\vec{W}_0)$ is

$$(\lambda+u)\frac{\partial(W_0^1/\alpha)}{\partial t_3} + \frac{W_0^1}{\alpha}\frac{\partial\lambda}{\partial t_3} - \frac{2}{\alpha^2}\mu W_0^1\frac{\partial\alpha}{\partial t_3}$$

so that

$$W_1^3 = -\alpha^2\frac{\partial(W_0^1/\alpha)}{\partial t_3} + \frac{2\mu}{(\lambda+\mu)}\frac{W_0^1\partial\alpha}{\partial t_3} - \frac{\alpha}{(\lambda+\mu)}\frac{W_0^1\partial\lambda}{\partial t_3} \qquad (2.28)$$

For P waves $\nabla\tau$ is parallel to $\hat{t}_1$ and we can state

$$\nabla\tau = \hat{t}_1/\alpha$$

Expansion of equation 2.17 and using 2.6 and 2.28 shows that

$$\vec{L}(\vec{W}_0)\cdot\nabla\tau = \frac{\rho\alpha\partial^2 W_0^1}{\partial t_2^2} + \frac{\mu}{\alpha}\left(\frac{\bar{K}\partial W_0^1}{\partial t_3} - W_0^1\bar{K}^2 + \frac{\partial^2 W_0^1}{\partial t_3^2}\right)$$
$$+ \frac{1}{\alpha}\frac{\partial(\rho\alpha^2)}{\partial t_1}\frac{\partial W_0^1}{\partial t_1} + \frac{1}{\alpha}\frac{\partial\mu}{\partial t_3}\left(\frac{\partial W_0^1}{\partial t_3} - W_o^1\bar{K}\right) \qquad (2.29)$$

and $\vec{M}(W_1^3\,\hat{t}_3)\cdot\nabla\tau = \frac{1}{\alpha^2}\left(\frac{\partial\mu}{\partial t_3} + (\lambda+3\mu)\bar{K}\right)\cdot\left[W_0^1\frac{\partial\alpha}{\partial t_3} - \right.$

$$\left. - \frac{\alpha\partial W_0^1}{\partial t_3} - \frac{\alpha W_0^1}{(\lambda+\mu)}\frac{\partial\lambda}{\partial t_3} + \frac{2\mu}{(\lambda+\mu)}W_0^1\frac{\partial\alpha}{\partial t_3}\right]$$

$$+ \frac{(\lambda+\mu)}{\alpha^2}\left[-\frac{\alpha\partial^2 W_0^1}{\partial t_3^2} + \frac{(\lambda+3\mu)}{(\lambda+\mu)}W_0^1\frac{\partial^2\alpha}{\partial t_3^2}\right.$$

$$\left. - \frac{\partial W_0^1}{(\lambda+u)}\frac{\partial^2\lambda}{\partial t_3^2} + \left(\frac{\partial W_0^1}{\partial t_3}\frac{1}{(\lambda+\mu)} - \frac{W_0^1}{(\lambda+\mu)^2}\frac{\partial(\lambda+\mu)}{\partial t_3}\right)\cdot\right.$$

$$\left.\frac{2\mu\partial\alpha}{\partial t_3} - \frac{\alpha\partial\lambda}{\partial t_3} + \frac{W_0^1}{(\lambda+\mu)}\frac{\partial\alpha}{\partial t_3}\left(\frac{2\partial\mu}{\partial t_3} - \frac{\partial\lambda}{\partial t_3}\right)\right] \qquad (2.30)$$

where $\bar{K}$ is the ray path curvature. $\bar{K}$ is taken as positive if the center of the circle describing the ray at a point lies stratigraphically above the ray.

The derivatives of Q where Q is any of the elastic parameters $\alpha, \rho, \lambda, \mu$ can be performed easily with the medium discussed in the previous section. Let T be the angle between the positive z axis and the unit vector $\hat{t}_1 (0 \le T \le \pi)$. Then it holds that

$$\frac{dQ}{dt_1} = \frac{dQ}{dz} \cos T,$$

$$\frac{d^2Q}{dt_1^2} = \frac{d^2Q}{dz^2} \cos^2 T,$$

$$\frac{dQ}{dt_3} = \frac{dQ}{dz} \sin T, - \frac{dQ}{dz} \frac{\sin^2 T}{V(z)} \frac{dV}{dz}$$

$$\frac{d^2Q}{dt_3^2} = \frac{d^2Q}{dz^2} \sin^2 T + \frac{dQ}{dz} \frac{\sin^2 T}{V(z)} \frac{dV}{dz}$$

and the derivatives with respect to z are readily available.

The t_1 and t_3 derivatives of W_0^1 require more care. Once the ray has impinged upon a boundary, it becomes impossible to write an expression for the displacement which lends itself to analytic differentiation. For this purpose, we propose the following algorithm:

(1) Determine the ray take-off angle at the source which causes the ray to emerge at a prescribed

epicentral distance. We term this ray the central ray.

(2) Partition each central ray segment into NPT+1 equal travel-time subsegments thus defining NPT points along each segment.

(3) Shoot two rays each to the left and right of the central ray. Locate the point where each of these auxiliary rays intersect the plane normal to the central ray at all NPT points (see Appendix A for algebraic details). At these points the displacement W_0^1 can be computed and by fitting a spline through the five $(t_3, W_0^1(t_3))$ points, values for $\partial W_0^1/\partial t_3$ and $\partial^2 W_0^1/\partial t_3^2$ can be calculated (see Figure 2.2).

(4) For computation of $\partial W_0^1/\partial t_1$ and $\partial^2 W_0^1/\partial t_1^2$ at the j-th point of the ray segment, employ values of W_0^1 at the j-2, j-1, j, j+1, j+2-th points of the ray segment. Consult Figure 2.3 for details. A spline can be fitted through the five points

$$t_{1,m},\ W_{0,m}^1$$

and the derivatives at m=j determined. Of course, this procedure requires an obvious modification if $j \leq 2$ or $j \geq NPT-2$.

Note that the methods outlined for computing directional derivatives of displacement will only give good results for

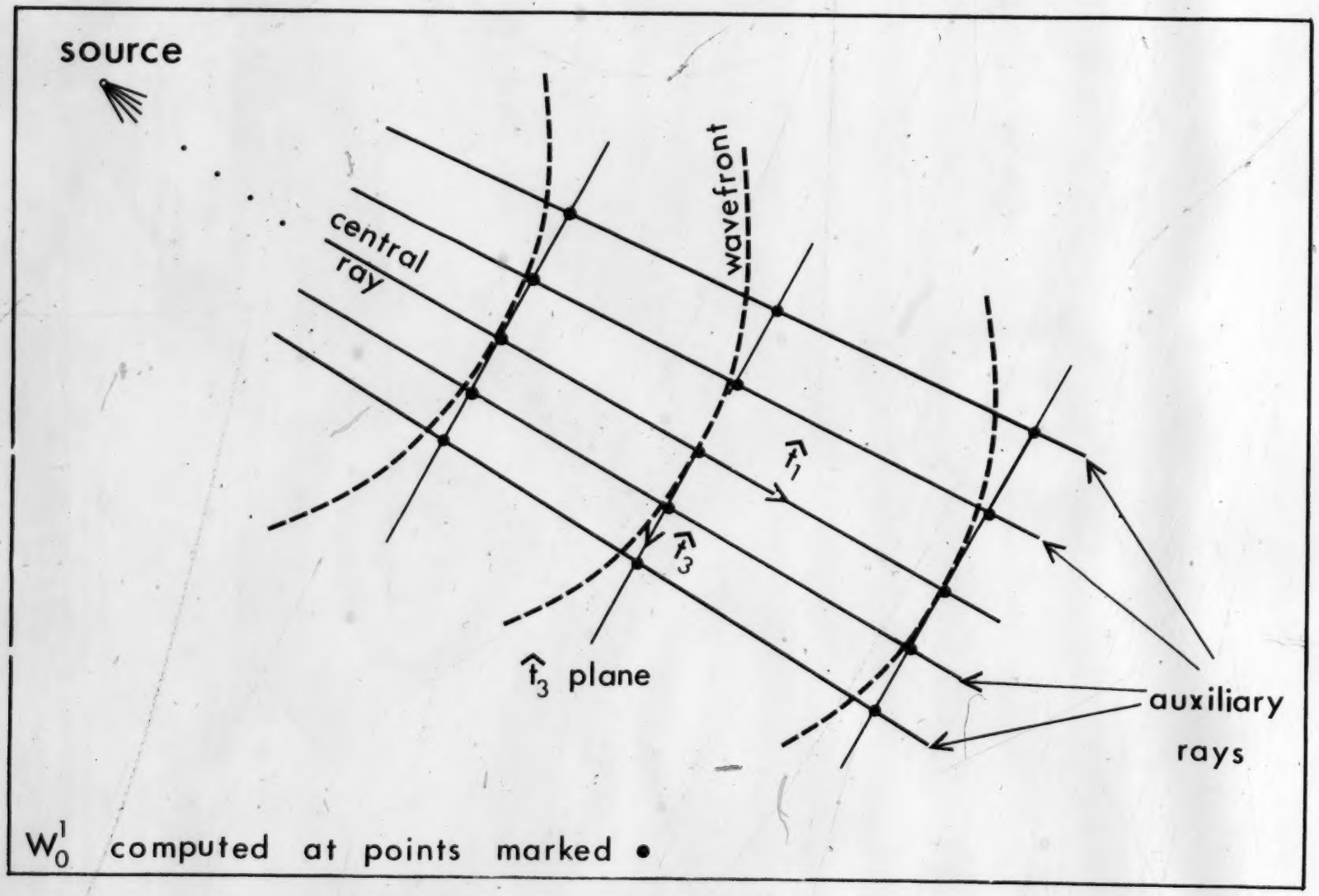

Figure 2.2 Evaluation of the $\hat{t}_3$ derivatives.

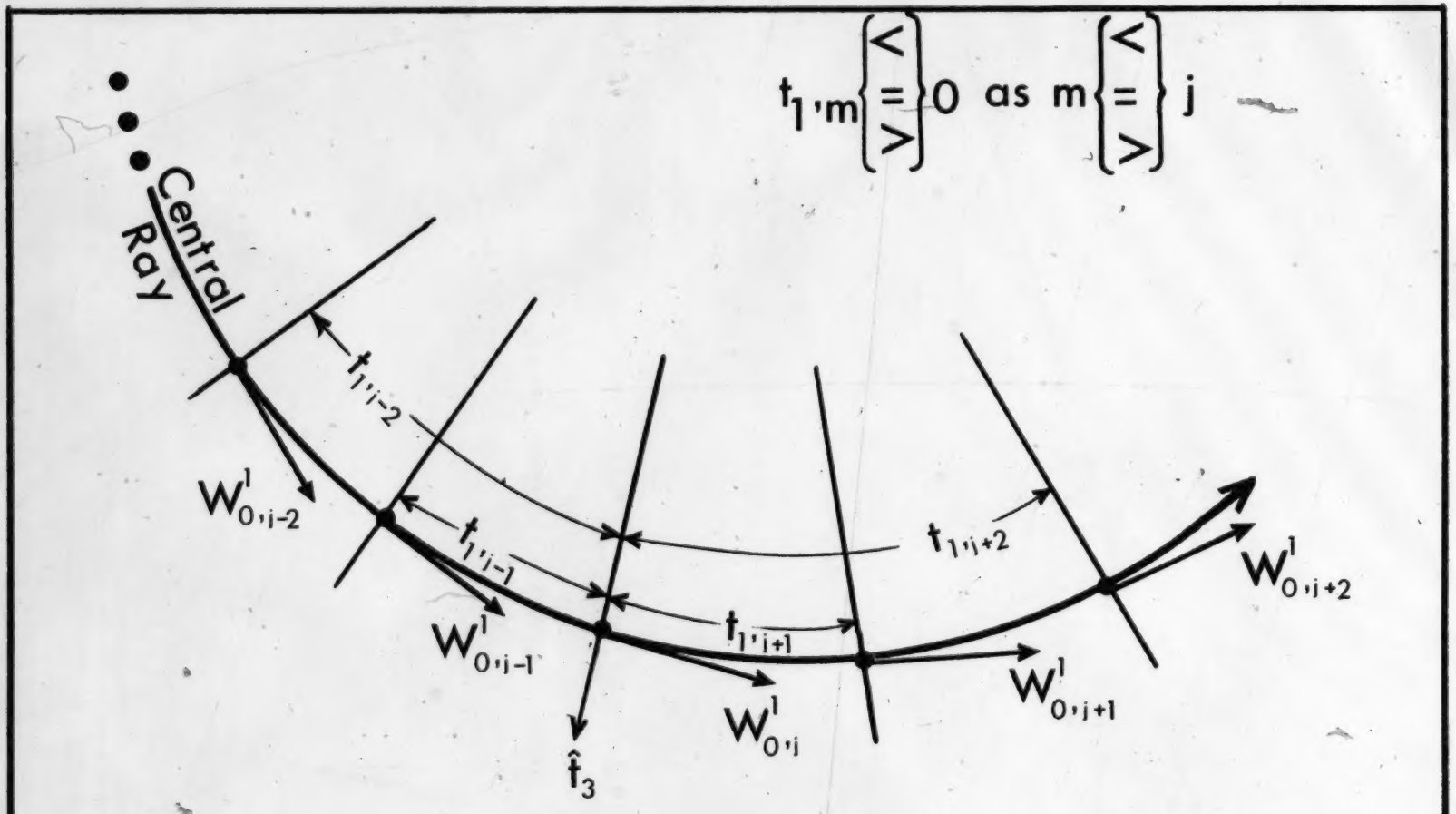

Figure 2.3 Evaluation of the $\hat{t}_1$ derivatives.

small values of ray curvature. For this reason, we have limited our study to rather weak inhomogeneities. If one were to extend these approaches to strongly inhomogeneous media, the technique would require the ray segmentation (step 2 above) to be finer for greater degrees of inhomogeneity.

Let t_0 be the initial time point of the ray segment or the time to reach the unit sphere surrounding the source if the very first ray segment is under consideration, and t be the time at which the central ray segment terminates on an interface. Then to evaluate the integral in equation 2.17 from t_0 to t, the vector operators $\vec{L}\cdot\vec{t}_1/\alpha$ and $\vec{M}\cdot\vec{t}_1/\alpha$ should be computed at the NPT points, and a spline passed through them. In this manner, the vector operators can be determined by substitution for any time $\xi, t_0 \leq \xi \leq t$, along the ray segment. Since the quantities $d\sigma(\xi)/d\sigma(t)$, $\alpha(\xi)$, $\rho(\xi)$ can be given by analytic expressions, integration of 2.19 is simplified. By computing values of W_k^1 and W_k^3 on the incident side of interface we have the necessary requirement to solve equation 2.27.

2.3.3 Evaluation of boundary conditions

Matrix $\overline{\overline{A}}$ in equation 2.27 is dependent only upon the elastic parameters on both sides of the interface and upon the angle of incidence. In the variables

F_1 to F_4 it is necessary to know the values of the four additional components corresponding to reflected and refracted waves at the interface. These can be computed by equations 2.13 for P waves (superscript n=1,3) and 2.14 for S waves (superscript n=2,4).

The evaluation of the x-derivatives of W_0^n (n=0,1,2,3,4) are also facile. Since we actually have five rays impinging on the interface, the boundary conditions for k=0 must be solved five times. The x-derivative problem then is a simple one of spline fitting through the five solutions.

The z-derivatives of W_0^n (n=0,1,2,3,4) are not quite as accessible. According to the zeroth order approximation, as a wave moves away from the interface, the only factor affecting W_o is

$$\left(\frac{\alpha_i}{\alpha(z)} \frac{\rho_i}{\rho(z)} \frac{d\sigma(u)}{d\sigma(z)} \right)^{\frac{1}{2}}$$

where the subscript "i" denotes the value of the variable at the interface and "u" represents the unit sphere surrounding the source. "RC" is the angle dependent reflection coefficient, available from the solution of equation 2.27 for k=0. For the wave travelling away from the interface, it is necessary to compute an expression relating the displacement of the wave at a vertical distance z from the

interface to the displacement at the interface, z=0. Following Cerveny and Ravindra (1971, pp. 74-88) for our medium and omitting the subscript 0 and superscript n

$$W(z) = W_i \frac{(v_i \rho_i \sin\theta_0)^{\frac{1}{2}}}{3^{\frac{1}{4}}(v(z))^{.625}} \left[r(z) \frac{\partial r(z)}{\partial \theta_0} (1-v^2(z)SV^2)^{-\frac{1}{2}} \right] \qquad (2.31)$$

where

W_i ... displacement at the boundary after reflection or refraction,

v_i, ρ_i ... velocity and density experienced by the incident, reflected, or refracted wave at the boundary,

θ_0 ... ray take-off angle with the positive z axis measured at the source

v_0 ... velocity at the source,

K ... velocity gradient in the layer in which the wave propagates,

$$SV = \sin\theta_0 / v_0 \qquad r(z) = r_i + \int_0^z \tan\theta(z)dZ$$

$$v(z) = v_i + Kz$$

$$\tan\theta(z) = v(z)(1-v^2(z)SV^2)^{-\frac{1}{2}} SV$$

r_i ... horizontal distance travelled from source to point of incidence with the interface.

The problem then is to evaluate $D = \frac{\partial W(z)}{dz}\Big|_{z=0}$

To accomplish this, one can find the x distance where the shallowest propagating ray impinges the interface, say at

$$X = X_o \qquad 2.32$$

The z coordinates where the other (four) rays intersect this vertical line are determined and the zeroth order displacements calculated there. The desired z derivative is then obtained by spline fitting.

It should be indicated that as the angle of incidence of waves upon the interface approaches a critical angle, the values of the z-derivatives of critically refracted waves tend to infinity. For this reason only subcritically reflected rays will be considered in our numerical calculations. This singularity will clearly be observable in the results of the next section.

2.4 Numerical results

In a medium composed of a laterally homogeneous layer overlying a laterally homogeneous halfspace, the equations discussed in the previous section can be evaluated numerically to give an indication of the magnitudes of the terms $k=0,1$ in the ray series. For each of several models studied, four graphs are shown. The first is a plot of the

magnitude of $\vec{w}_0 = w_0^1 \hat{t}_1$ versus distance from the source. Also given are plots of the magnitudes of w_1^1 and w_1^3 versus distance from the source. In all cases, the displacements are relative to a unit displacement on the unit sphere surrounding the source. The fourth graph is a plot of $U = |\vec{w}_1|/(2\pi|\vec{w}_0|) \times 100\%$. This is a ratio between the magnitudes of the k=1 and k=0 terms in the ray series. The greater this value, the greater the effect of the non-leading term in the ray series. This ratio must be divided by the source frequency, f, in Hertz, to obtain the frequency dependence. Thus, reference to a value of U such as 25/f%, for example, means that for source frequency of, say, 10 Hertz, the ratio of the k=1 term to the k=0 term is 25/10=2.5%. Also given in each set of graphs are velocity depth profiles of the media under consideration. The label numbers on these profiles correspond to those on the individual curves. Note that all reflections are subcritical in keeping with the discussion of the previous section.

In the first model, we study P waves propagating through a homogeneous layer and reflecting from a homogeneous halfspace. The refractive index at the reflecting interface is assigned an increasing value in each of the four cases with the interface becoming nearly transparent in the last one. These results are displayed in Figure 2.4. The curves for

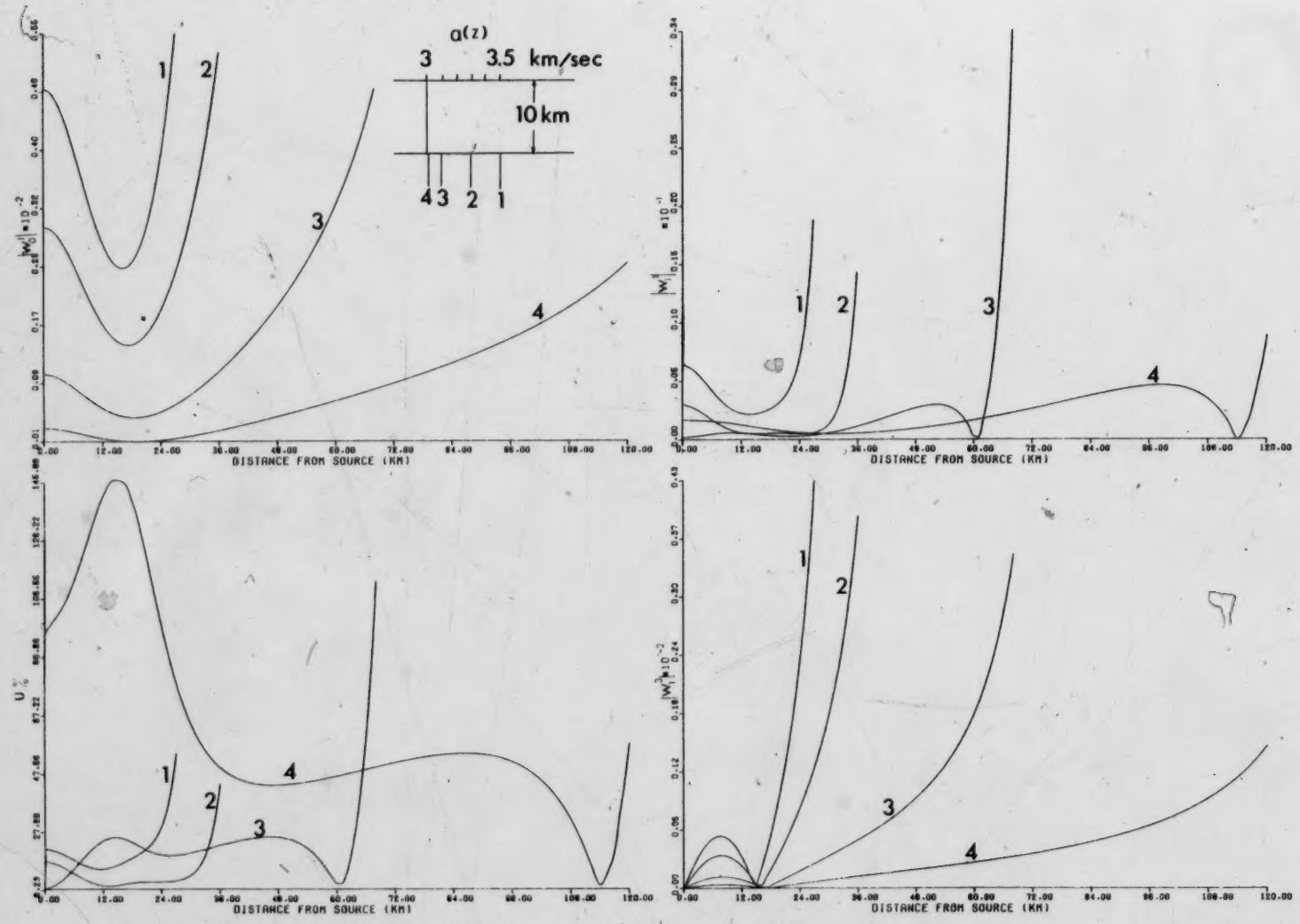

Figure 2.4 Magnitudes of the terms k=0,1 and their ratio for P waves in a homogeneous layer reflected from a homogeneous halfspace.

$|W_0^1|$ behave as expected with the amount of reflected energy being directly linked with the refractive index across the reflector. As well, the derivatives of the $|W_0^1|$ curves tend to infinite values as one approaches the critical distance. It is interesting to examine the curves for $|W_0^1|$ in conjunction with those for the additional component $|W_1^3|$, noting that the latter varies roughly as the derivative of the former. In general, the points where the curves for $|W_1^1|$ and $|W_1^3|$ dip to 0 indicate approximate points where W_1^1 and W_1^3 have polarity reversals. The curves for the ratio U indicate that for rays incident on the reflector at substantially less than critical angles, the magnitude of the k=1 term is approximately 25/f% for all but the most transparent interface.

The second test, displayed in Figure 2.5, examined P waves propagating through an inhomogeneous layer and reflected from a homogeneous halfspace. Both positive and negative velocity gradients in the layer were considered. In order to retain some degree of similarity between the models, the refractive index at the reflecting interface was kept constant. Once again, note the similarity between the curves for $|W_1^3|$ and the derivatives of the $|W_0^1|$ curves. However, it must be recalled that in inhomogeneous media, W_1^3 depends on spatial derivatives of the elastic parameters as well as the derivatives of the zeroth order approximation W_0^1.

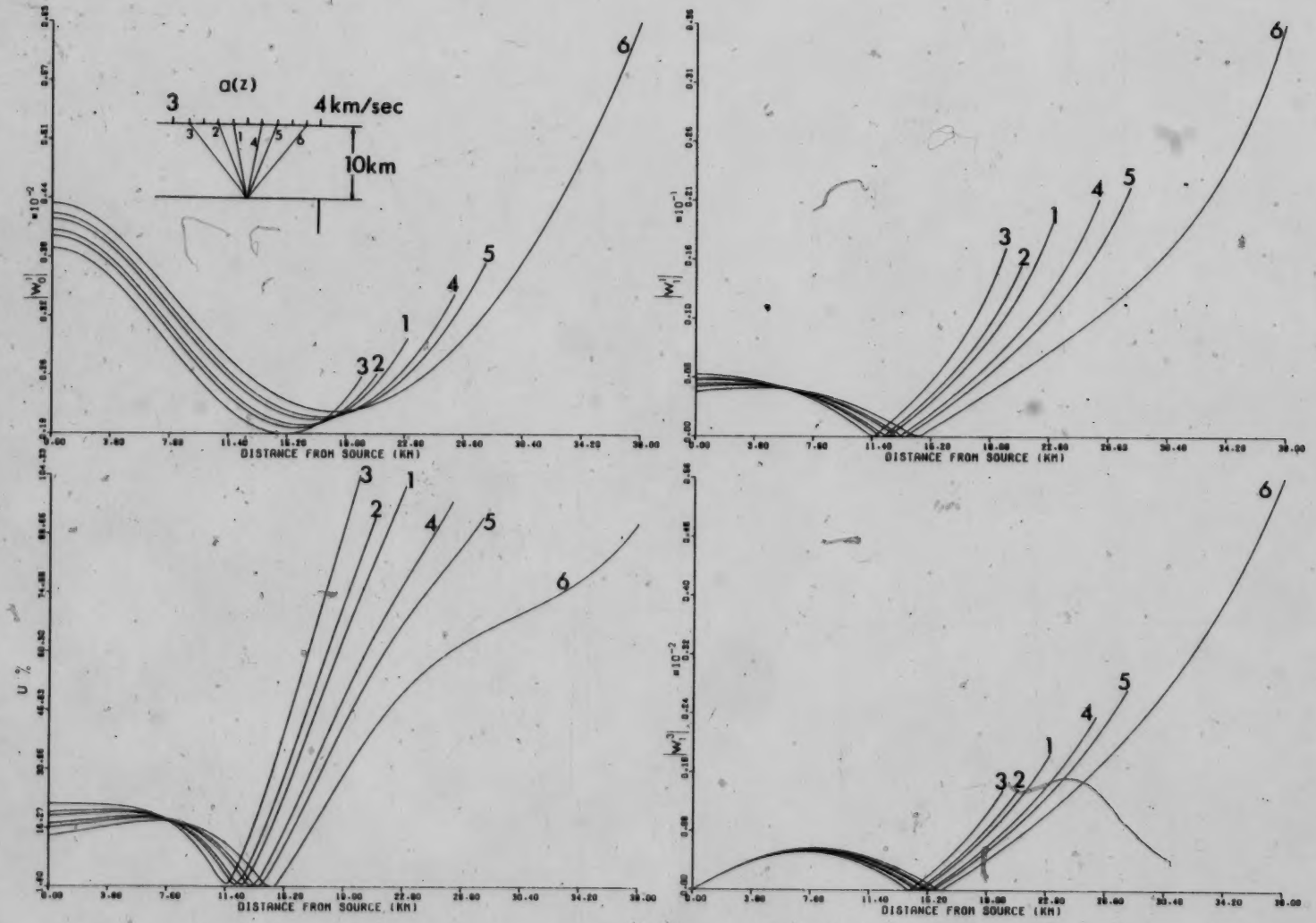

Figure 2.5 Magnitudes of the terms k=0,1 and their ratio for P waves in a vertically inhomogeneous layer reflected from a homogeneous halfspace.

The zeroes in the $|W_1^1|$, $|W_1^3|$ and U correspond to polarity reversals in the functions. The singularity in the term k=1 as the receiver approaches the critical distance is evident. However, for subcritical reflection in the model, the effect of the non-leading term in the first order approximation is no more than 25/f%. It can also be inferred from inspection of these curves that as one increases the value of the absolute velocity gradient (and hence the degree of inhomogeneity of the medium), the magnitude of the k=1 term also increases.

A commonly used technique in refraction seismology employs refracted waves that occur when the velocity varies continuously with depth. It is interesting to study the relationship between the geometrical ray theory result, $|W_0^1|$ $|W_1^3|$ and $|W_1^1|$ for refracted rays in an inhomogeneous halfspace. Computed results for such an inquiry are shown in Figure 2.6. Curves for $|W_0^1|$, $|W_1^3|$ and $|W_1^1|$ all have the same basic nature, namely, monotonic decrease with distance from the source. The graph of the ratio U versus distance indicates two conclusions. First, that the effect of the k=1 term is rather small for rays refracted through an inhomogeneous halfspace and second, that the ratio of magnitudes, U, varies almost linearly with the degree of inhomogeneity.

The zeroth order approximation to the solution of the elastodynamic equation predicts that the amplitude of a wave

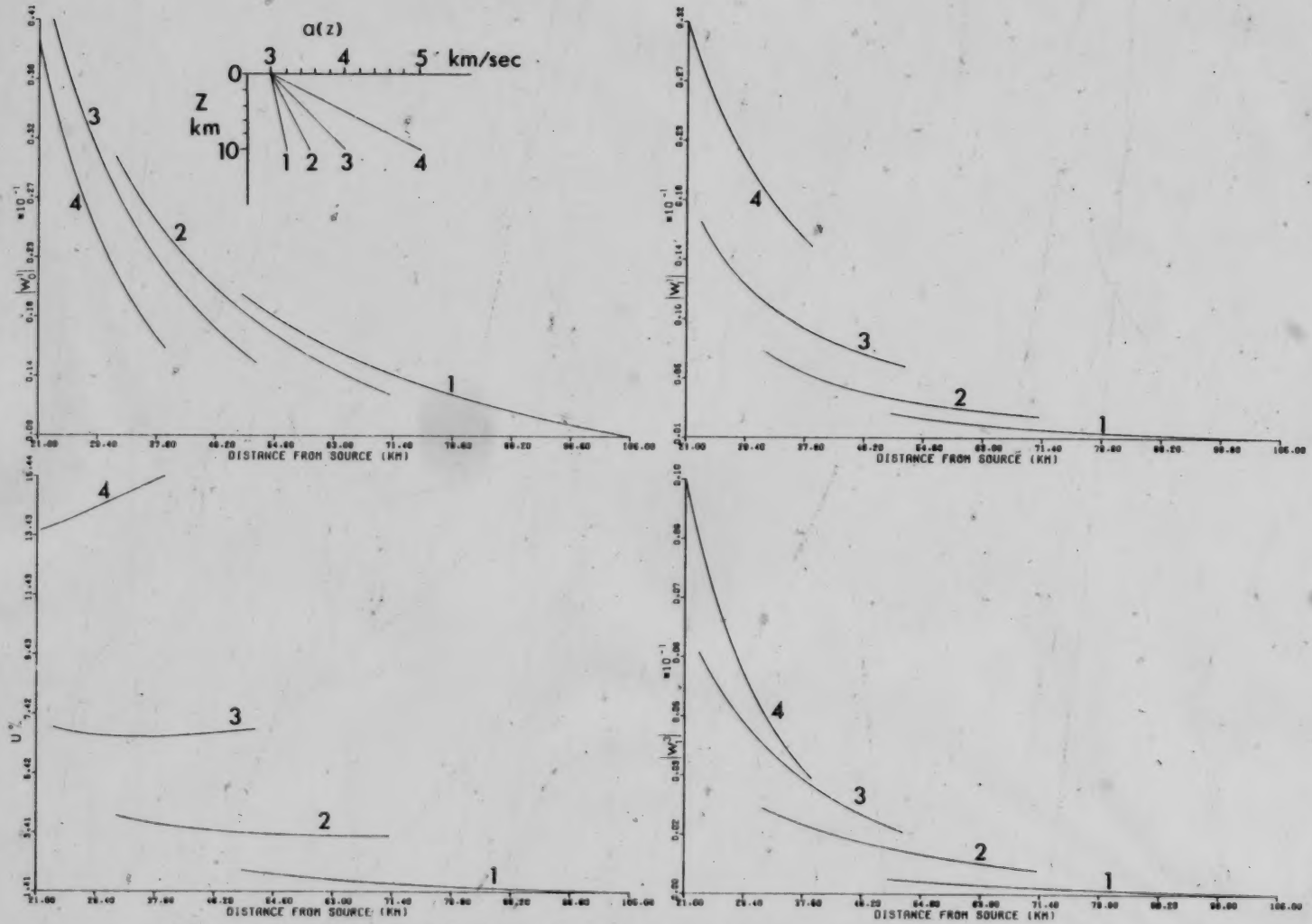

Figure 2.6 Magnitudes of the terms k=0,1 and their ratio for P waves refracted through a vertically inhomogeneous halfspace.

reflected from an inhomogeneous halfspace will not depend on the degree of inhomogeneity of the halfspace. In the first order approximation this is no longer so. Brekhovskikh (1960) studied a similar problem for plane electromagnetic waves propagating through a homogeneous layer and reflected from an inhomogeneous halfspace. For spherical elastic waves propagating in an elastic solid, no previous results have been published on a similar problem, to the author's knowledge.

The next model tested considers P waves propagating in a homogeneous layer and reflected from an inhomogeneous halfspace. The degree of vertical inhomogeneity of the halfspace has been varied, but the refractive index across the interface has been kept constant. With this condition, it is not surprising to notice in Figure 2.7 that the $|W_0^1|$ curve for all seven cases is identical. $|W_1^3|$, since it depends on the derivative of W_0^1, behaves similarly. $|W_1^1|$ and the ratio between the terms, U, are however, inhomogeneity dependent. With an increase in the value of the velocity gradient of the halfspace, both $|W_1^1|$ and U increase. The singular nature of the curves as the receiver approaches the critical point is also evident.

In this model it is instructive to examine the solutions to the boundary conditions (equation 2.27) for k=0 and k=1. These are displayed in Figure 2.8 for the models

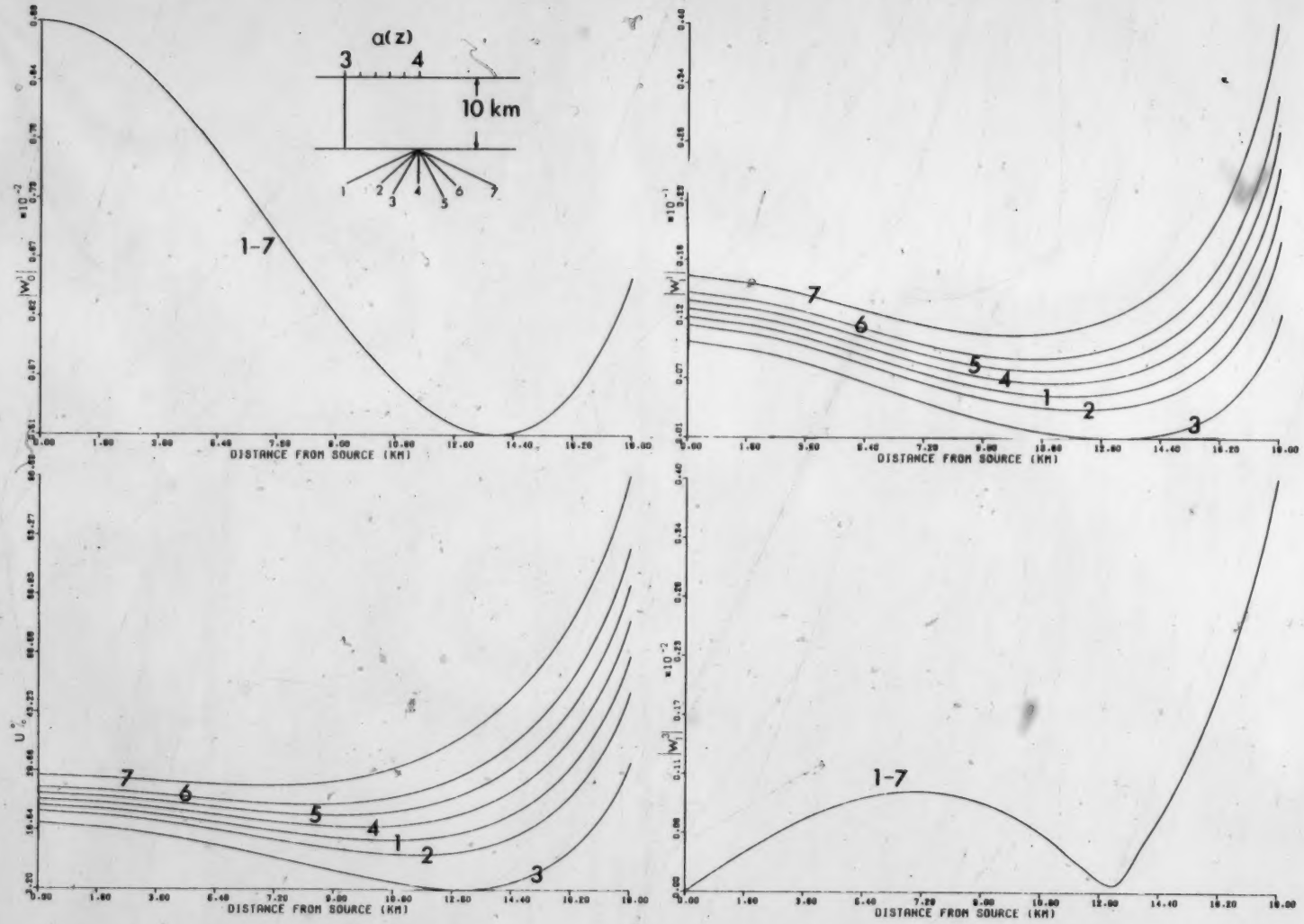

Figure 2.7 Magnitudes of the terms k=0,1 and their ratio for P waves in a homogeneous layer reflected from a vertically inhomogeneous halfspace.

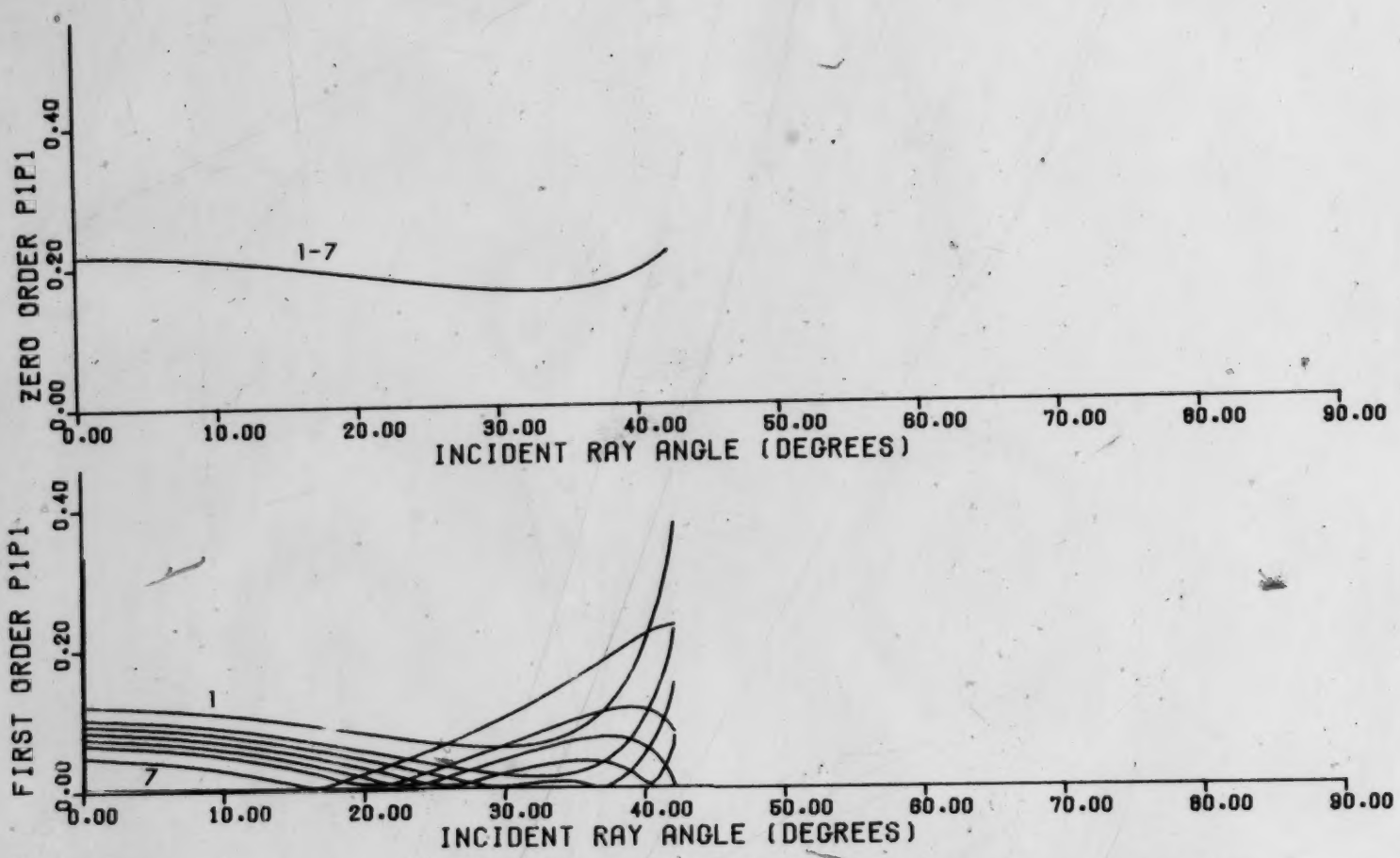

Figure 2.8 Solutions to the k=0 and k=1 boundary conditions for P waves reflected from a vertically inhomogeneous halfspace. The velocity distribution at the interface is given in Figure 2.7.

under consideration. Using the notation of equation 2.27, the curves give the ratio of the reflected compressional displacement, $W^1_{k,P}$, to the incident compressional displacement, W^0_k for k=0,1. This ratio for k=0 is more commonly known as the reflection coefficient. For k=1, this simplicity is lost due to the increased complexity of the higher order boundary conditions.

It is desirable to remove the effect of the singularity at the critical point and be able to study the effect of the k=1 term for rays which are incident upon plane interfaces at angles near 90°. To achieve this the programs have been run for a homogeneous layer overlying an inhomogeneous halfspace with the velocity in the layer exceeding that at the top of the halfspace. These results are presented in Figure 2.9. Again, for all seven velocity depth profiles, the curves for $|W^1_0|$ $|W^3_1|$ are the same. The results for drop sharply with distance from the source, pass through zero between 30 and 50 km and decay very slowly as the rays approach grazing incidence. The effect of this upon the curve of the ratio, U, between the magnitudes of the k=0 and k=1 terms is to gradually increase as the grazing angle is approached. It is evident that in this case, the effect of the term $\tilde{W}_1$ is less than 50/f%.

In homogeneous media, a tractable expression can be derived for the additional component of once reflected P

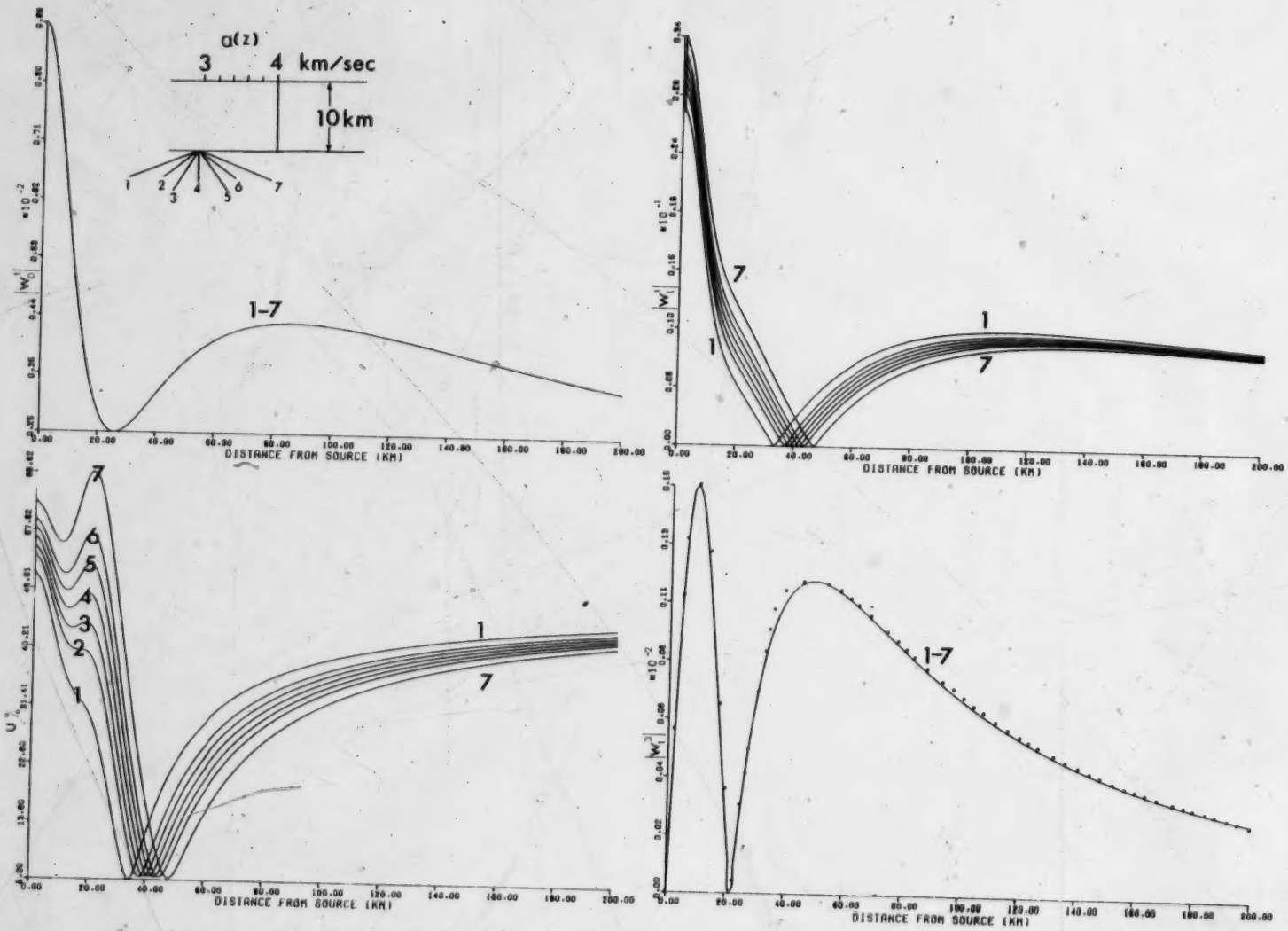

Figure 2.9 Magnitudes of the k=0,1 terms and their ratio for P waves in a homogeneous layer reflected from a vertically inhomogeneous halfspace. The dotted line on the graph of the additional component was computed by analytical methods.

waves. If $R(\theta)$ is the plane wave reflection coefficient as a function of incident angle, θ, (see the solution of equation 2.27 for K=0) then some elementary algebra and geometry shows that

$$W_1^3 = \frac{\alpha \cos^2\theta}{4h^2} \frac{dR(\theta)}{d\theta}$$

where α is the P wave velocity in a layer of thickness h. The evaluation of this expression is shown by the dotted line in Figure 2.9. Clearly, the matching between analytic and numerical techniques is very good in this simple medium.

The solutions to the boundary conditions for this model are presented in Figure 2.10. It can be shown that the zeroth order solution to the boundary conditions tends to -1 as the incident angle approaches 90°. The first order solution increases without limit for rays approaching grazing angles. However, the $|W_1^1|$ curves remain finite due to the fact that the geometrical spreading term $d\sigma(t_0)/d\sigma(t)$ in equation 2.17 tends to zero at a faster rate.

2.5 Conclusions

A commonly used technique for describing the propagation of seismic body waves in an inhomogeneous medium is the asymptotic ray series. Most seismologists have been satisfied with the zeroth order approximation which is correct for $\omega \to \infty$.

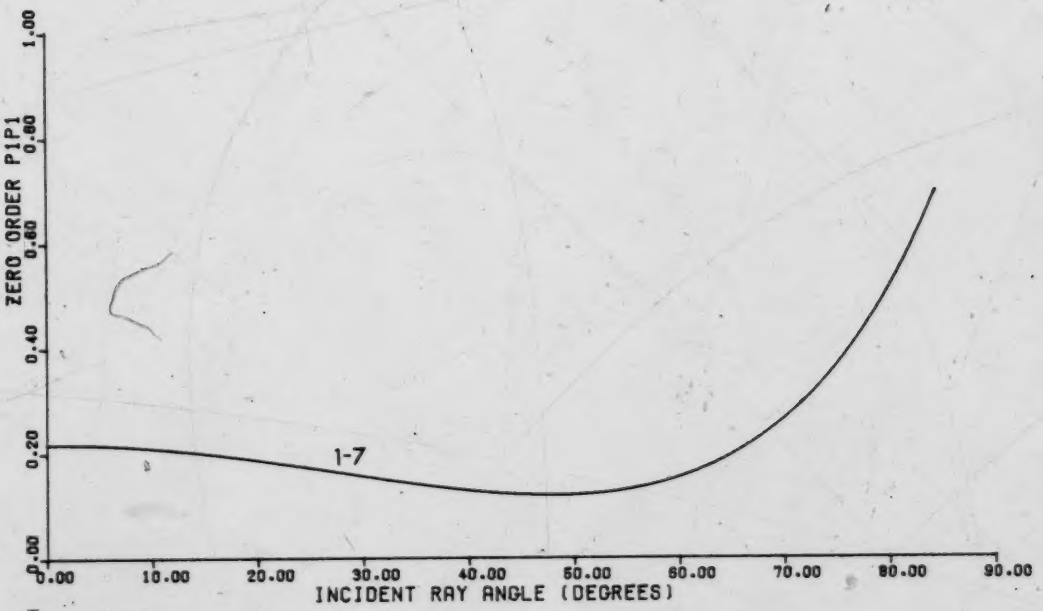

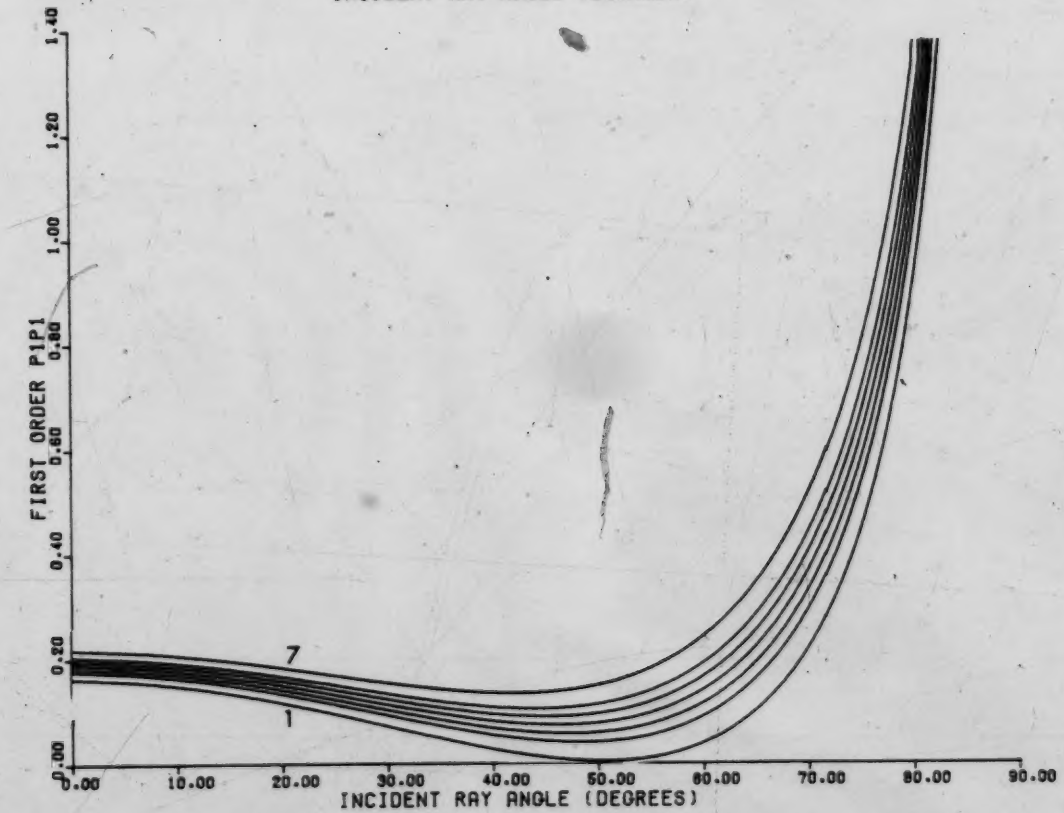

Figure 2.10 Solutions to the k=0 and k=1 boundary conditions for P waves reflected from a vertically inhomogeneous halfspace. The velocity distribution at the interface is given in Figure 2.9.

This relies on the assumption that the higher terms in the ray series ($k \geq 1$) could be neglected. This chapter has presented the formulae for the first order approximation in a numerically practical form. These equations have been evaluated for some common problems in relection and refraction seismology. On the basis of these tests we wish to establish a "rule of thumb" on the magnitude of the $k=1$ term relative to the leading term which embodies geometrical ray theory. For subcritical reflection from an interface separating vertically inhomogeneous media, the error in neglecting the $k=1$ term is generally less that $75/f\%$ where f is the source frequency in Hertz. For refracted arrivals the error is considerably less than that. Since a reasonable seismic source frequency for crustal explosion seismology is of the order of 10 Hertz, the error is less than 8%. For exploration seismic work, the error drops even lower to 1-5%, which will be imperceptible on individual seismic records.

This problem of higher terms in the ray series could be further researched by extending the presented techniques to more complicated media. One of these would be to generalize the processes to an arbitrary number of layers. Then the first order approximation could be studied for waves propagating in layers that are thin compared to the wavelength. The effect of interface curvature on the first order approximation could also be investigated. Results for

the zeroth order approximation in media with curved boundaries are presented in Chapter 6 of this thesis. Finally, the effect of the k=1 term may play a considerable role in diffraction phenomena, since these are known to be generally frequency dependent.

3. NUMERICAL CONFIRMATION OF METHODS OF COMPUTING SEISMIC WAVE AMPLITUDE

3.1 Introduction

A number of geophysical programs today are employing asymptotic ray theory as a primary means of theoretically investigating seismic wave propagation. Notable among these are Cerveny and Ravindra (1971), Hron and Kanasewich (1971) and Cerveny et al (1977). The reasons for the widespread use are the theory's versatility in complex media and the great computational efficiency over full wave techniques such as the method of finite differences. It is important to determine the degree of accuracy of the ray theory in order to justify its extensive uses in both crustal studies and oil exploration geophysics. This accuracy may be determined by direct numerical integration of the displacement integrals.

A recent study (Marks 1976, Marks and Hron 1979a) has presented a technique, based on the parabolic cylinder function (or Weber function), which eliminates the singularity that asymptotic ray theory produces when the receiver lies at the critical point of a head wave. Direct numerical integration can also be utilized to verify the amplitudes produced by the Weber function approach. At this point the reader may find it beneficial to consult Appendix

B for a review of the principles of the Weber function approach in plane-layered media. Asymptotic ray theory was discussed in Chapter 2. We shall employ only the zeroth order approximation here.

3.2 Theory for numerical integrations

According to Brekhovskikh (1960) or Ewing et al (1957), among others, the following integral expression describes the potential at the earth's free surface of a P wave with bottoming reflection on the L-th interface of a plane, parallel-layered medium with all layers homogeneous and isotropic

$$\Phi(r,z) = \frac{e^{-i\omega t}}{2} \int_{-\infty}^{\infty} R(a_L q/a_1)\sigma(a_L q/a_1)H_0^1(krq) \exp(ik\,\bar{B}(q))q(1-q^2)^{-\frac{1}{2}}dq \qquad (3.1)$$

where

$k=\omega/a_1$ = wave number in first layer,

$\omega = 2\pi f$ = circular frequency of source,

a_i, b_i = compressional and shear wave group velocities in the i-th layer,

R = plane wave reflection coefficient appropriate to the type of reflection occuring at the L-th interface,

σ = product of all other reflection, transmission, free surface and surface conversion coefficients

encountered by the ray in its propagation from source to receiver,

H_0^1 = Hankel function of the first kind and zeroth order,

$$\bar{B}(q) = N_{S1}h_1(a_1^2/b_1^2-q^2)^{\frac{1}{2}} + ((N_{P1}-1)h_1+z)\cdot (1-q^2)^{\frac{1}{2}} + \sum_{i=2}^{L} N_{pi}h_i(a_1^2/a_i^2-q^2)^{\frac{1}{2}} + \sum_{i=2}^{L} N_{si}h_i(a_1^2/b_i^2-q^2)^{\frac{1}{2}}$$

= phase function of the ray with N_{pi} P type ray segments and N_{si} S type ray segments in the i-th layer,

h_i = thickness of the i-th layer,

z = height of receiver above the first (non-free) interface.

By application of the well known equations, one may write the expressions for the horizontal (u) and vertical (w) components of displacement as

$$\begin{Bmatrix} u \\ w \end{Bmatrix} = \begin{Bmatrix} -1 \\ i \end{Bmatrix} \frac{ke^{-i\omega t}}{2} \int_{-\infty}^{\infty} R\sigma \begin{Bmatrix} H_1^1(krq) \\ H_0^1(krq) \end{Bmatrix} \exp(ik\bar{B}(q))q \begin{Bmatrix} q \\ 1 \end{Bmatrix} \begin{Bmatrix} 1 - q_1^2)^{-\frac{1}{2}} \end{Bmatrix} dq$$

where

H_1^1 is the Hankel function of first kind and order and the arguments have been dropped from R and σ.

By the proper choice of integration contours and by limiting ourselves to high frequencies, the Hankel functions may be expanded asymptotically as (Abramowitz and Stegun 1965)

$$H_0^1(z) \approx (2/\pi z)^{\frac{1}{2}} \exp(iz - i\pi/4)$$

$$H_1^1(z) \approx (2/\pi z)^{\frac{1}{2}} \exp(iz - 3i\pi/4)$$

With these approximations and by placing the receiver at the free surface ($z = h_1$), the displacements may be rewritten as

$$\begin{Bmatrix} u \\ w \end{Bmatrix} = \left(\frac{k}{2\pi r}\right)^{\frac{1}{2}} \exp(-i\omega t + i\pi/4) \int_{\overline{D}} R\sigma$$

$$\exp(ikB)\, q^{\frac{1}{2}} \begin{Bmatrix} q(1-q^2)^{-\frac{1}{2}} \\ 1 \end{Bmatrix} dq \qquad (3.2)$$

where

$$B = rq + \sum_{i=1}^{L} N_{pi} h_i \, q(a_1^2/a_i^2 - q^2)^{-\frac{1}{2}}$$

$$+ \sum_{i=1}^{L} N_{si} h_i \, q(a_1^2/b_i^2 - q^2)^{\frac{1}{2}} \qquad (3.3)$$

The path

$\bar{D}$ utilized in equation 3.2 must be decomposed depending on the receiver's location relative to the critical point. For epicentral distances less than the critical point the path consists of two parts: path D_0 and path D_1 (see Figure 3.1). The former is a semicircle in the upper half plane of the complex variable q , while the latter is given parametrically by

$$(1-q^2)^{\frac{1}{2}} = (1-x^2) + p\cdot\exp(-i\pi/4) \qquad (3.4)$$

for real p in the domain $(-\infty,\infty)$. The variable x, which is the real-valued saddle point for the ray, may be obtained by solving the condition of steepest descent

$$\left.\frac{dB}{dq}\right|_{q=x} = r$$

Upon performing this operation, we arrive at an equation for rays.

Beyond the critical distance, r^* , one must consider the branch cuts of the radical $(a_1^2/v_{L+1}^2 - q^2)^{\frac{1}{2}}$ which correspond to the generation of P-type (if v=a) or S type (if v=b) head waves from the L-th interface. In order that the deformed path D end on the same sheet of the Riemann surface as it began on, it is necessary to circumvent the cuts due to the above radical by path

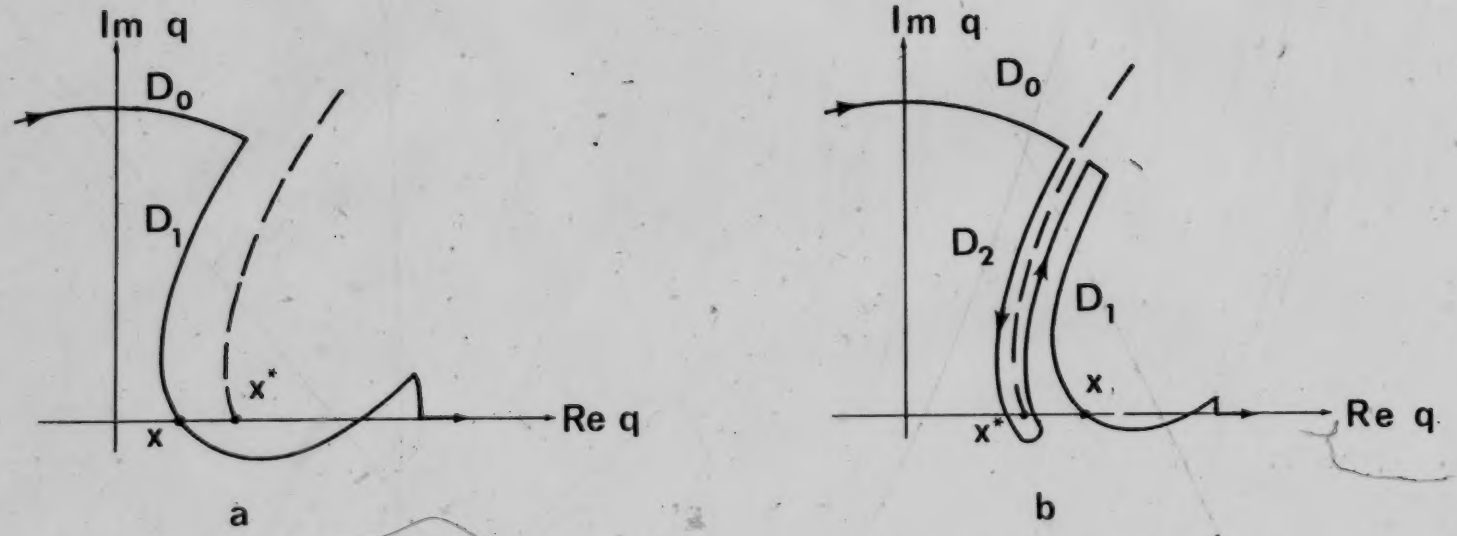

Figure 3.1 Contours of integration.

D_2 (see Figure 3.1b). This cut is chosen as

$$(1-q^2)^{\frac{1}{2}} = (1-x^{*2})^{\frac{1}{2}} + p\cdot\exp(-i\pi/4) \qquad (3.5)$$

for real values of p in the domain $[0, \infty)$ and for $x^* = a_1/v_{L+1}$. Physically, it is clear that x^* is the critical ray parameter in the first layer. The radical will have a different sign on either bank of the branch cut since it crossed onto a different Riemann sheet.

The use of the contours of integration shown in Figure 3.1 and described parametrically by equations 3.4 and 3.5 have been discussed at length by many authors. Rigourous justifications of these paths can be found in Cerveny (1962, 1965, 1967) and Marks and Hron (1979a). Recently, Daley and Hron (1979) studied a similar problem for SH waves in transversely istropic media.

For epicentral distances less than the critical point, only the reflected wave will exist. In this case, the exponential term in the integrand may be expanded as

$$ikB = ikB(x) - k(r-\tilde{r})p^2/2x^3 + \ldots$$

where

$$\tilde{r}/x^3 = \sum_{i=1}^{L} N_{pi}h_i\,(a_1^2/a_1^2 - 1)(a_1^2/a_i^2 - x^2)^{-3/2}$$

$$+ \sum_{i=1}^{L} N_{si}h_i\,(a_1^2/b_i^2 - 1)(a_1^2/b_i^2 - x^2)^{-3/2}$$

We also note that $B(x)$ is related to the two way travel time of the reflected ray by $B(x)/a_1 = t_r$. This yields a result which lends itself to numerical integration

$$\begin{bmatrix} u \\ w \end{bmatrix} = e^{-i\omega(t-t_r)} \left(\frac{k}{2\pi rx}\right)^{\frac{1}{2}} \int_{-\infty}^{\infty} R\sigma \cdot$$

$$\exp(-k(r-\tilde{r})p^2/2x^3) \begin{Bmatrix} q \\ (1-q^2)^{\frac{1}{2}} \end{Bmatrix} dp \quad . \tag{3.6}$$

Along the circumvention of the branch cut a similar expansion may be produced as

$$ikB = ikB(x^*) - k(1-x^{*2})^{\frac{1}{2}}(r-r^*)(1+i)p/2^{\frac{1}{2}}x^*$$

$$-k(r-\tilde{r}^*)\ p^2/2x^{*3} + \ldots$$

where $\tilde{r}^*$ is just $\tilde{r}$ evaluated at $x=x^*$. Again, $B(x^*)$ is related to the travel time of the head wave by $B(x^*)/a_1 = t_h$.

The plane wave reflection coefficient R can be cast in the form

$$R = E - D(a_1^2/v_{L+1}^2 - q^2)^{\frac{1}{2}} = E - DS \tag{3.7}$$

where E and D are functions of $a_L q/a_1$. E and D do not depend on the radical S, but only on even powers of S. By substituting equations 3.5 and 3.7 into 3.2, and recalling that the sign of S differs from left to right bank of the

path, we arrive at an integral expression for the head wave displacement:

$$\begin{Bmatrix} u^* \\ w^* \end{Bmatrix} = -e^{-i\omega(t-t_h)} \left(\frac{k}{2\pi r x^*} \right)^{\frac{1}{2}} 2 \int_0^{\infty} DS\sigma$$

$$\exp(-k(1-x^{*2})^{\frac{1}{2}} (r-r^*)(1+i)p/2^{\frac{1}{2}}x^* -$$

$$k(r-\tilde{r}^*)\ p^2/2x^{*3}) \begin{Bmatrix} q \\ (1-q^2)^{\frac{1}{2}} \end{Bmatrix} dp \qquad (3.8)$$

Equations 3.6 and 3.8 are the final expressions that we wish to evaluate along the integration paths shown in Figure 3.1. Care must be taken to ensure that the correct sign is used for all radicals in the reflection and transmission coefficients in the integrands. The integrands are, in general, complex valued and thus the integrals must be evaluated once for the real part and once for the imaginary part.

3.3 Numerical results

An efficient and versatile algorithm for numerical integration employs cautious Romberg extrapolation, ably discussed by de Boor (1971). On the basis of a FORTRAN program with the algorithm at its hub, amplitude - distance curves were obtained for various rays and source frequencies for the medium listed in Table 3.1. This medium is basically

that due to Cumming and Kanasewich (1966). The top two layers have been thickened to increase the ratio of thickness to wavelength to values acceptable by asymptotic ray theory.

The cost of computing results via numerical integration exceeds those derived by asymptotic ray theory or the Weber function by a factor of 160 to 200, depending on the frequency and ray path selected. However, this integration technique may be taken as exact and the Weber function approach and asymptotic ray theory will be shown to be very economical approximate methods.

Figures 3.2 - 3.6 are a series of plots of vertical amplitudes versus distance from the source calculated by means of asymptotic ray theory, the Weber function approach for interference reflected head waves or direct numerical integrations. Each diagram has a schematic sketch of the ray(s) under consideration. A solid line in this sketch implies propagation in the compressional (P) mode, while a broken line denotes the shear (S) mode. The predominant source frequency (F) is indicated where necessary.

Figure 3.2 displays an amplitude distance curve for an unconverted P wave reflected from the third interface. It can be observed that the amplitude curves derived by direct numerical integration (numbers 2 - 4) preserve the same

TABLE 3.1

The Alberta Model

P Wave Velocity km/sec	S Wave Velocity km/sec	Volume Density g/cm^3	Layer Thickness km
2.31	1.33	2.04	8
3.06	1.77	2.21	8
6.50	3.75	2.73	∞

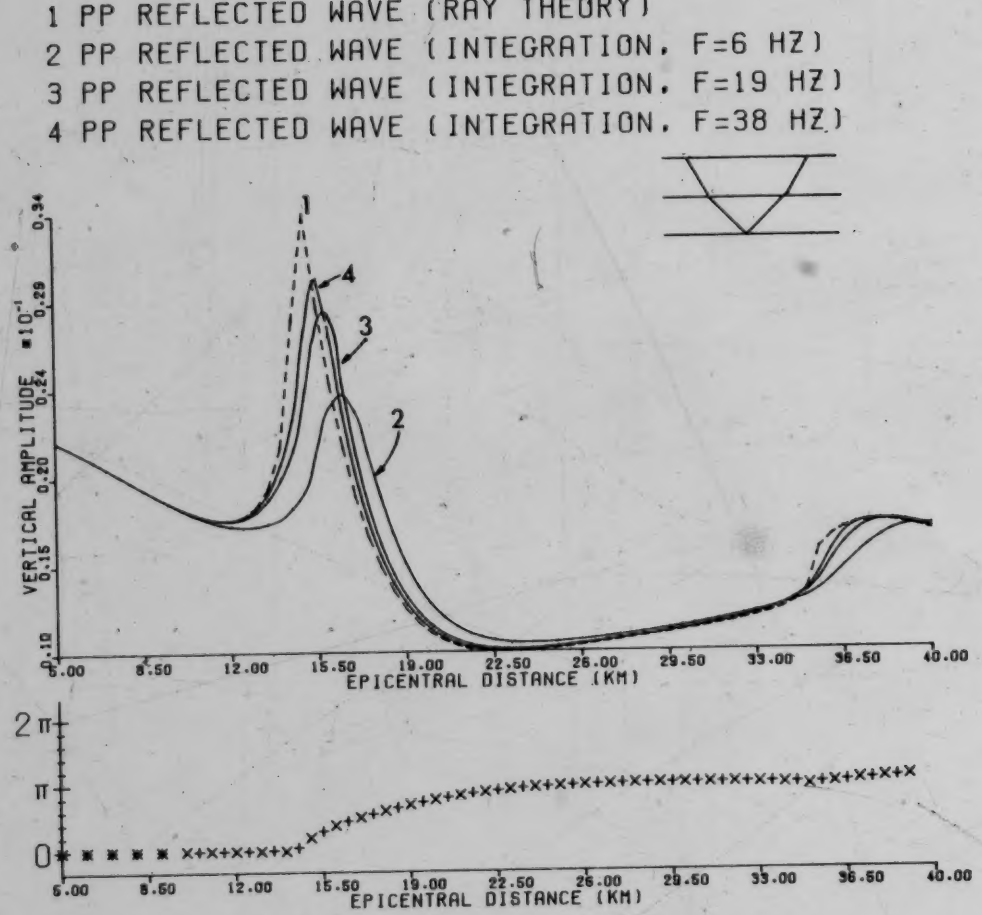

Figure 3.2 Reflected unconverted wave displacement computed by ray theory and integration.

general shape of the ray theoretical curve (number 1). At higher frequencies, the integration curves attain sharper maxima and more closely follow the ray theoretical curve. The good fit between phase shifts between curves 1 and 4 should also be noted.

In Figure 3.3, the common logarithm of amplitude is displayed against the distance for a reflected and converted wave. The location of the critical points for the SPS and SSS head waves (marked Rcp and Rcs, respectively) are indicated. Following this, Figure 3.4 displays the amplitude of an SSS head wave, which has its critical point at the location marked by Rcs in Figure 3.3. The end of the interference zone between the reflected and head waves is indicated by Ri. Thus, outside this region, there is a near perfect fit between the results of the two methods.

Figure 3.5 shows confirmation of the frequency dependence of head waves. Curves 1 and 2 were computed by ray theory which predicts an inverse frequency dependence for head wave amplitude. Curves 3 and 4, calculated by direct integration, produce a very good fit with asymptotic ray theory outside the interference zones. The end of the interference zone for the lower (higher) frequency is indicated by the rightmost (leftmost) Ri. The phase shifts are also shown corresponding to curves 2 and 4.

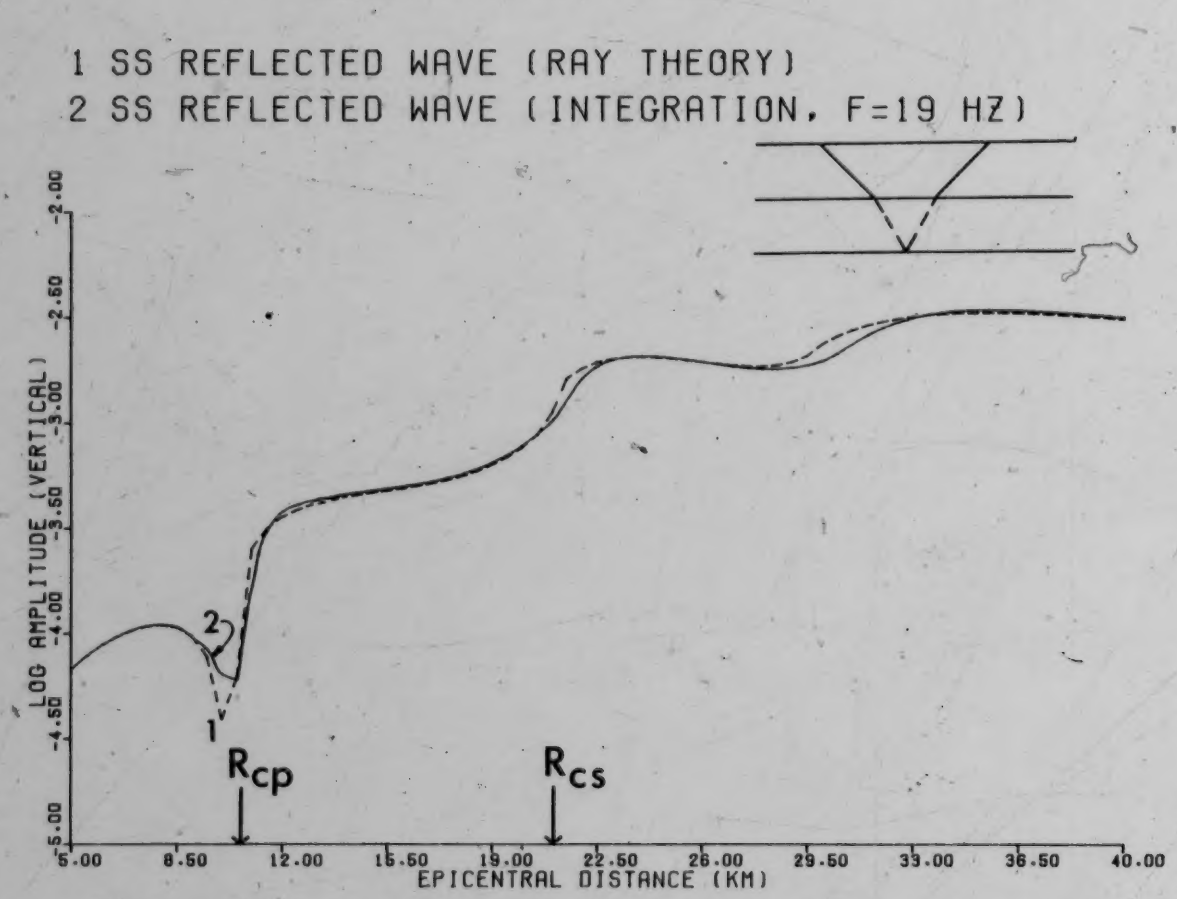

Figure 3.3 Reflected converted wave displacement computed by ray theory and integration.

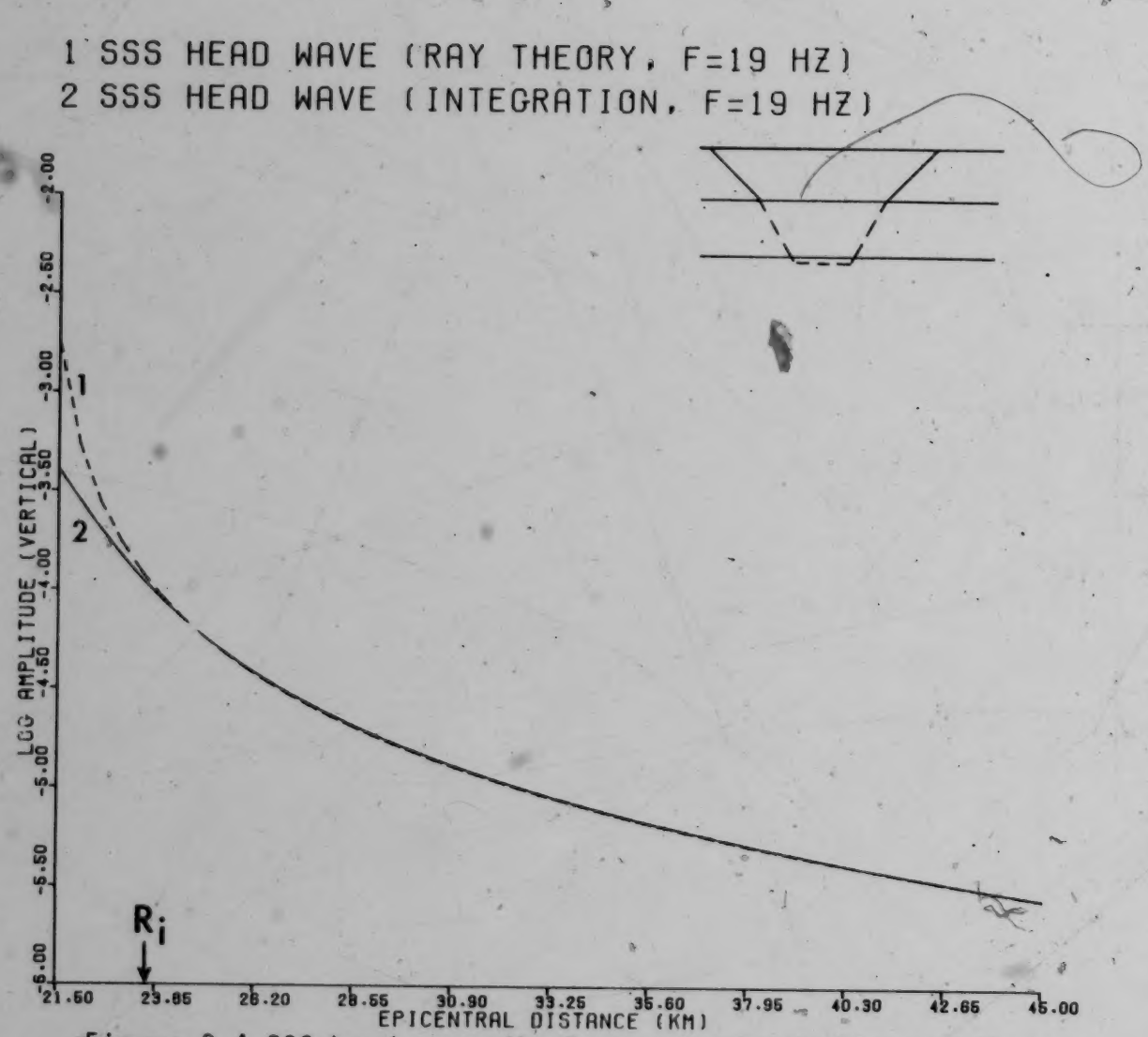

Figure 3.4 SSS head wave displacement computed by ray theory and integration.

1 PPP HEAD WAVE (RAY THEORY, F=6 HZ)
2 PPP HEAD WAVE (RAY THEORY, F=19 HZ)
3 PPP HEAD WAVE (INTEGRATION, F=6 HZ)
4 PPP HEAD WAVE (INTEGRATION, F=19 HZ)

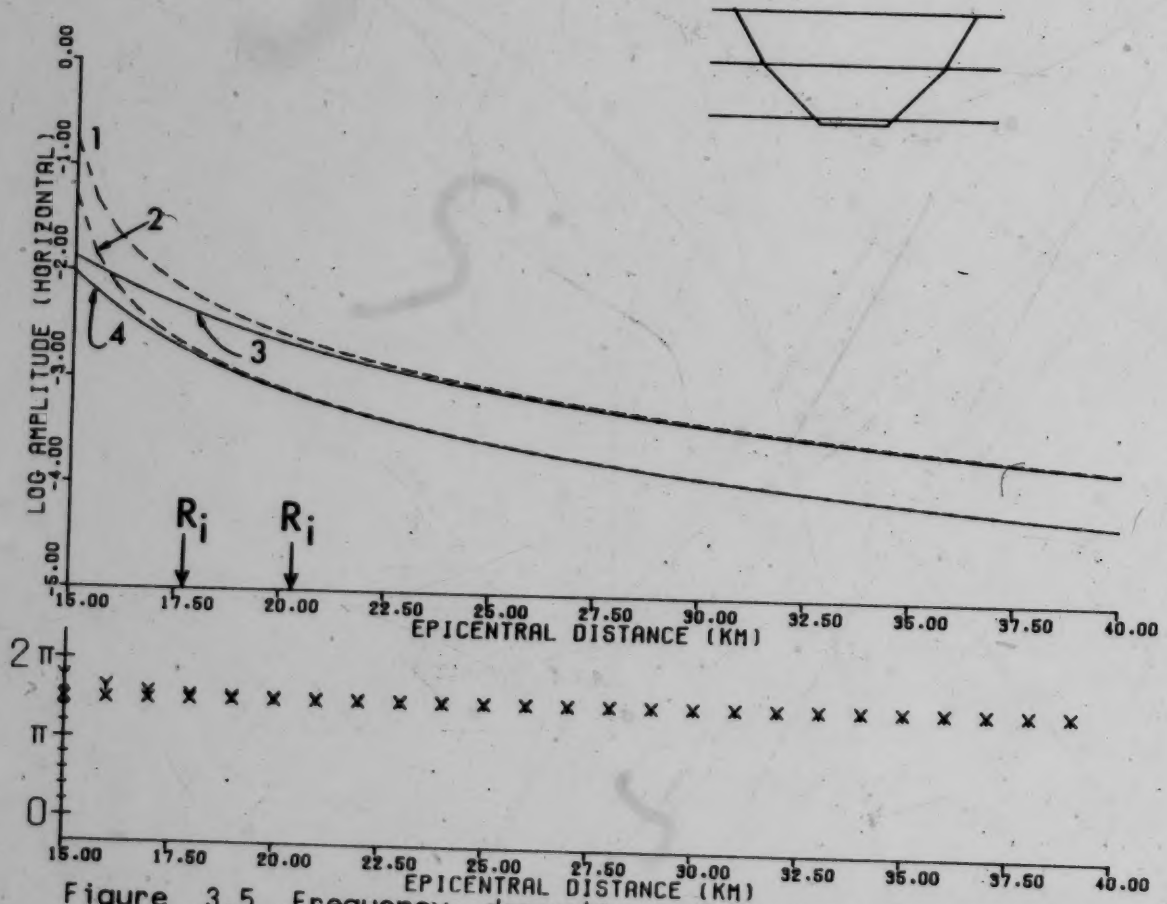

Figure 3.5 Frequency dependence of head waves computed by different means.

Within the interference zone, it is necessary to consider the composite of the reflected wave and head wave since they do not exist independently there. It was for the purpose of investigating the interference reflected head wave that the Weber function approach was developed. It should be noted that discrepancies in amplitude between direct integration and the Weber function techniques outside the interference zone may be overlooked, since certain approximations used in developing the theory required the epicentral distance to be close to the critical point. Results, displayed in Figure 3.6, indicate the correctness of the Weber function approach within the interference zone.

3.4 Conclusions

Approximate methods of determining seismic ray amplitude have recently become in vogue for the theoretical investigation of wave propagation in homogeneous, plane-layered media. Two of these, asymptotic ray theory and the Weber function approach for interference reflected head waves, have been shown to match very closely with a more exact method of direct numerical evaluation of the displacement potentials. The matching between the integration method and the two high frequency approximations became better as the source frequency was increased.

1 PP-PPP INTERFERENCE WAVE (WEBER FUNCTION, F=11 HZ)
2 PP-PPP INTERFERENCE WAVE (INTEGRATION, F=11 HZ)

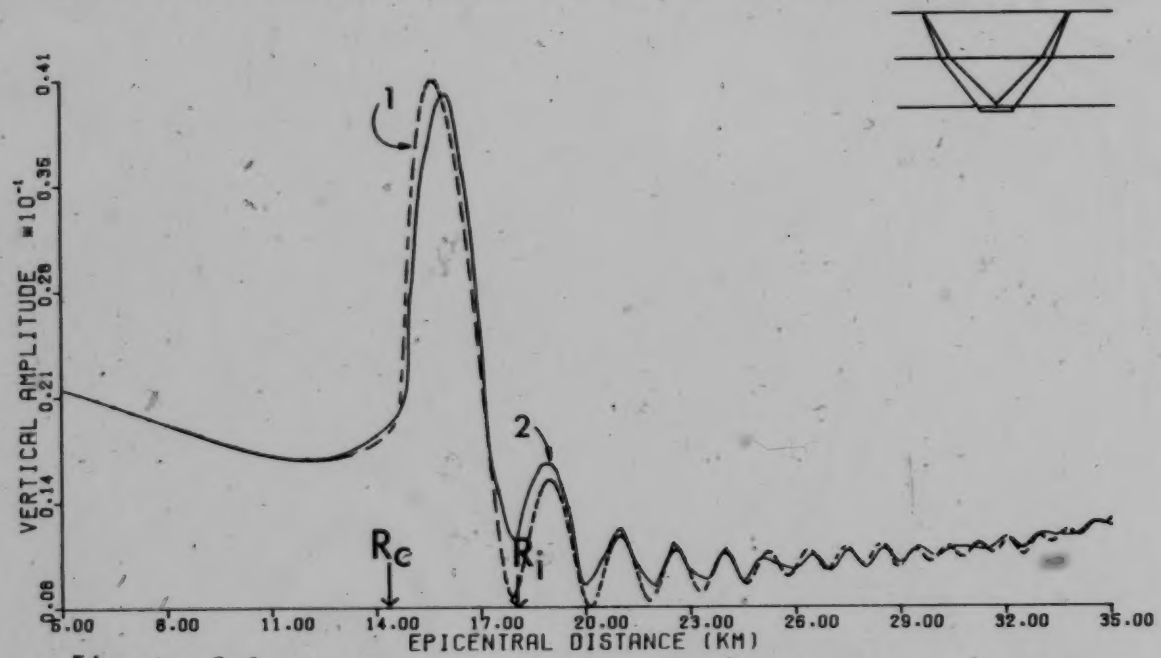

Figure 3.6 Comparison of the Weber function approach and integration.

In summary, this chapter has provided a numerical investigation of two methods of seismic ray amplitude computation: asymptotic ray theory and the Weber function approach. These methods complement each other in reference to their regions of applicability. This renders them especially useful for purposes of constructing synthetic seismograms.

4. RAY TRACING BY CLASSICAL METHODS

4.1 Introduction

Classical methods of computing ray paths for seismic energy have been known for some time. One of these consists of a variational approach of Fermat's Principle. We shall term this technique "The Bending Method". Another classical method consists of numerically solving a system of first order differential equations. For certain simple velocity distributions (i.e. simple enough to be specified by a certain analytic function of position) ray paths may be analytically determined by complex analysis. The remaining ray tracing methods rely upon solving a set of coupled non-linear differential equations. For this purpose, computationally costly numerical methods must be implemented. A newer method, employing local velocity gradients for which analytic expressions are known will be presented in the next chapter.

4.2 The bending method for ray tracing

The bending method as described by Julian and Gubbins (1977) was considered for purposes of tracing seismic rays through two-dimensional media. Additional authors include Wesson (1970) and Chander (1975). The method basically perturbs an initial guess at the true ray path between the

source and receiver until a stationary time path is obtained. The differential equations for the ray, obtained by the calculus of variations, are expressed in terms of changes in the ray path coordinates. The system of equations is linearized and solved by standard techniques. This solution represents corrections to the ray path. The process is reiterated until either the RMS path perturbation between consecutive iterations is less than some prescribed error bound or the variational equations for the ray (expressed by finite differences) are solved. This method is computationally expedient if an efficient method is used to solve the linear algebraic equations. For this purpose, one may take advantage of the fact that the coefficient matrix involved is tridiagonal and apply Gaussian elimination algorithms as ably discussed in Henrici (1962).

Figure 4.1 gives an example of the use of this technique. The solid path is the true ray path for the velocity structure $v(z)=3+1.3z$. This ray is an arc of a circle, the equation for which is given in many standard texts (Nettleton 1940). The initial guess at the ray path was taken to be a straight line joining source and receiver. The corrected path is shown after N=2,4,9 iterations. We have also displayed the error in the ray.

For purposes of ray tracing alone, this technique appears to be of great service. The method has the desirable

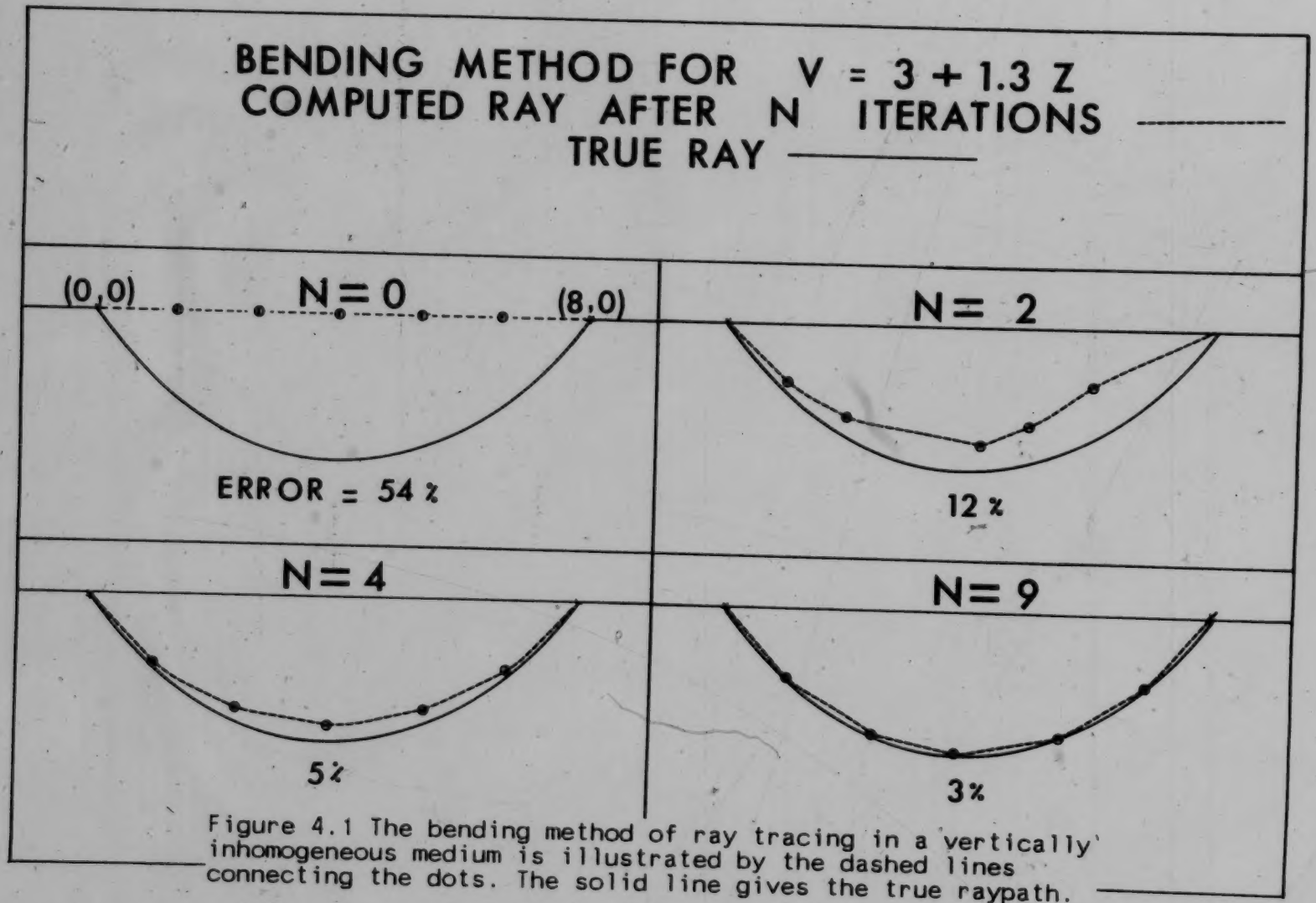

Figure 4.1 The bending method of ray tracing in a vertically inhomogeneous medium is illustrated by the dashed lines connecting the dots. The solid line gives the true raypath.

feature of allowing the user to specify the receiver point, which other methods seek to reach by varying the take-off angle of the ray at the source. However, for purposes of synthetic seismogram computation at several receiver locations in a complicated model, the method has some drawbacks. Let us define a family of rays as all those rays which travel outward from the source, strike the same interfaces in the same order, are converted from P to S mode or vice versa, and finally arrive at the free surface. Due to a complex two-dimensional velocity structure (Psencik 1972) or curvilinear interfaces (Hron 1973) or both, this family of rays may produce a large number of individual travel time branches. For a receiver at some distance from the source the bending method would have to be utilized to find the ray path corresponding to each arrival (i.e. for each branch which exists at the distance). This would require some initial guess for each of these ray paths. It is at this point that the method is insufficient. Firstly, the ray paths in complex models may be rather exotic (Hron et al 1977) and an initial estimate may be very difficult. Secondly, a poorly conjectured initial path will converge to a ray lying on a different branch than the one desired. Finally, this method does not give information on the total number of travel time branches related to the same family of rays, nor, more crucially, whether a particular arrival lies on a forward or reverse branch. This information is indispensible in determining the phase shift

$\pi/2$ associated with the geometrical spreading (Cerveny and Ravindra 1971, p. 76, Choi 1978) for rays having passed through a number of caustics. For these reasons, we must seek alternative approaches for seismic ray tracing.

4.3 Complex analysis

A rather limited approach to the problem was presented by Barnes and Solomon (1971). Their technique requires an analytic expression for the velocity field of the medium. For certain fields, ray paths can be derived using the theory of complex variables. However, it is difficult to find a function which would even partially correspond to the velocity distribution of a real medium. For this purpose we will not further investigate this method.

4.4 Differential equations for ray tracing

Ray paths for seismic energy may be computed by solving a system of first order differential equations. Various authors have used different approaches to arrive at these equations, including Eliseevnin (1964), Chen and Ludwig (1972), Psencik (1972), Green (1976) and White (1978), among others.

In two-dimensional media with a point source, three

differential equations must be solved for the coordinates of the endpoint of the ray, $(x(t), z(t))$, and the angle that the ray makes with the vertical, $\theta(t)$, as a function of time, t. Following Psencik (1972) these may be written as

$$\frac{d}{dt}\begin{bmatrix} x \\ z \\ \theta \end{bmatrix} = \begin{bmatrix} v \sin\theta \\ v \cos\theta \\ v_z \sin\theta - v_x \cos\theta \end{bmatrix}, \quad 0 \le \theta < 2\pi \qquad (4.1)$$

where $v(x,z)$ is the velocity of propagation (P or S wave mode) at the point under consideration. v_x, v_z are its spatial derivatives. These equations must be solved subject to the initial conditions

$$x(0) = x_0, \quad z(0) = z_0, \quad \theta(0) = \theta_0$$

where (x_0, z_0) is the source location and θ_0 is the take off angle. Note that for equation 4.1 to hold θ must be measured counter-clockwise from the negative z axis to the tangent of the ray path. We take the positive z axis to point into the earth from the free surface.

The solution to equation 4.1 requires knowledge of the velocity field and its spatial derivatives everywhere that the ray travels. The input velocities may be specified on a rectangular grid rather than an analytical expression. This is due to the difficulty in finding a function which reasonably approximates true velocity-position relationships

in the earth. In order to determine v and its derivatives within any rectangle of the grid one may use linear interpolation among the four corner points. This approximation was utilized by Psencik (1972). However, this will lead to second order discontinuities in the ray from rectangle to rectangle. An improved technique has been implemented to employ bicubic splines for the velocity field. By this method the velocity at any point is dependent upon not only the velocity at the four nearest grid points, although these are weighted more heavily, but also by the general trend of the velocity in the entire layer.

Consider a point (x,z) which lies within a grid rectangle with (x_ℓ, z_ℓ) as coordinates of its upper left corner. By employing all the velocity-position data given within the layer that houses (x,z) we may compute bicubic spline coefficients in the form of 4x4 matrices, C_{ij}, i,j=1,2,3,4, (Ahlberg et al 1967, Chapter 7). A spline interpolation may then be made as

$$v(x,z) = C_{ij}(x-x_\ell)^{i-1}(z-z_\ell)^{j-1}$$

where we sum over i and j. If one wishes to use the same velocity model for many rays in different computer runs, a considerable saving of central processing unit (CPU) time may be achieved by computing all spline coefficients once, writing them on a permanent direct access file in the computer memory, and subsequently scanning the file for the appropriate coefficients as the program progresses.

The effect of geological curvilinear interfaces where the ray directions change discontinuously must be taken into account in solving equation 4.1. By the principle of the isolated element and Snell's Law, we may determine the initial parameters for solving equation 4.1 after the ray impinges an interface. The location of interfaces may be spcified by a series of (x,z(x)) coordinates. We may smooth this initial data by the use of cubic splines (Ahlberg et al 1967, Chapter 2). This approach will also allow us to determine the interface normals quite easily.

Although the formulation for ray tracing presented here will give us ray paths which can be considered to be correct, it has a serious impediment. This is the extremely large amount of CPU time needed to solve the differential equations with a reasonable degree of accuracy. The severity of this is compounded when many rays are considered, as in the construction of synthetic seismograms. To alleviate this the next chapter presents a ray tracing concept which consumes only a fraction of the CPU time required by the differential equation process and still yields reasonably accurate results.

5. RAY TRACING BY CIRCULAR APPROXIMATION

5.1 Introduction

Chapter 4 described techniques for tracing rays through two-dimensional media with curvilinear boundaries. The differential equation method is precise in that it takes into account all the known values of velocity within a given layer to compute the velocity at any point. However, from a computational viewpoint, the method is extremely expensive. An approximate method has been developed which gives reasonably close results to the exact theory. Much computational effort may be spared if one approximates the velocity field v(x,z) within a small region of the model to be expressible as

$$v(x,z) = v_0(x_0,z_0) + \text{grad } v \cdot d\vec{r}$$

where v_0 and (grad v)=K are constants. With this representation, one may solve classical equations to direct the ray endpoint to its proper location as a function of time. Similar techniques were developed independently by Gebrande (1976), Will (1976), Aric and Gutdeutsch (1978) and Dantz (1978). All of these techniques require the approximation of the isovelocity lines of the medium.

Rather than using the computationally expensive cubic splines to represent a geological interface from a set of

discrete data, we shall approximate the interface by a set of piecewise continuous parabolae. The use of these second degree equations will allow us to compute analytical rather than numerical solutions for the intersection between a ray and an interface.

5.2 Circular approximation ray tracing without interfaces

Consider an elastic isotropic medium whose velocity field $v(x,z)$ is specified by velocities given on the nodal points of a rectangular grid. The spacing between grid points may vary over the whole grid. Let the coordinate system by which these grid points are given be termed the home coordinates. Place a point source of harmonic waves somewhere within this medium, say at (x_s, z_s). Let us define another set of coordinate axes parallel to the home coordinates and with origin at the source. This system of coordinates will be termed the translated coordinates.

The rectangle in which the source lies may be divided into two equal triangles with the source lying in either the upper or lower triangle. This decomposition of the model's blocks into triangles is the basic advantage of this ray tracer, for we may employ velocities at the three corner points of the triangle

$v_i(x_i,z_i)$, i=1,2,3 to compute a unique linear mapping

$$v(x,z) = Ax + Bz + C \qquad (5.1)$$

by solving three linear algebraic equations for the three unknown coefficients A,B,C. Numerical experimentation demonstrated that it is most beneficial to divide the rectangle by the diagonal joining the two points adjacent to the corner point of the rectangle nearest to the source point.

Figure 5.1 shows a typical geometry for this situation. If the local velocity field is given by equation 5.1, we do not really have a depth-dependent velocity as pledged. However, if the coordinate axes are rotated through an angle ϕ,

$$\phi = -\tan^{-1}(A/B), \quad -\pi/2 \le \phi \le \pi/2 \qquad (5.2)$$

then we can define a set of translated, rotated coordinates (x',z') such that

$$\begin{bmatrix} x' \\ z' \end{bmatrix} = \begin{bmatrix} \cos\phi & \sin\phi \\ -\sin\phi & \cos\phi \end{bmatrix} \begin{bmatrix} x \\ z \end{bmatrix} \qquad (5.3)$$

In Figure 5.1, note that ϕ is positive when measured in the clockwise direction. In the

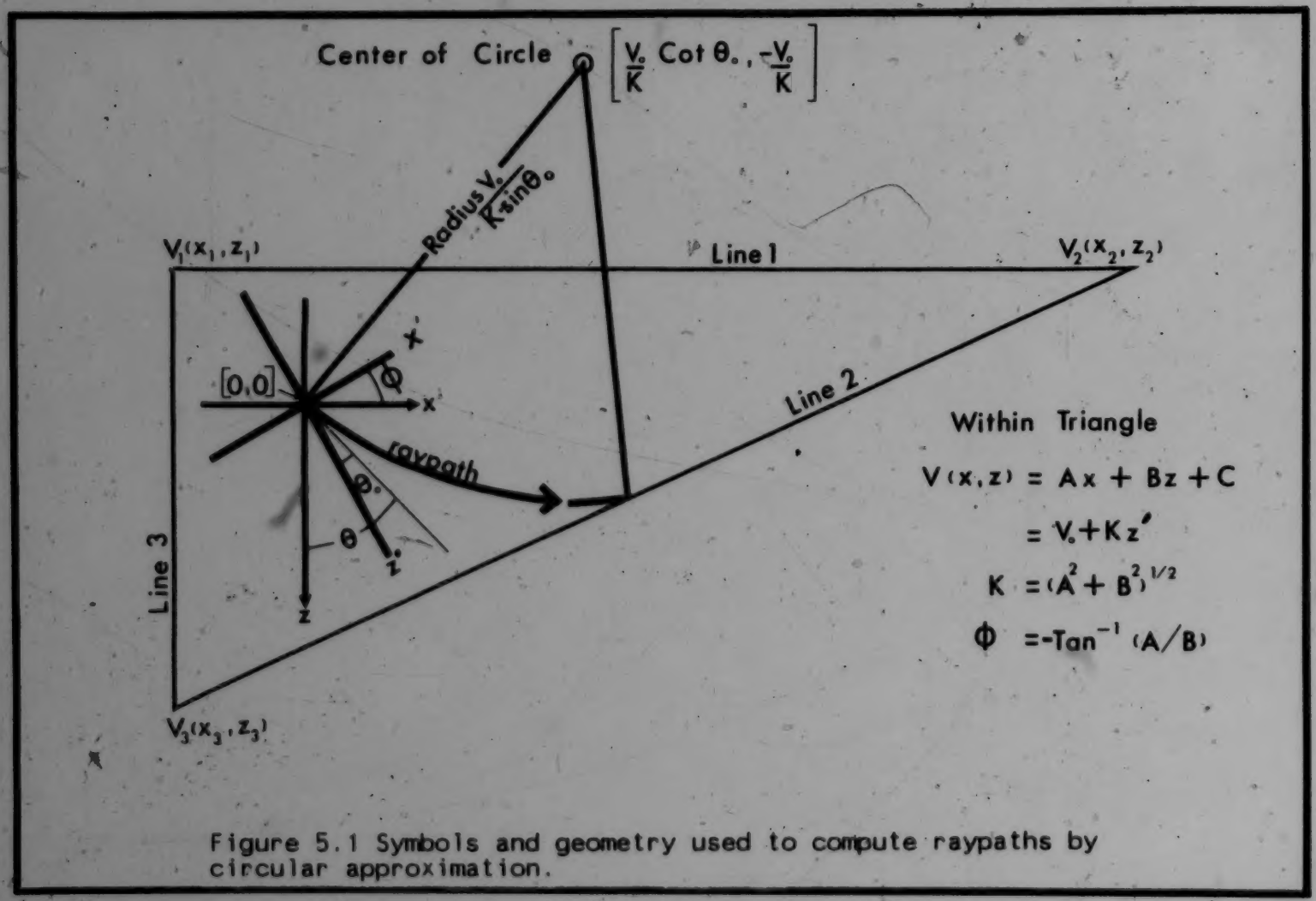

Figure 5.1 Symbols and geometry used to compute raypaths by circular approximation.

(x',z') coordinates the velocity field is given by

$$v(x',z') = v(0,0) + (A^2+B^2)^{\frac{1}{2}} z' \qquad (5.4)$$

Nettleton (1940) has derived analytic expressions for seismic ray paths for a medium whose velocity field is given by $v = v_0 + kz$. Essentially, these paths are circles in the (x',z') plane defined by

$$\left(x' - \frac{v_0 \cot\theta_0}{k}\right)^2 + \left(z + \frac{v_0}{k}\right)^2 = \left(\frac{v_0}{k \sin\theta_0}\right)^2 \qquad (5.5)$$

where θ_0 is the take off angle (measured from the vertical) of the ray, $0 \leq \theta_0 < 2\pi$. As well, the travel time T to reach any point (x',z') on the ray path is

$$T = \frac{1}{k} \cosh^{-1}\left[\frac{k^2(x'^2+z'^2)}{2vv_0} + 1\right] \qquad (5.6)$$

Of course, if $v_1 = v_2 = v_3$, the block is homogeneous and the rays degenerate to straight lines.

The ray can now be traced through the triangle up to its exit point. Determination of the exit point can be posed as the problem of finding the intersection between a circle (equation 5.5) and a straight line

$z' = Mx' + B$. These straight lines are the lines bounding the triangle in the translated rotated coordinates. We must find the point of intersection (x'_e, z'_e) and the corresponding time, t_e . Since there may be up to six intersection points, the criteria for determining the correct one are:

(1) those for which (x'_e, z'_e) lies within the specified endpoints of the lines $z = Mx' + B$

(2) that for which the time te , is minimal.

The ray may either have entered the second triangle of this block (by crossing line 2) or a completely new block (by crossing lines 1 or 3). If the former event results, the procedure is repeated starting with the calculation of coefficients A,B,C. If the latter presides, the operation is initiated beginning with division of the new block.

This technique of ray tracing requires considerably less CPU time than the exact differential equation method described in Chapter 4. The chief saviour is the use of analytic expressions. However, one difficulty must be highlighted. Since the velocity field is only specified locally, the ray will "see" the lines, separating the blocks as second order interfaces resulting in a discontinuous derivative of the ray angle upon crossing these lines. Numerically, the effect is minimal, as the next chapter will

bear out.

5.3 Determining the ray as a function of time

For purposes of producing ray diagrams it may be beneficial to know the location of the ray endpoint and the angle with respect to the rotated vertical as a function of time. The time, t, is measured from the moment the ray enters the triangle. To disclose these quantities one must solve equation 4.1 with a velocity $v = v_0 + kz$ and $x(0) = x_0$, $z(0) = z_0$, $\theta(0) = \theta_0$. The solutions to these equations are

$$x(t) = \frac{v_0}{k} \tan\frac{\theta_0}{2} (e^{2kt} - 1)(1+ae^{2kt})^{-1}$$

$$z(t) = \frac{v_0}{k} (e^{kt}(1+a)(1+ae^{2kt})^{-1} - 1)$$

$$\theta(t) = 2\tan^{-1}(e^{kt} \tan\frac{\theta_0}{2}) \qquad (5.7)$$

$$v(t) = v_0(1+a)e^{kt}(1+ae^{2kt})^{-1}$$

where

$$a = \tan^2\frac{\theta_0}{2}$$

5.4 The effect of an interface

The approximation of interfaces by piecewise continuous parabolae is discussed in Appendix C. If curvilinear interfaces are to be introduced into the model, record must be kept of which blocks are cut by these interfaces. If the

ray enters a block which contains an interface, specific steps must be taken. The first of these is to eliminate the velocity datum on any corner point of the block which lies on the other side of the interface from which the ray is incident. The datum must be replaced by extrapolation among the velocities at the points nearest the point in question. In practice, this can be performed by linear extrapolation utilizing the three nearest points.

The second modification required in blocks cut by an interface, is to determine the location and time of the ray's intersection with the interface (if any). If we have a parabola described as $z(x)=(ax+b)x+c$ and a circle given by $(x-A)(x-A)+(z-B)(z-B)=r*r$ then the (at most 4) points of intersection are the roots of the following fourth degree polynomial

$$a^2x^4 + 2abx^3 + (b^2+2a(c-B)+1)x^2$$

$$+2(b(c-B)-A)x + (A^2-r^2 + (c-B)^2) = 0$$

The equations for the circle, parabola and intersection points are to be taken in the unrotated, translated coordinates with the origin at the point where the ray enters the triangle containing the interface. The fourth degree polynomial can be solved numerically or sometimes even analytically. The requirements for an intersection point to be the true one are the same as for the

ray-triangle boundary case.

Using parabolae to approximate interfaces makes it simple to compute the interface normals at the point of incidence. Knowing these, as well as the incident angles at the time of intersection (equation 5.7), it is an elementary operation to reflect or refract rays according to Snell's Law.

The next chapter will discuss ways that this method, as well as the method of differential equations, can be utilized to calculate ray amplitude at the earth's surface.

6. GEOMETRICAL SPREADING OF WAVEFRONTS IN LATERALLY INHOMOGENEOUS MEDIA

6.1 Introduction

Computation of ray paths in laterally inhomogeneous media has been discussed in the preceeding chapters. Applicable methods for this task include solution of a system of differential equations and the method of circular approximation. The problem of determination of geometrical spreading, and hence amplitude, is solvable by techniques similar to those for ray paths. In this chapter equations will be given and numerical tests performed to obtain ray amplitudes and travel times.

6.2 Differential equation solution for ray amplitude

Differential equations have been derived by Cerveny et al (1974), among others, by which the cross sectional area of the ray tube may be expressed. A brief summary of these equations will be given here. For more in-depth discussion, the reader is referred to the original publication. Basically, the equations are an extension of the ray tracing equations discussed in Chapter 4.

We introduce ray coordinates

q_1, q_2, τ where q_1, q_2 specify the ray under consideration and τ the position of a point along the ray. Physically, q_1 may represent the declination of the ray at take-off and q_2 the azimuthal angle. Thus any point along the ray may be described by $\vec{x} = (x_i(q_1, q_2, \tau))$ $i=1,2,3$. The cross sectional area of an elementary ray tube, $d\sigma$ can be evaluated by

$$d\sigma = J \, dq_1 dq_2 \tag{6.1}$$

where

$$J = \left| \frac{\partial \vec{x}}{\partial q_1} \times \frac{\partial \vec{x}}{\partial q_2} \right| \tag{6.2}$$

and $\vec{x} = (x_1, x_2, x_3)$. In zeroth order ray theory, the amplitude, A, of a wave at time τ_1 is expressible as

$$A(\tau_1) = \left[\frac{v(\tau_0)}{v(\tau_1)} \frac{\rho(\tau_0)}{\rho(\tau_1)} \frac{J(\tau_0)}{J(\tau_1)} \right]^{\frac{1}{2}} A(\tau_0) \tag{6.3}$$

where v denotes velocity and ρ density. τ_0 is some reference time. It is convenient to take this time to correspond to the wave front on the unit sphere about the source. Within this sphere, the medium is assumed homogeneous. The components of the slowness vector

$(p_i(\tau))$ can be written in terms of the azimuth angle A and declination D

$$p_1 = \frac{\cos A \sin D}{v}, \quad p_2 = \frac{\sin A \sin D}{v}, \quad p_3 = \frac{\cos D}{v}$$

Let us introduce the following notation:

$$y_{\alpha i}(q_1,q_2,\tau) = \frac{\partial x_i(q_1,q_2,\tau)}{\partial q_\alpha} \tag{6.4}$$

$$z_{\alpha i}(q_1,q_2,\tau) = \frac{\partial p_i(q_1,q_2,\tau)}{\partial q_\alpha} \tag{6.5}$$

for $\alpha = 1,2$. Using the Laplace identity, namely

$$(\vec{a}\times\vec{b})\cdot(\vec{c}\times\vec{d}) = (\vec{a}\cdot\vec{c})(\vec{b}\cdot\vec{d}) - (\vec{b}\cdot\vec{c})(\vec{a}\cdot\vec{d})$$

we can rewrite 6.2 in a more useful form

$$J = (EF - G^2)^{\frac{1}{2}} \tag{6.6}$$

where

$$E = y_{1i}y_{1i}, \quad F = y_{2i}y_{2i}, \quad G = y_{1i}y_{2i}$$

and summation convention is assumed. Functions $y_{\alpha i}$ are obtained by means of partial differentiation of equation 4.1 with respect to q_α . These are

$$\frac{dy_{\alpha i}}{d\tau} = p_i y_{\alpha j}\, 2v \frac{\partial v}{\partial x_j} + v^2 z_{\alpha i}$$

$$\frac{dz_{\alpha i}}{d\tau} = \frac{y_{\alpha j}}{v^2}\left[\frac{\partial v}{\partial x_i}\frac{\partial v}{\partial x_j} - v\frac{\partial^2 v}{\partial x_i \partial x_j}\right] \tag{6.7}$$

Similar equations to these are available in Wesson (1970) or in Green (1976) for spherical geometry. The system must be solved simultaneously with the ray tracing equations, 4.1, to obtain both kinematic and dynamic properties of waves in inhomogeneous media. The numerical problems in solving this system are the same as those discussed in Chapter 4. The user can now expect a substantial increase in CPU time to solve the extra equations.

6.3 The effect of an interface

The differential equations 4.1 and 6.7 can be solved in a region where $v(x_i)$ is a smooth function of the coordinates, i.e. up to the point where the ray intersects with an interface of first order. We assume that this interface is given by an equation $f(x_i) = 0$, where f is to have continuous partial derivatives up to second order in some neighborhood of the intersection point. The components of the unit normal are

$$N_i = \varepsilon \frac{\partial f}{\partial x_i} \Big/ \left[\frac{\partial f}{\partial x_j} \frac{\partial f}{\partial x_j} \right]^{\frac{1}{2}}$$

where $\varepsilon = \pm 1$, chosen so that the normal vector points into the layer from which the ray is incident. At such interfaces the quantities

$p_i, Y_{\alpha i}, Z_{\alpha i}$ change discontinuously. Cerveny et al (1974) have presented equations for the change in $Y_{\alpha i}, Z_{\alpha i}$ while the change in p_i is obtainable through Snell's Law. Let quantities which are to be evaluated at the interface be written in upper case. Variables with a tilde represent the value on the reflected or refracted side of the interface while non-tilded variables are measured on the incident side. The reflected side coincides with the incident side of the interface, in that energy is carried away from the interface into the same medium from which it arrived. According to equations 38 and 39 of the above paper

$$\tilde{Y}_{\alpha i} = Y_{\alpha i} + (V^2 P_i - \tilde{V}^2 \tilde{P}_i) \frac{\partial T}{\partial q_2} \tag{6.8}$$

$$\tilde{Z}_{\alpha i} = Z_{\alpha i} - N_i (1 \pm AB^{-1}) \left[P_k \frac{\partial N_k}{\partial q_\alpha} + N_k Z_{\alpha k} \right.$$

$$\left. - \frac{N_k}{V} \frac{\partial V}{\partial x_k} \frac{\partial T}{\partial q_\alpha} \right] - \frac{1}{V\tilde{V}} \left[\frac{V \partial \tilde{V}}{\partial x_i} - \frac{\tilde{V} \partial V}{\partial x_i} \right]$$

$$- (A \pm B) \frac{\partial N_i}{\partial q_\alpha} \pm \frac{N_i}{B} \left[\tilde{V}^{-3} \frac{\partial \tilde{V}}{\partial q_\alpha} - V^{-3} \frac{\partial V}{\partial q_\alpha} \right] \tag{6.9}$$

where

$$\frac{\partial T}{\partial q_\alpha} = -N_j Y_{\alpha j} / V^2 N_k P_k$$

$$0 \leq A = P_i N_i$$

$$B = (\tilde{V}^{-2} - V^{-2} + A^2)^{\frac{1}{2}} > 0$$

The upper sign is used for a refracted wave and the lower for a reflected one. The derivative of an arbitrary function $G(x_i)$ with respect to q_α along the interface is

$$\frac{\partial G}{\partial q_\alpha} = \frac{\partial G}{\partial x_i} \left[Y_{\alpha i} + V^2 P_i \frac{\partial T}{\partial q_\alpha} \right]$$

To determine the amplitude at a time τ_{1+K} along a ray that has encountered K interfaces we employ the following equation from asymptotic ray theory

$$A(\tau_{1+k}) = A(\tau_0) \left[\frac{v(\tau_0)}{v(\tau_{1+K})} \frac{\rho(\tau_0)}{\rho(\tau_{1+K})} \frac{J(\tau_0)}{J(\tau_{1+K})} \right]^{\frac{1}{2}} \cdot \prod_{j=1}^{k} \left[\frac{\tilde{v}(\tau_j)}{v(\tau_j)} \frac{\tilde{\rho}(\tau_j)}{\rho(\tau_j)} \frac{\tilde{J}(\tau_j)}{J(\tau_j)} \right]^{\frac{1}{2}} R_j \qquad (6.10)$$

where R_j are the corresponding plane wave reflection, refraction or surface conversion coefficients (see Cerveny and Ravindra 1971) and τ_j are the times of intersection with the interfaces. It should be noted that $\tilde{J}(\tau_j)/J(\tau_j) = \cos \tilde{i}/\cos i$ where i ($\tilde{i}$) is the angle of incidence (reflection or refraction) Cerveny et al (1977).

Thus, the computation of rays and ray amplitude in laterally inhomogeneous media can be performed by the

following procedure:

(1) Integrate equations 6.7 and 4.1 up to the point of intersection with an interface. In this fashion we obtain $\tilde{P}_i, \tilde{Y}_{\alpha i}, \tilde{Z}_{\alpha i}$

(2) From the relations 6.8-6.9 obtain values for $\tilde{Y}_{\alpha i}, \tilde{Z}_{\alpha i}$. $\tilde{P}_i$ is obtained from Snell's Law.

(3) At the interface compute the product term required in equation 6.10.

(4) Use the values of $P_i, Y_{\alpha i}, Z_{\alpha i}$ as new initial values and begin solving equations 6.7 and 4.1 subject to the new initial values.

(5) Steps (1)-(4) are repeated until either another interface is reached, the ray is terminated at a receiver or the ray is traced out of bounds.

Numerical examples of this method will be discussed further in this chapter.

6.4 Ray amplitude by dynamic ray tracing

In a recent work, Cerveny and Hron (1979) studied the problem of computation of ray amplitude in a generally inhomogeneous medium with curvilinear interfaces. They introduced the process of "dynamic ray tracing", which employs second derivatives of the seismic time field with respect to the ray coordinates. For a laterally

inhomogeneous two-dimensional medium, the dynamic ray tracing system reduces to two non-linear differential equations. The phase matching method is used to determine discontinuities of individual quantities in the system when the wave impinges a curved boundary separating two generally inhomogeneous media. The final equations only and some numerical examples will be presented in this chapter of the thesis.

In a two-dimensional model, in which elastic and geometrical characteristics do not change in one fixed direction, the propagation of seismic waves can be investigated in the plane perpendicular to this fixed direction. Under these circumstances, the dynamic ray tracing system of Cerveny and Hron (1979) reduces to

$$\frac{dM}{d\tau} = v^2 - \frac{M^2}{v} V11$$

$$\frac{dN}{d\tau} = v^2 \qquad (6.11)$$

subject to $M(0) = N(0) = 0$. Equation 6.11 corresponds to equation 93 of the above reference. The variable M represents the product of the wavefront's radius of curvature (in the plane of propagation) multiplied by the velocity of propagation at that time,

τ . The variable N is similar but for the radius of curvature perpendicular to the plane of propagation. V11 represents the second derivative of velocity in the direction tangent to the wavefront.

Unfortunately, the spreading function, J, employed in equation 6.10 for ray amplitude is not readily available from M and N. It is given by

$$J(\tau) = J(\tau_0) \exp\left(\int_{\tau_0}^{\tau} v^2 \left(\frac{1}{M} + \frac{1}{N} \right) d\xi \right) \qquad (6.12)$$

If the first ray segment emanating from the source is under consideration, then $\tau_0 = v_0^{-1}$, corresponding to a homogeneous unit sphere surrounding the source. v_0 is the velocity at the source and $J(\tau_0) = \sin\theta_0$ where θ_0 is the ray take off angle as measured from the vertical at the source. Otherwise, τ_0 is the time at the beginning of the current ray segment.

When the ray impinges a curved interface between two different media, the quantities M and N in equation 6.11 will become discontinuous. The initial values of M and N on the reflected or refracted side of the interface, denoted by a tilde, must be computed in order to begin solving equation 6.11 again. According to the theory of dynamic ray tracing,

$$\tilde{M} = \left(\frac{\cos i}{\cos \tilde{i}} \right)^2 \left(\frac{1}{M} + K + I \right)^{-1}$$

$$\tilde{N} = N \qquad (6.13)$$

where $$K = \frac{uC}{(\cos \tilde{i})^2}$$

$$I = \left(\frac{\sin i}{v \cos \tilde{i}}\right)^2 \frac{\partial \tilde{v}}{\partial x} \sin \tilde{i} + \frac{\partial \tilde{v}}{\partial z} \cos \tilde{i}$$

$$- \frac{\partial v}{\partial x} \sin i - \frac{\partial v}{\partial z} \cos i$$

$$u = \frac{\cos i}{v} \pm \frac{\cos \tilde{i}}{\tilde{v}}$$

$i(\tilde{i})$ is the positive acute angle that the incident (reflected or refracted) ray makes with the interface normal. $v(\tilde{v})$ is the velocity of the incident (reflected or refracted) wave at the incident. In u, the upper (lower) sign is taken for reflected (refracted) waves. C is the curvature of the curved boundary, which is taken as positive (negative) for those parts of the boundary which are seen as convex (concave) by an observer located in the medium from which the ray is incident.

K is termed the curvature term, describing the effect of interface geometry upon ray amplitudes. On the other hand, I, depending on variations of the elastic parameters near the interface, is termed the inhomogeneity term. This is a key advantage of dynamic ray tracing, in that it allows one to study separately the effect of inhomogeneity and

interface geometry upon ray amplitude. Numerical examples of this will be presented later in this chapter.

6.5 Ray amplitude by circular approximation

The amplitude of a wave propagating in an arbitrarily inhomogeneous, isotropic medium is given by (Cerveny and Ravindra 1971, equation 2.107)

$$A(M) = \frac{\tilde{g}(q_1,q_2)}{L}\left[\frac{v_0\rho_0}{v(M)\rho(M)}\right]^{\frac{1}{2}} \prod_{j=1}^{K}\left[\frac{\tilde{v}(O_j)\tilde{\rho}(O_j)}{v(O_j)\rho(O_j)}\right]^{\frac{1}{2}} R_j \qquad (6.14)$$

where

$\tilde{g}$ ... directivity function of the source (taken as unity for this study),

O_j ... point of incidence of the ray upon the j-th interface that it encounters,

$v_0\rho_0$ ... wave velocity and density at source,

M ... receiver location,

M_0 ... some reference location,

$\theta(O_j)$ ... angle of incidence upon the j-th interface,

$$L = \left[\frac{d\sigma(M)}{d\sigma(M_0)}\right]^{\frac{1}{2}} \prod_{j=1}^{K}\left[\frac{d\sigma(O_j)}{d\tilde{\sigma}(O_j)}\right]^{\frac{1}{2}}$$

The product in the geometrical spreading function, L, can be

evaluated as the ratios of cosines of angles of incidence and reflection (or refraction) as in Cerveny et al (1974). This term represents a compensation for the discontinuity of geometrical spreading across the interfaces. The tilded quantities are to be evaluated on the reflected or refracted side of the interface. All quantities in equation 6.14 are easily computable except $d\sigma(M)$. We shall develop an algorithm to compute $d\sigma(M)$ for laterally inhomogeneous media with curvilinear interfaces by means of the circular approximation discussed in Chapter 5.

From the geometry of Figure 6.1

$$d\sigma(M) = \cos\theta(M) \frac{\partial y}{\partial \phi_0} \, dr \, d\phi_0$$

$$= \frac{\partial r}{\partial \theta_0} \cos\theta(M) \frac{\partial y}{\partial \phi_0} \, d\theta_0 \, d\phi_0$$

where r is the magnitude of the vector pointing from source M_o to receiver M. Within the unit sphere surrounding the source we assume the model to be homogeneous allowing us to express $d\sigma(M_0) = \sin\theta_0 \, d\theta_0 \, d\phi_0$. Thus

$$\frac{d\sigma(M)}{d\sigma(M_0)} = \frac{\partial r}{\partial \theta_0} \frac{\cos\theta(M)}{\sin\theta_0} \frac{\partial y}{\partial \phi_0} \qquad (6.15)$$

Numerically,

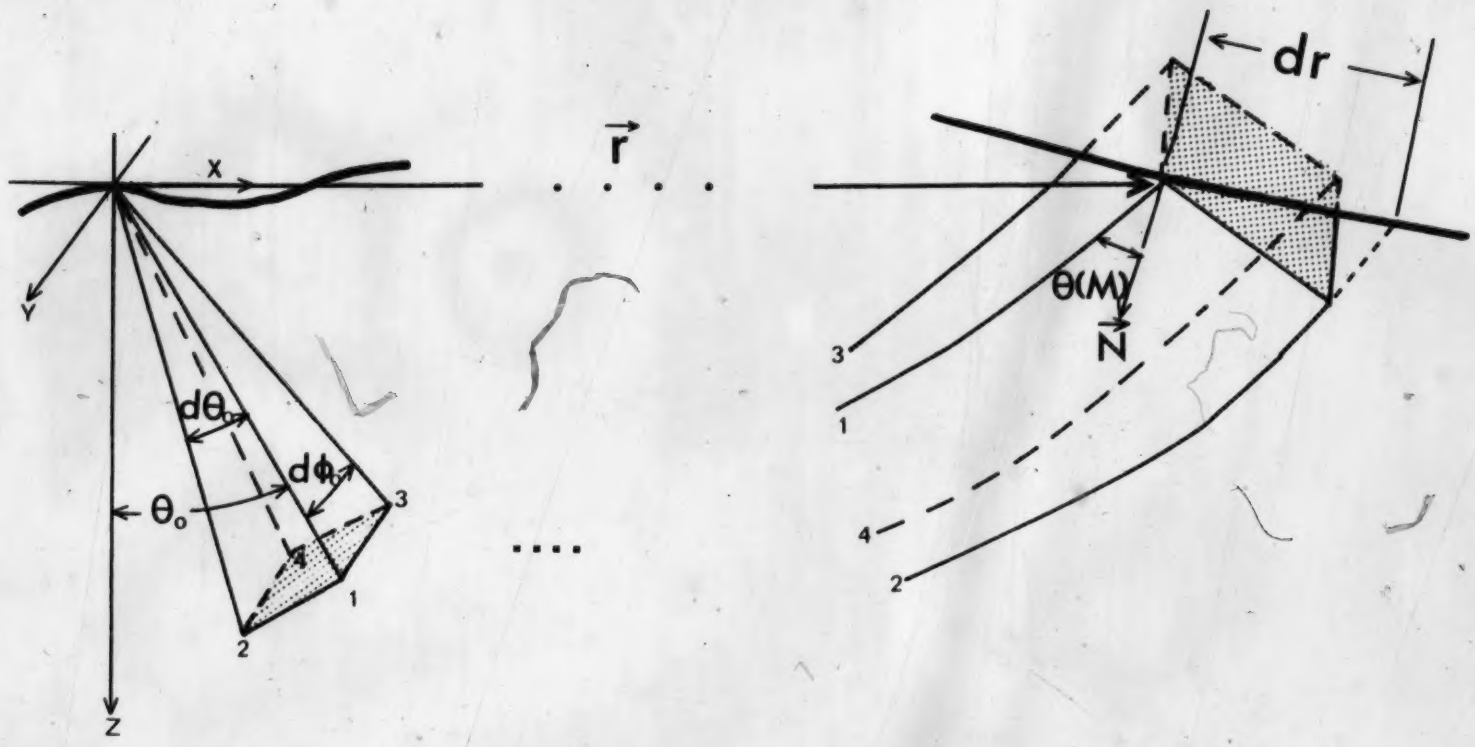

SOURCE (M_o)

RECEIVER (M)

$\vec{N}$ = unit vector normal to Earth's surface at M

Figure 6.1 Geometry of the ray tube at source and receiver The heavy lines represent the earth's surface. The angle θ_0 is confined to the X-Z plane, while $\phi_{0'}$ is confined to the Y-Z plane.

$\partial r/\partial\theta_0$ may be determined at point M by the following procedure:

(1) Shoot three rays on either side of the ray arriving at the receiver. This may be done by subtracting or adding small amounts $\Delta\theta_0$ ($\Delta\theta_0 \sim 10^{-4}$ radians) from the take-off angle. The change in θ_0 should yield a change in epicentral distance.

(2) Fit a cubic spline through the seven (θ_0, r) data.

(3) Evaluate the derivative $\partial r/\partial\theta_0$ at the take-off angle which causes the ray to arrive at the receiver M.

According to Cerveny et al (1974), $g = \partial y/\partial\phi_0$ is defined by the following differential equation for the two-dimensional medium which is under consideration in this study:

$$\frac{dg}{dt} = \frac{\sin\theta_0}{v_0} v^2(t)$$

Furthermore, g is invariant at any (zero strike) interface. Integrating this and summing over all N triangles that the ray passes through we have

$$g = \frac{\sin\theta_0}{v_0} \sum_{i=1}^{N} v_{0i}^2 (1+a_i)^2 \int_{t_{i-1}}^{t_i} e^{2k_i(t-t_{i-1})} \left(1+a_i e^{2k_i(t-t_{i-1})}\right)^{-2} dt$$

where

v_{0i} ... velocity at entry point of i-th triangle,

$a_i = \tan^2 \frac{\theta_{0i}}{2}$

θ_{0i} ... angle of incidence (in rotated coordinates) upon entry of i-th triangle,

k_i ... velocity gradient in i-th triangle,

t_{i-1}, t_i ... total ray travel time upon entry (exit) to (from) i-th triangle.

Note that $t_0 = 0$ and t_N = total travel time for the ray. Upon performing the integration and inserting the result in equation 6.15 we have

$$\frac{d\sigma(M)}{d\sigma(M_0)} = \frac{\partial r}{\partial \theta_0} \frac{\cos\theta(M)}{v_0} \sum_{i=1}^{N} \frac{v_{0i}^2(1+a_i)}{2k_i} \cdot \left(e^{2k_i(t_i-t_{i-1})} - 1 \right) \left(1+a_i e^{2k_i(t_i-t_{i-1})} - 1 \right) \tag{6.16}$$

If, in any of the triangles, $k_i = 0$ the term to be added must be $v_{0i}^2(t_i-t_{i-1})$. The computation of ray amplitudes in two dimensionally inhomogeneous media with curvilinear interfaces is now given by equations 6.14 and 6.16.

6.6 Numerical tests

FORTRAN programs have been written to compute kinematic and dynamic characteristics of waves in two-dimensional inhomogeneous media by solving differential equations and by the circular approximation. In this section, numerical comparisons will be presented between these methods. In all these models, the shear wave velocity amd volume density are given by

$$V_S(x,z) = V_P(x,z)/3^{\frac{1}{2}}, \quad \rho(x,z) = 3^{\frac{1}{2}} V_P^{\frac{1}{4}}(x,z)$$

from Gardner et al (1974).

As a first model we present a two-layered laterally inhomogeneous medium with curved interfaces. Since this is a mathematically contrived model, the P wave velocity-position function, V(x,y), and the interfaces are given analytically. Figure 6.2 is a description of the model showing P1P2P2P1 ray paths and amplitude distance characteristics. These amplitudes were computed by three different means, namely, the differential equations of Cerveny et al (1974), the dynamic ray tracing (D.R.T.) system of Cerveny and Hron (1979) and the circular approximation discussed in this chapter. Results are given as a per cent of curve 1. The differential equations technique and dynamic ray tracing both required about two minutes of CPU time, while the circular approximation only consumed about 20 seconds. With

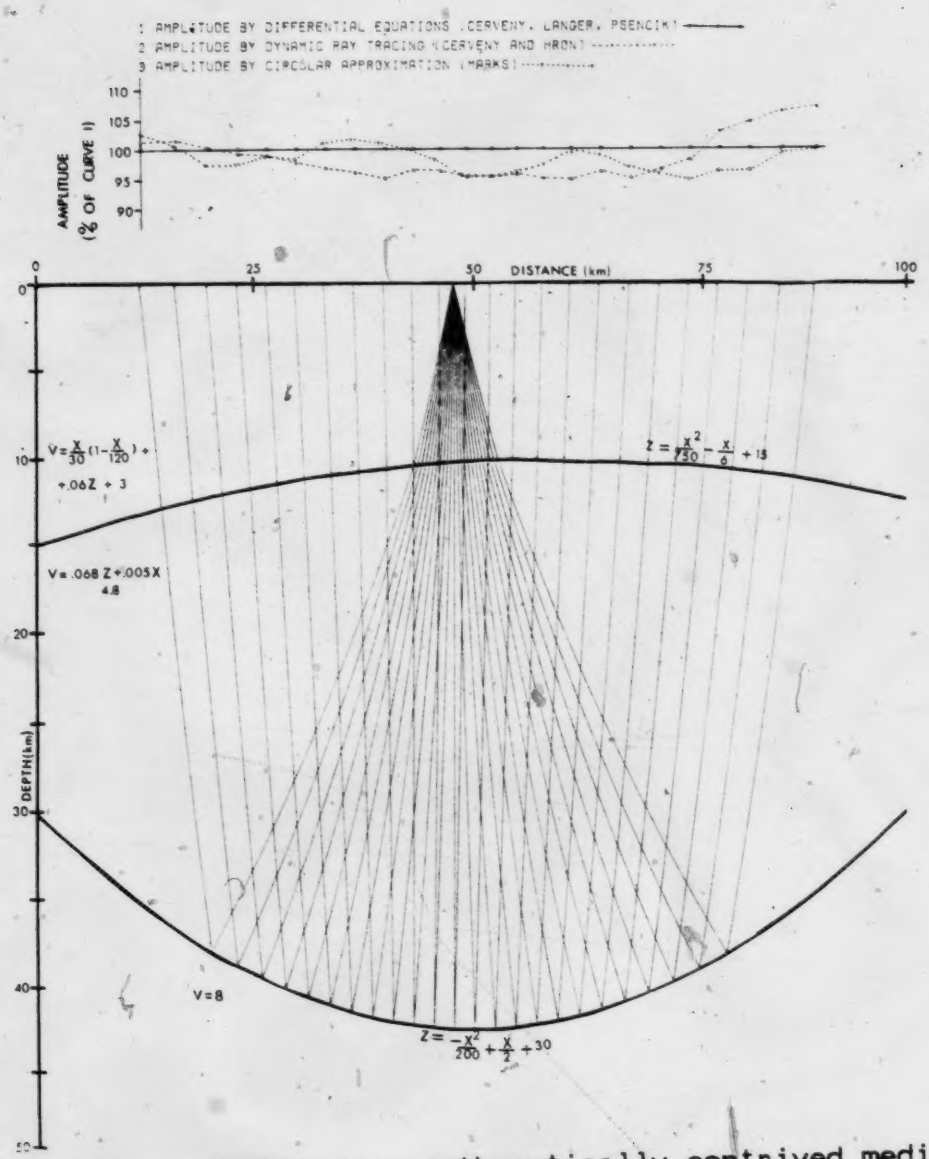

Figure 6.2 P1P2P2P1 in a mathematically contrived medium. The amplitudes are given as a per cent of curve 1.

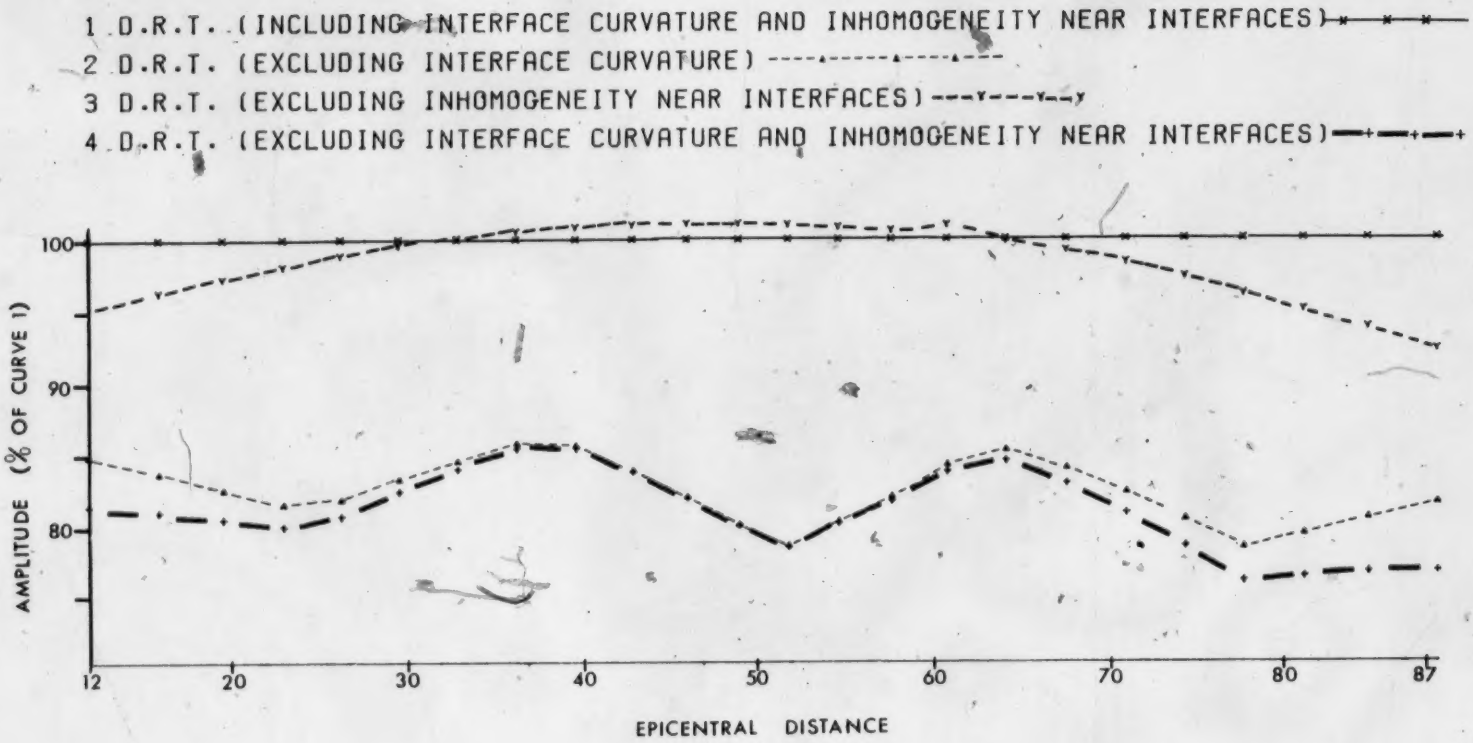

Figure 6.3 The effect of the curvature and inhomogeneity terms in the dynamic ray tracing (D.R.T.) system for the rays and model presented in the previous figure.

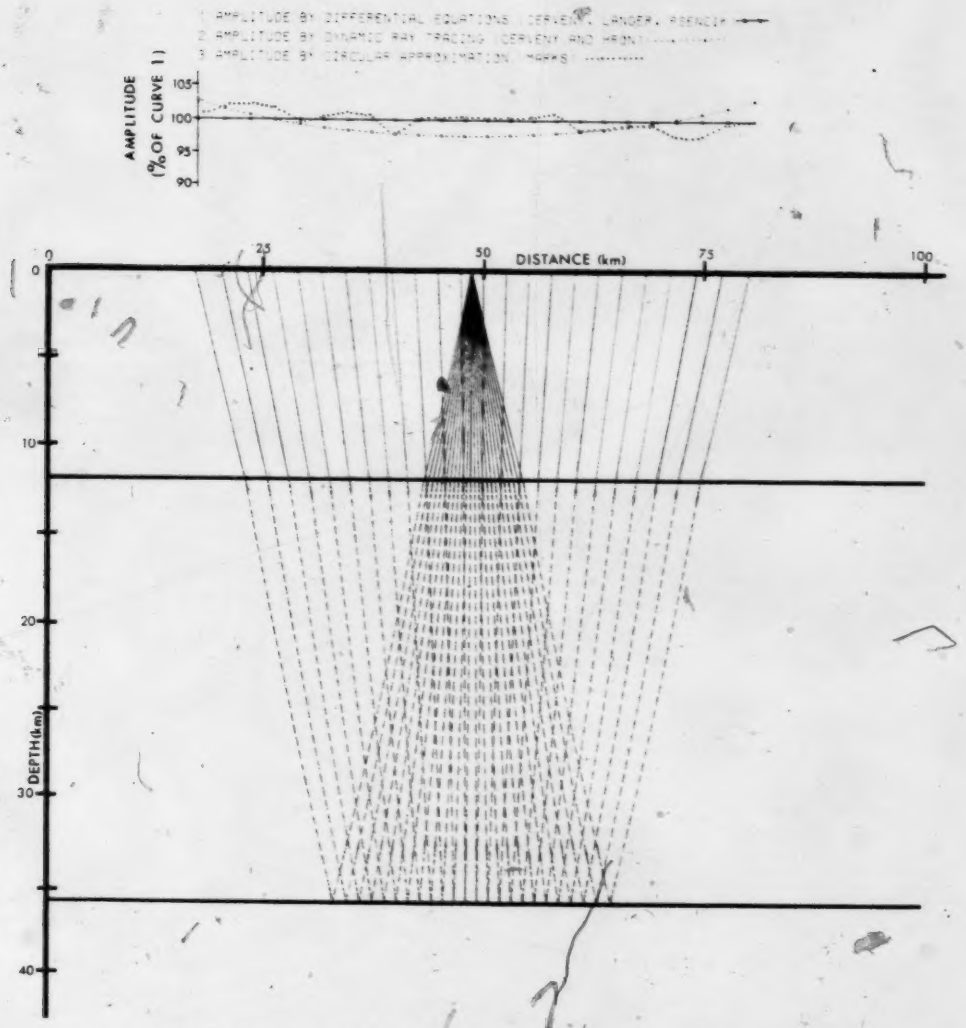

Figure 6.4 Rays P1S2S2P1 propagating in a plane layered medium. The seismic wave velocities are given by the mathematical equations presented in Figure 6.16.

BOHEMIAN MASSIF

V_p Isovelocity Contours (Km/Sec)

Seismic Profile VI , Czechoslovakia

$V_s = V_p / 3^{1/2}$ $\rho = 1.73\, V_p^{1/4}$

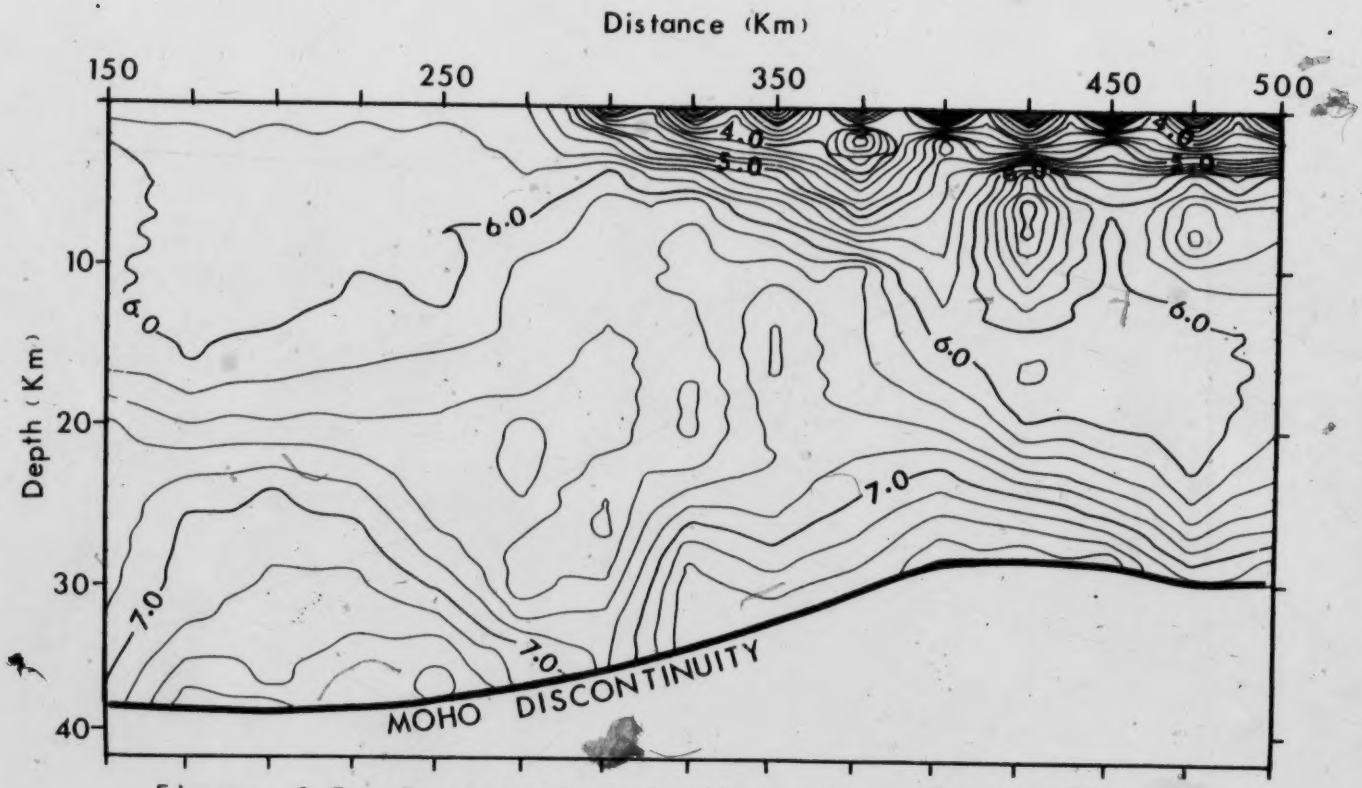

Figure 6.5 P wave isovelocity contours for the Bohemian Massif.

this saving in computational time, the few per cent discrepancy is quite acceptable.

Dynamic ray tracing allows one to study the effect upon amplitude of interface curvature and velocity inhomogeneity near the interfaces. This is achieved by setting either K=0 or I=0 in equation 6.13. Figure 6.3 displays the result of this experimentation for the model shown in Figure 6.2. Setting K=0 is equivalent to considering a plane interface at the point of incidence. This leads to a 15-22% change in amplitude. Setting I=0 is equivalent to considering a homogeneous medium surrounding the interface at the point of incidence. This yields only a 5% change in amplitude. Clearly, for the model shown, interface curvature plays a key role in determining seismic ray amplitude. To examine this phenomenon more closely, the two curved interfaces can be replaced by flat interfaces at depths of 12 and 36 km as in Figure 6.4. To demonstrate the programs' capability to handle converted phases, results are displayed for the ray P1S2S2P1. With the removal of curved interfaces, the discrepancy between the results computed by three different methods decreases.

The Bohemian Massif is a laterally inhomogeneous medium taken from a seismic survey of profile VI in Czechoslovakia (Psencik 1972). Figure 6.5 exhibits the P wave isovelocity contours for this model. The lateral inhomogeneity of the

V(X , Z)

PROFILE VI

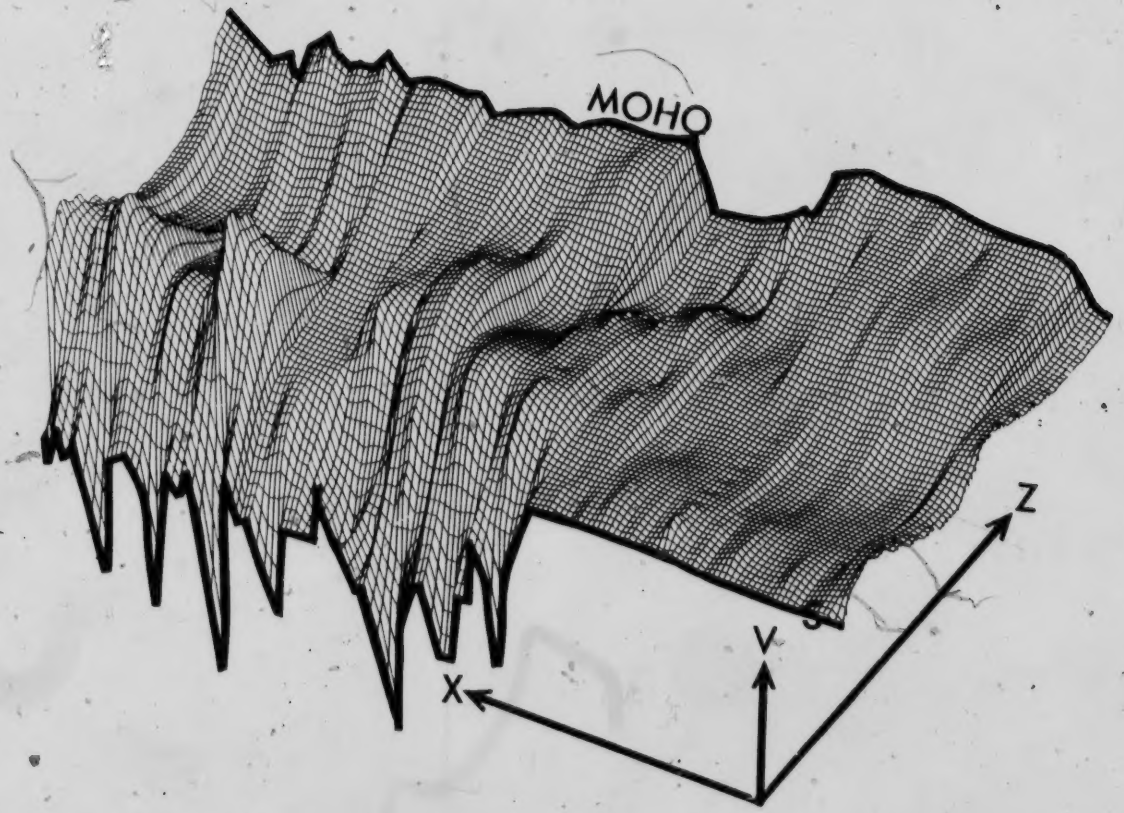

Figure 6.6 Transect plot of P wave velocity for the Bohemian Massif.

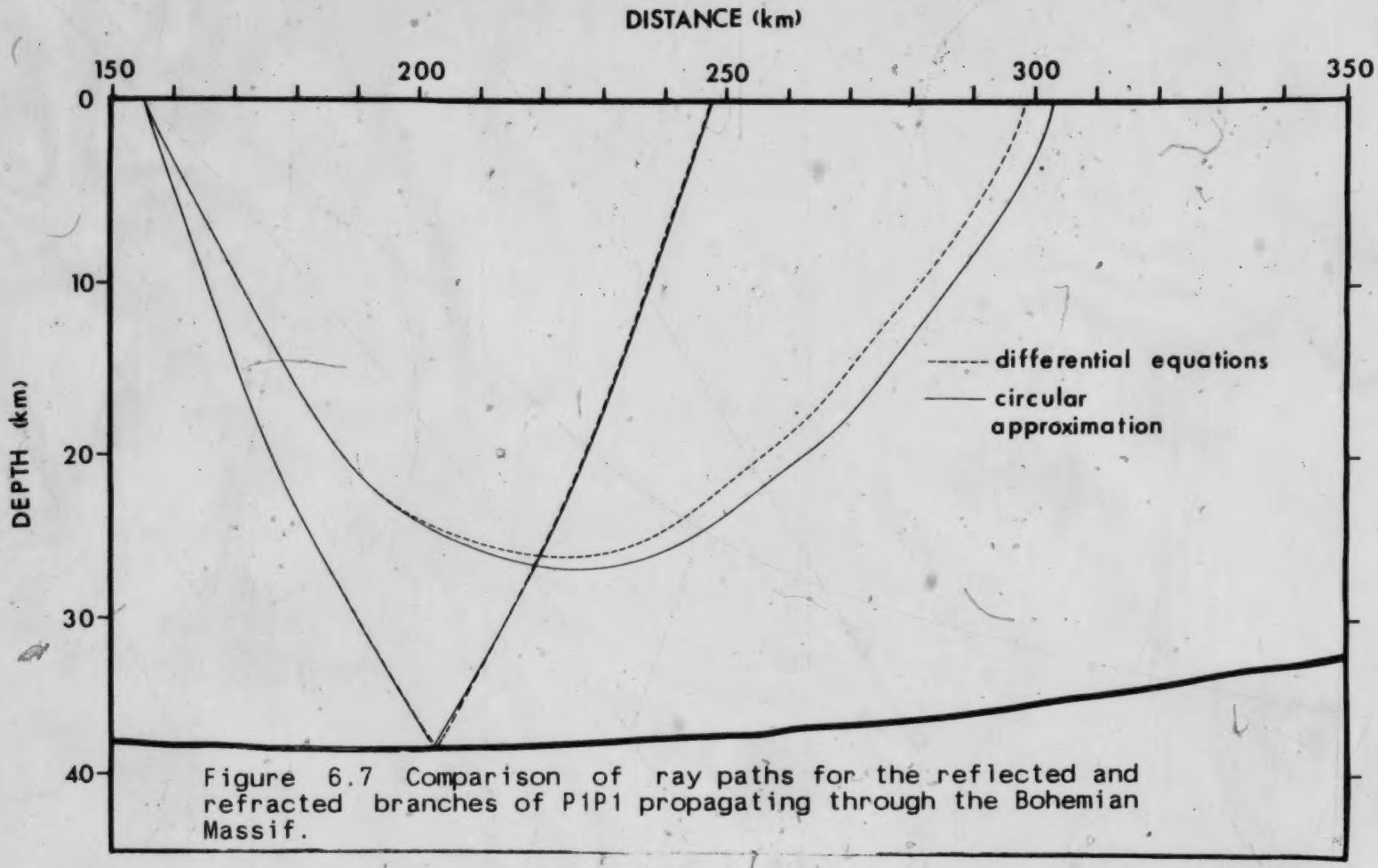

Figure 6.7 Comparison of ray paths for the reflected and refracted branches of P1P1 propagating through the Bohemian Massif.

model is well illustated in the transect plot of the velocity field shown in Figure 6.6.

Figure 6.7 illustrates a comparison between ray paths computed for identical take off angles at the source (155.2 km). The dashed ray segments were calculated by the differential equation approach, while the solid ones were computed by the circular approximation. Table 6.1 is a detailed account of the results of this test. Note that an additional 11 seconds of computer time were required to evaluate the bicubic spline coefficients for the velocity field. This was performed on a prior computation.

Figure 6.8 shows a comparison between the travel times for the ray P1P1. In Figure 6.9 we have compared the logarithm of the vertical amplitude (excluding reflection coefficient). Here we see some discrepancy due to the different methods of computing geometrical spreading, L. However, since the deviation is roughly of the same magnitude as errors in determining the velocity from inversion of seismic data, the technique of circular approximation appears to be a viable instrument.

TABLE 6.1

Comparison of P Rays Computed by Two Methods

Source at 155.2 km

Ray (method of computation)	Take Off Angle (deg)	Arrival Time (sec)	Angle with Vertical (deg)	Emergent Distance (km)	CPU Time (sec)
Refracted (differential equations)	50	24.419	32.731	298.546	1.000
Refracted (circular approx.)	50	25.120	29.643	303.074	.044
Reflected (differential equations)	40	18.301	40.339	247.454	1.000
Reflected (circular approx.)	40	18.355	40.148	247.680	.045

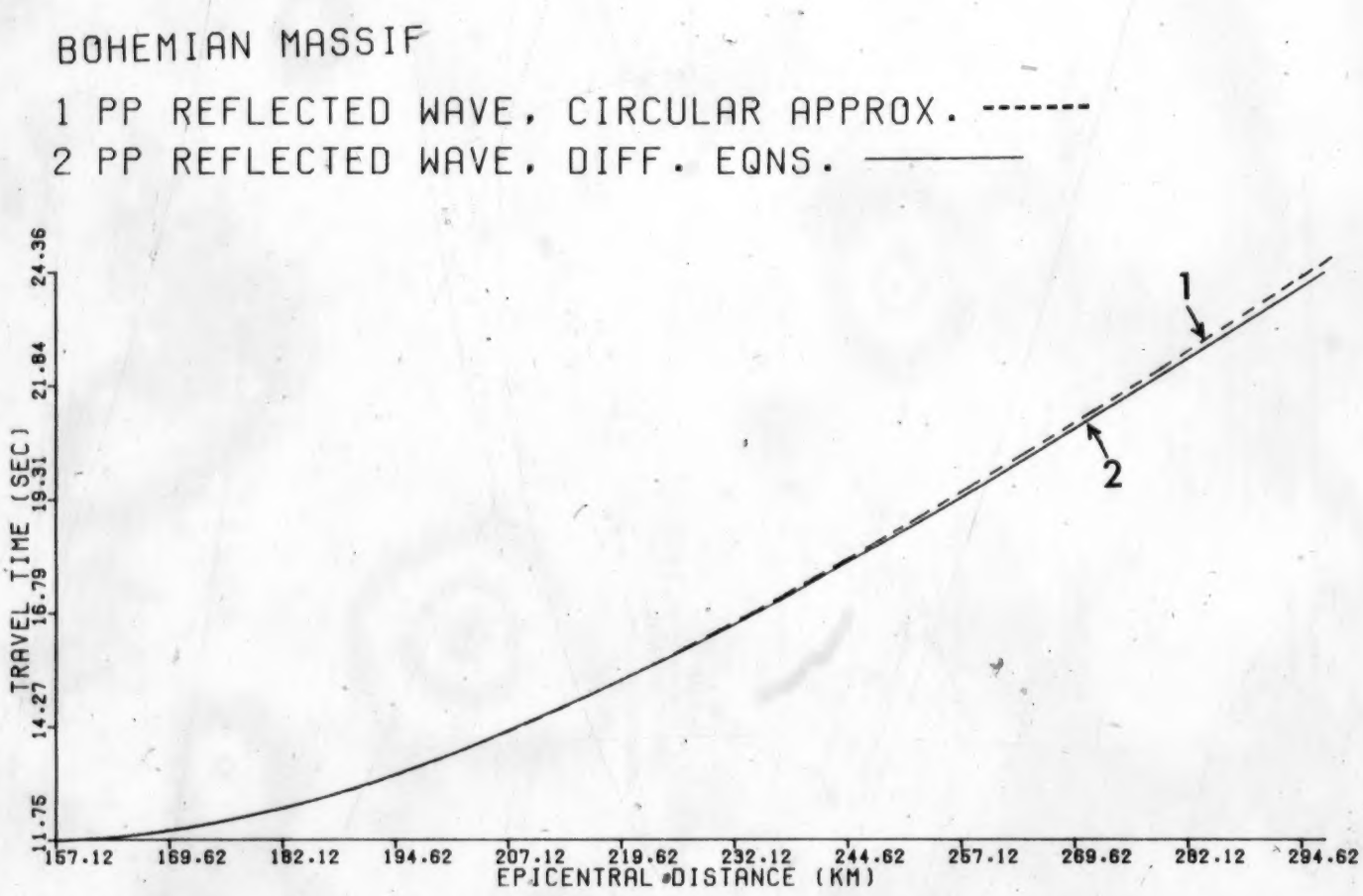

Figure 6.8 Comparison of travel times for the reflected branch of P1P1 through the Bohemian Massif.

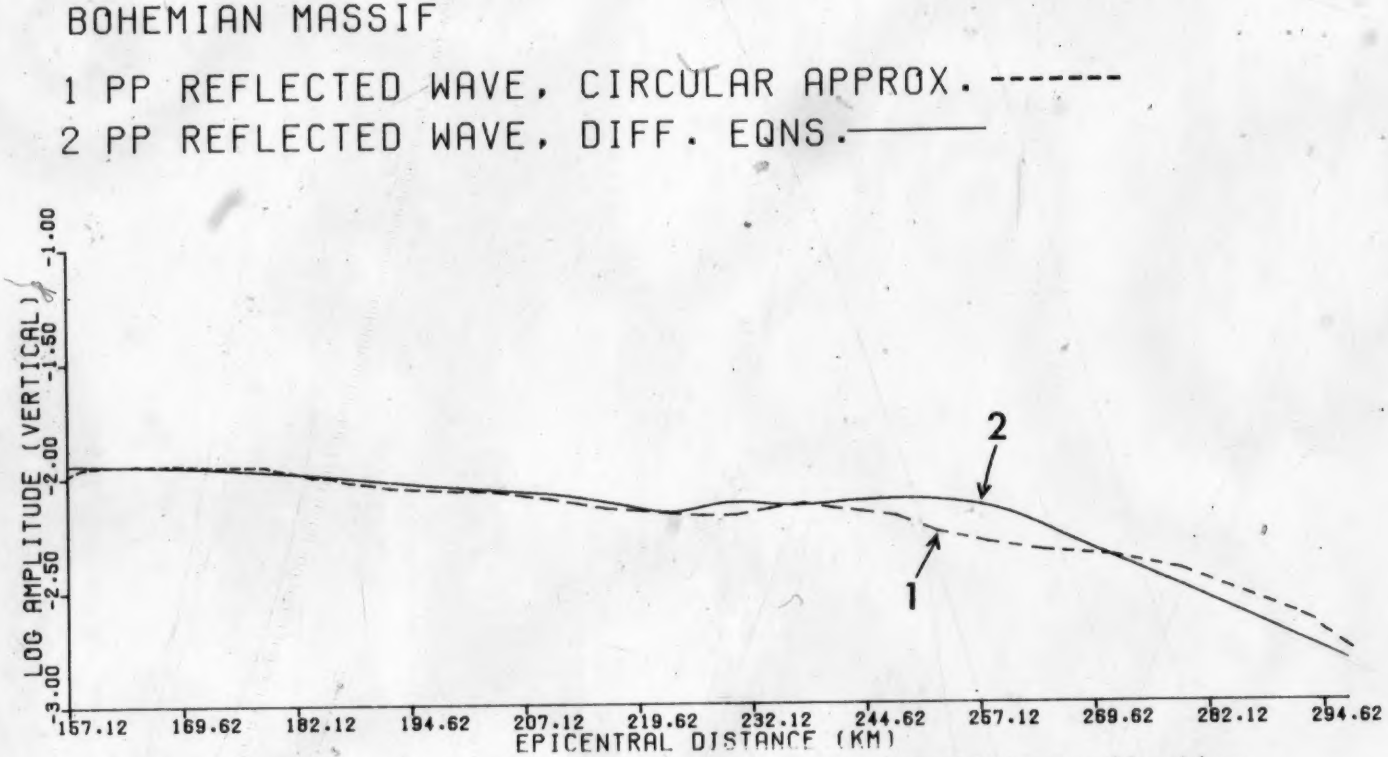

Figure 6.9 Comparison of amplitudes (excluding reflection coefficient) for the ray P1P1 as computed by the methods of differential equations and circular approximation.

7. NUMERICAL MODELLING OF SEISMIC BODY WAVES IN LATERALLY INHOMOGENEOUS MEDIA

7.1 Introduction

Methods of tracing seismic rays and computing geometrical spreading of wave fronts in two-dimensional laterally inhomogeneous media have been discussed in previous chapters. In this chapter, a general procedure linking all these processes together to produce synthetic seismograms will be presented. At the hub of this package of computer programs is the rapid, yet accurate circular approximation method of seismic ray tracing.

7.2 The relationship between take off angle, epicentral distance, travel time and amplitude in a complex medium

It is well known that in a complex geological medium, the travel time curve of any phase may be of a very complicated nature. Inhomogeneities or curved interfaces lead to discontinuities or cusps in the travel time branches. Triplication or even higher order multiplicity of travel time is possible. If one hopes to compute ray theoretical seismograms then a necessary requirement is to determine the ray parameter and arrival time at the receiver of all phases of any ray. One may then iterate this process with as many rays as necessary to provide a reasonable

approximation to the total wave field.

Special care must be taken to locate the exact position of cusps and discontinuities of individual travel time branches related to the same ray. Since we are dealing with flat Earth models of finite horizontal extent, it is necessary to specify left and right boundaries of our model. Thus, rays will be traced out of the bounds of the model for some take off angles at the source. Let us introduce T1 and T2 as two take off angles which cause the rays associated with them to be traced out of the bounds of the model. Furthermore, assume that all take off angles between T1 and T2 are associated with rays which emerge at the Earth's surface within the bounds of the model. Then the travel time-distance relationship formed for angles between T1 and T2 is defined as a branch of the total travel time curve for this ray. A branch may consist of several branch parts in which epicentral distance is a monotonic function of take off angle at the source. Physically, the point of intersection between two adjacent branch parts may correspond to either a caustic or a grazing ray. An intelligent ray tracing technique should be able to distinguish which is correct. As a simple schematic of this situation consider Figure 7.1. The portion of the curves from A to B corresponds to reflection from an interface, while segments B to F are related to the refracted phases of the same ray. For some epicentral distances up to four

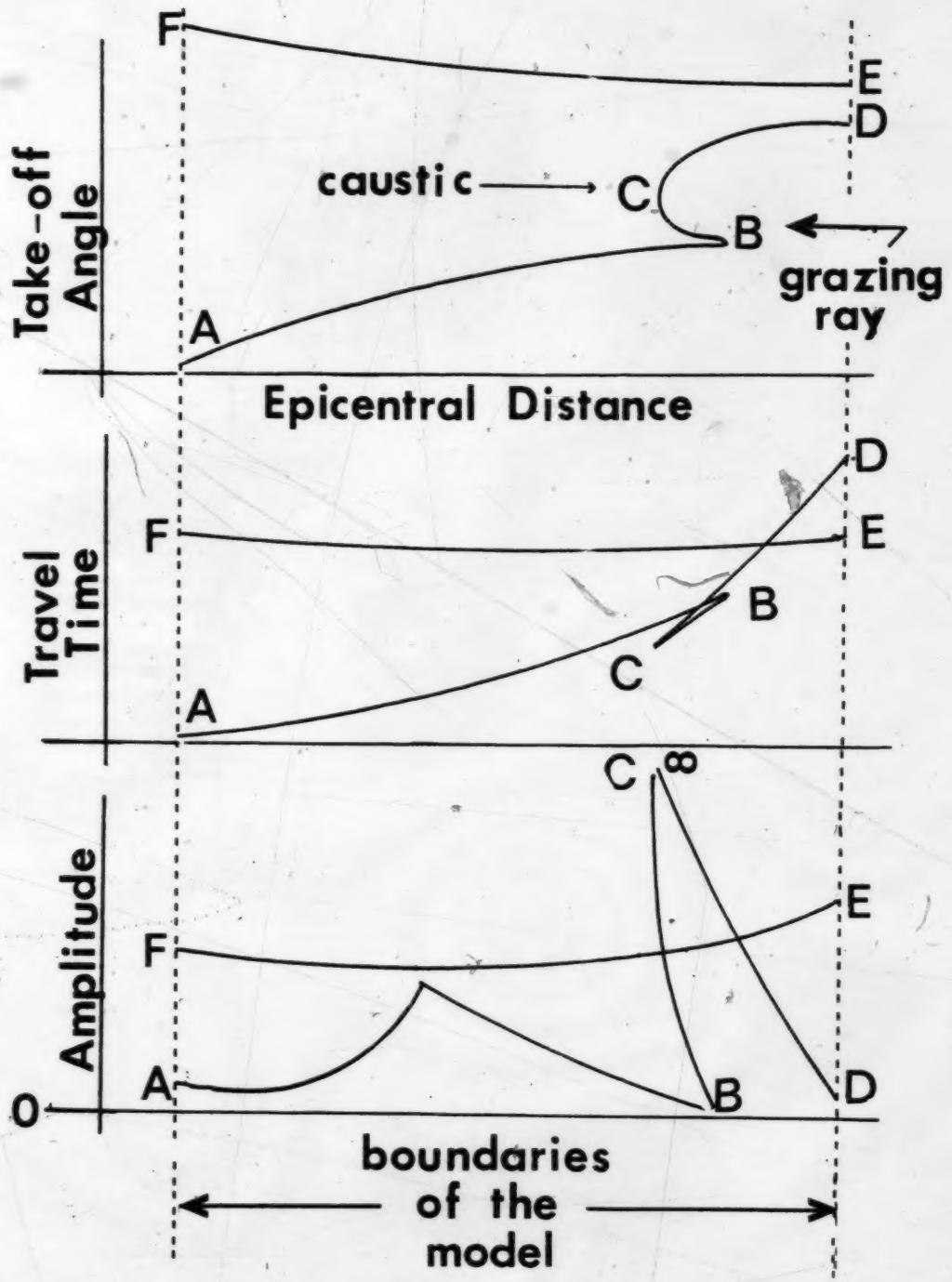

Figure 7.1 Take off angle, epicentral distance, travel time and amplitude in a complex medium.

arrivals will contribute to a synthetic seismograms. For a complex geological model, the number of individual travel time branches as well as the number of monotonic parts contained within each branch may rise to rather large values. In order to divide the individual branches into their component parts, a sophisticated algorithm must be employed. To make this procedure as inexpensive as possible, two criteria must be met. First, the number of samplings of the take off angle-distance curve must be minimized and second, the tracing of each single ray, which yields one datum on the curve, must be as fast as possible. The latter problem can be solved by using circular approximation ray tracing. The former has also been dealt with successfully by Hron (personal communication) and will not be discussed in this thesis. One important feature of Hron's process of determining travel time branch parts should be mentioned. When using the linear method of approximating velocity required by circular approximation ray tracing, we are in essence introducing false interfaces of the second order. Cerveny and Pretlova (1977) have examined this problem in detail and have drawn the conclusion that some degree of smoothing is necessary to ensure meaningful amplitude distance curves. Hron has implemented a smoothing operation into his program for computing travel time branches (personal communication).

One further remark should be mentioned regarding Figure

7.1. The infinite amplitude predicted by asymptotic ray theory at the caustic C is due to the shrinking of the ray tube. It is well known that asymptotic ray theory is not valid in the vicinity of points where the phase function is not analytic (see Cerveny et al 1977 for a complete discussion of these points). In such a case it is necessary to seek a solution to the elastodynamic equation in the form of another asymptotic expansion. A method of solution in the vicinity of a caustic, which somewhat resembles the ray method, is developed in Appendix D. This alternative high frequency approximation will be used in the vicinity of all caustic points.

7.3 General modelling procedure for laterally inhomogeneous media

A general approach to producing ray theoretical synthetic seismograms is given in the flow chart of Figure 7.2. The process is for a harmonic source with a single predominant frequency, but could be adapted to sources with more complicated frequency spectra.

The efficiency of the method outlined in Figure 7.2 relies heavily upon the ray tracing procedure employed. Circular approximation provides accurate, yet rapid results and is well suited for implementation.

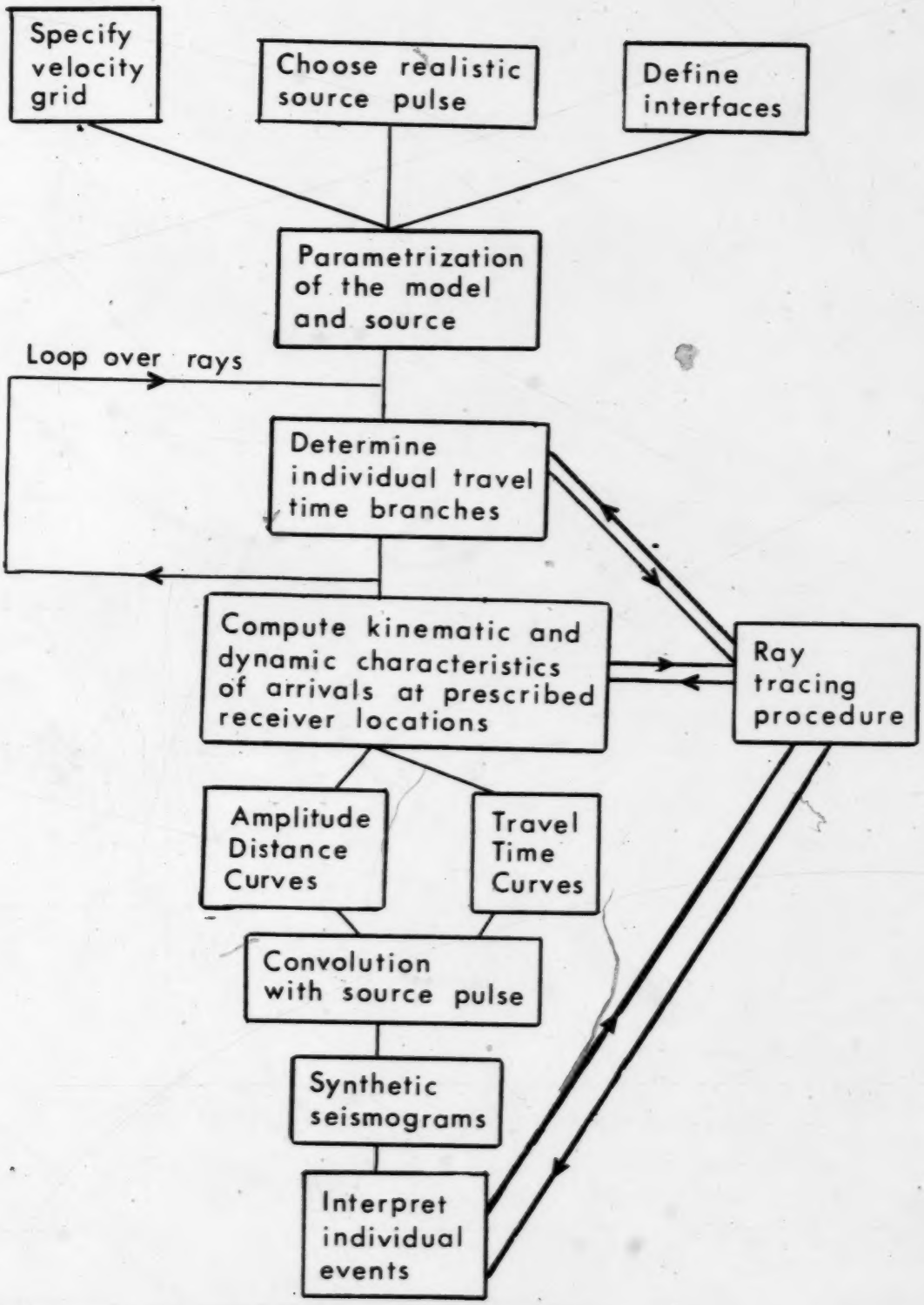
Specify velocity grid
Choose realistic source pulse
Define interfaces
Parametrization of the model and source
Loop over rays
Determine individual travel time branches
Compute kinematic and dynamic characteristics of arrivals at prescribed receiver locations
Ray tracing procedure
Amplitude Distance Curves
Travel Time Curves
Convolution with source pulse
Synthetic seismograms
Interpret individual events

Figure 7.2 General modelling procedure for laterally inhomogeneous media.

Computationally, the most costly portion of the modelling process is the determination of individual travel time branches. However, once computed, these results can be conveniently stored on a disk file in the computer memory for scanning and implementation in subsequent parts of the procedure. This feature also allows one to determine the effect on synthetic seismograms of individual parts of various travel time branches. As well, a unique code number can be assigned to every part of each travel time branch. This code number can then be used to identify events on the synthetic traces. This is a key advantage of ray methods over full wave methods, such as finite differences, in that the user can determine what portions of the subsurface have been sampled in order to produce a particular event.

The loop over rays in Figure 7.2 employs a modification of the numerical ray generation scheme as proposed by Hron (1972). Since the presence of lateral inhomogeneities precludes the assemblage of rays into kinematic and dynamic analogs, that portion of the algorithm has not been utilized. Instead the rays are considered for tracing and amplitude calculations individually. The author has compiled a complete package of FORTRAN programs employing the process shown in Figure 7.2. Some subroutines were utilized which were coded by F. Hron, namely the approximation of interfaces as described in Appendix C, discrimination of travel time branches and plotting of synthetic seismograms.

These programs have been tested against known results for simple media. Numerical results for two-dimensional laterally inhomogeneous media follow in the remaining sections of this chapter.

7.4 Cerveny model

We will first consider a vertically inhomogeneous model utilized by Cerveny and Zahradnik (1972) to study the wave field near a caustic. It consists of an upper layer with linear velocity gradients overlying a homogeneous halfspace. The ray diagram for primary P waves and a description of P wave velocity in the model are shown in Figure 7.3. Also illustrated are the travel time curves for these waves. The threefold travel time branch consists of one reflected part and two refracted parts which form a caustic on the surface. By analytical techniques (Brekhovskikh 1960, section 38, or Choi 1978) the location of this caustic can be shown to be at 120 km which is very close to the result obtained by circular approximation ray tracing.

The vertical amplitude distance curves of the three branch parts are also given in Figure 7.3. The method of circular approximation was used in all regions except the vicinity of the caustic where the Airy approximation (see Appendix D) was utilized. The frequency of the source was taken as 15 Hz. The dotted line represents the amplitude

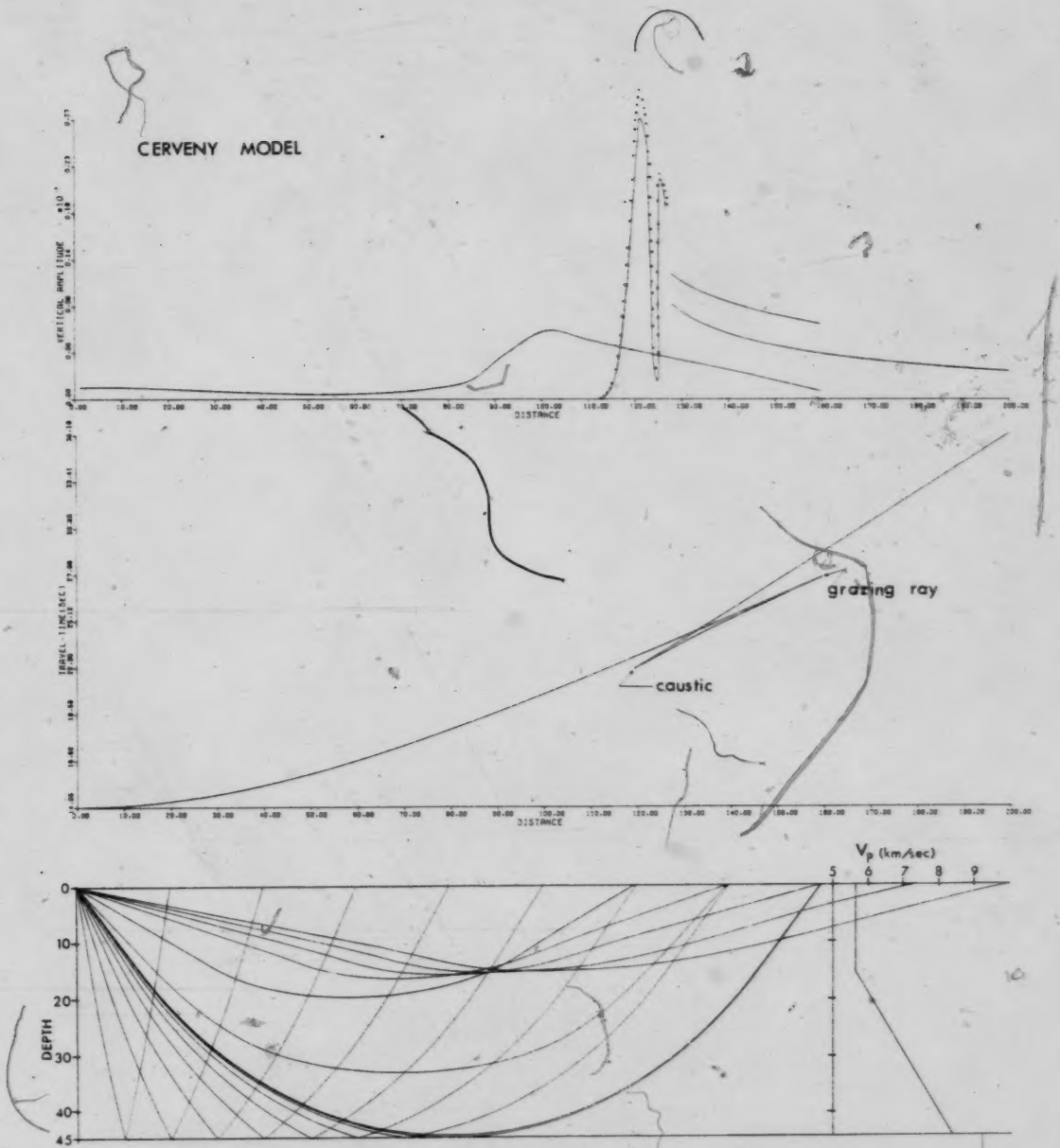

Figure 7.3 Rays, travel times and amplitudes for the Cerveny model. The dotted curve was computed by analytical means (Choi 1978).

predicted by the analytical approach of Choi (1978) valid in the neighborhood of a caustic in a vertically inhomogeneous medium. The results match very well over the entire zone of applicability. Calculation of wave amplitude by the Airy function approach was limited to those regions for which the difference in travel times between rays lying on each branch part was less than the time duration of the source pulse.

Figure 7.4 shows synthetic seismograms computed for the Cerveny model in the vicinity of the caustic. The reduced travel time branch, corresponding to reflected and refracted paths has been overlaid onto the seismograms. The increased energy at the caustic is clearly visible in these seismograms.

7.5 Bohemian Massif

The Bohemian Massif, illustrated and employed in Chapter 6, was used extensively by Psencik (1972) to study travel times of primary P waves. This model for the earth's crust allows a full demonstration of the general modelling process for seismic waves in laterally inhomogeneous media. Figure 7.5 shows the ray diagram of reflected and refracted P rays from a source at 155.2 km for rays arriving at prescribed receiver points. For some receiver locations there may be up to six arrivals, although some may be of very low amplitude. The presence of internal caustics

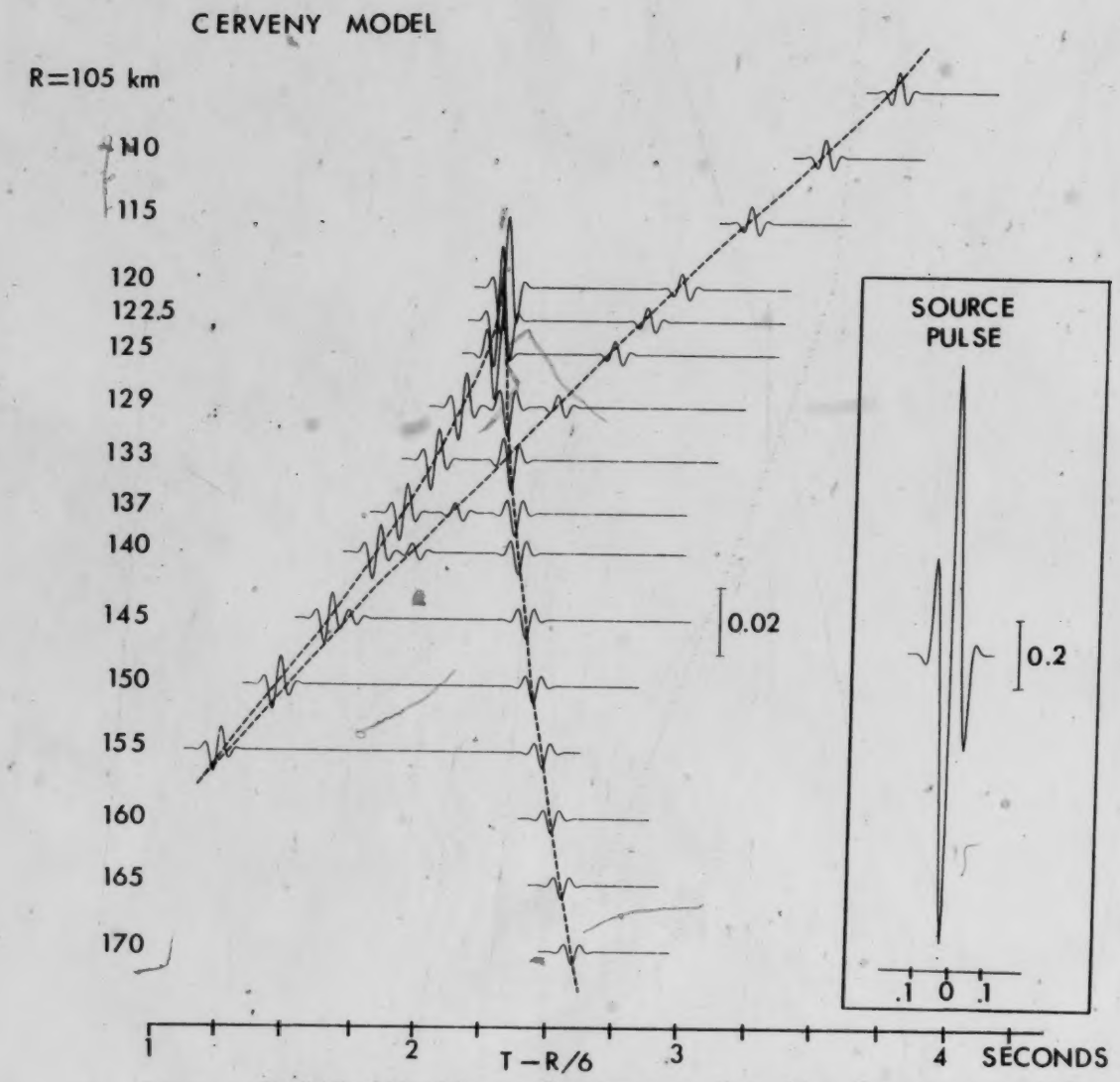

Figure 7.4 Synthetic seismograms for the Cerveny model.

REFLECTED & REFRACTED P RAYS IN THE BOHEMIAN MASSIF

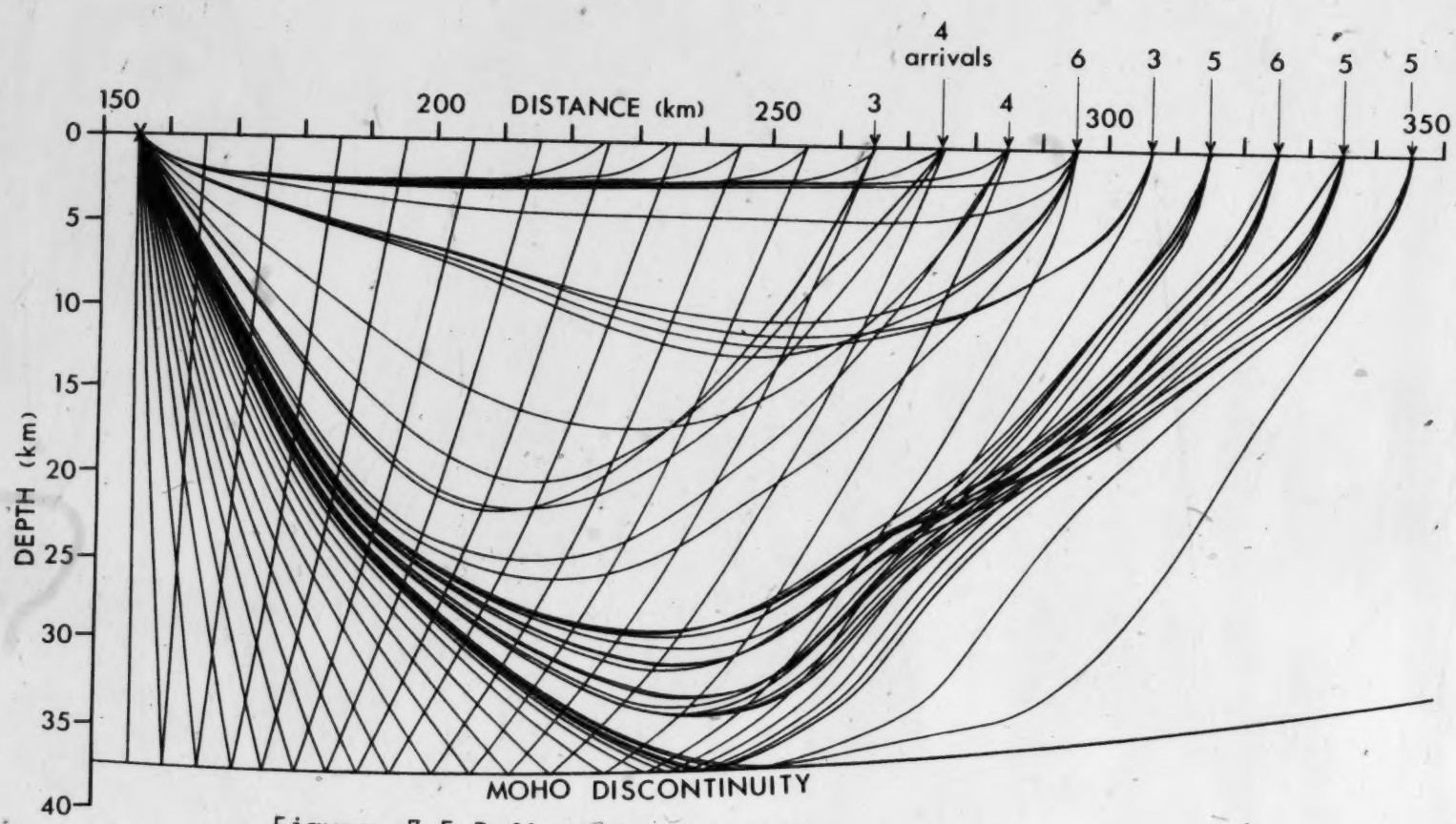

Figure 7.5 Reflected and refracted primary P waves arriving at prescribed receiver locations in the Bohemian Massif.

(corresponding to points where the ray tube vanishes) can be ascertained by examination of Figure 7.5.

For reflected and refracted P waves, a computer program, employing circular approximation ray tracing and an optimized search technique of the distance - take off angle function, distinguished 11 travel time branches. Some of these branches had up to four parts. Time-distance and amplitude) distance curves of some of the arrivals are shown in Figure 7.6. Only the stronger arrivals have had their amplitude plotted. The Airy function approach for a laterally inhomogeneous medium was employed to compute amplitudes near two of the caustic points, showing that some of these amplitudes may be of non-trivial magnitude. The predominant source frequency was taken as 10 Hz.

Synthetic seismograms for the Bohemian Massif have been constructed and are displayed in Figure 7.7. In addition to primary P waves, labelled P1P1, converted phases, P1S1, S1P1, and a multiply reflected wave $(P1)^4$ were included. Other rays were not admitted because of either low amplitude relative to P1P1 or else very late arrival times.

One can observe several phenomena present in the synthetic seismograms displayed in Figure 7.7: a strong interference of multiple arrivals, abrupt appearance and disappearance of wavelets, and a great range of amplitudes.

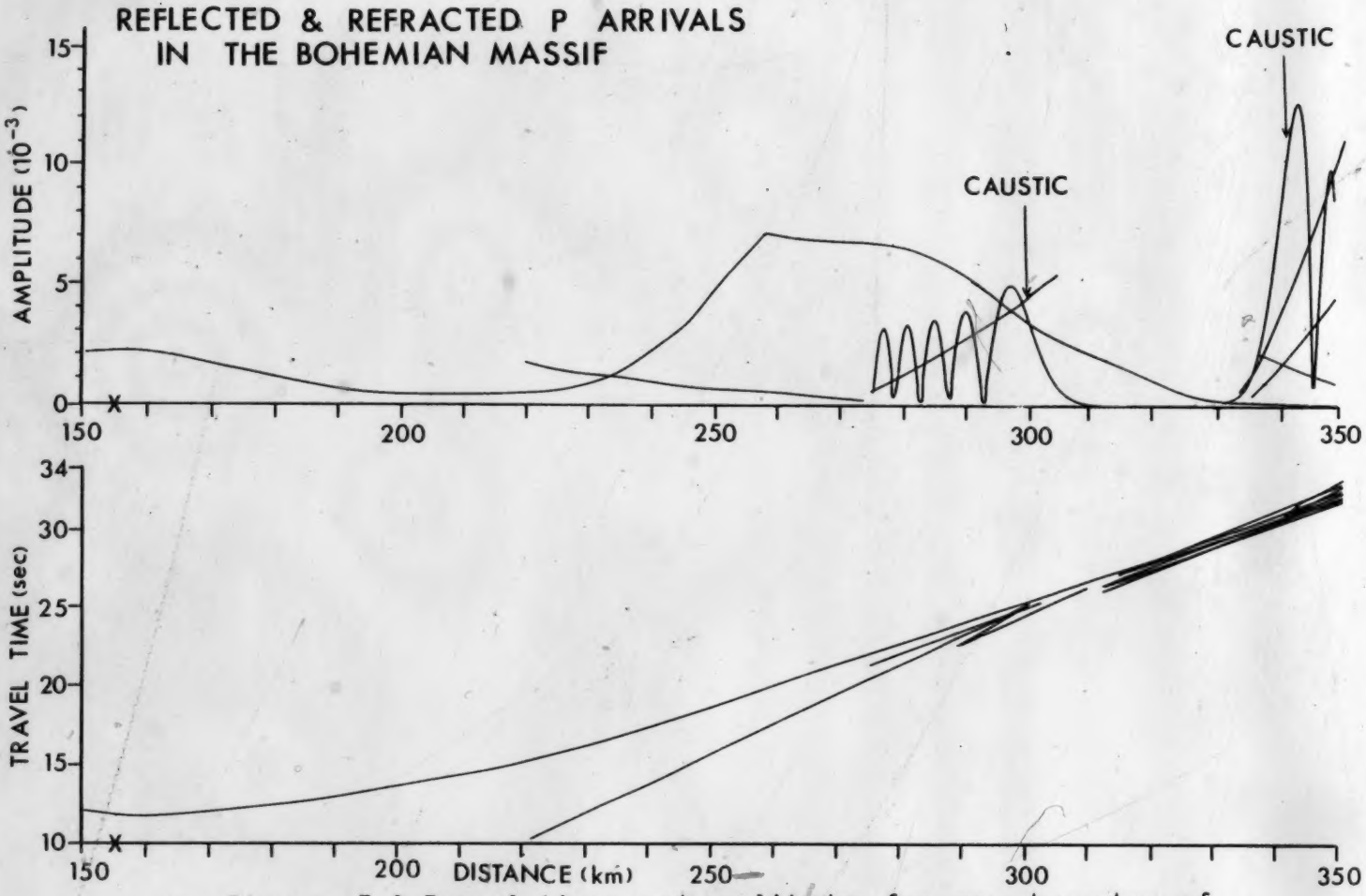

Figure 7.6 Travel times and amplitudes for some branches of the primary P wave in the Bohemian Massif.

Figure 7.7 Synthetic seismograms for the Bohemian Massif. Only reflected phases have been interpreted with travel times. All other arrivals correspond to refracted branches of P1P1 or $(P1)^4$.

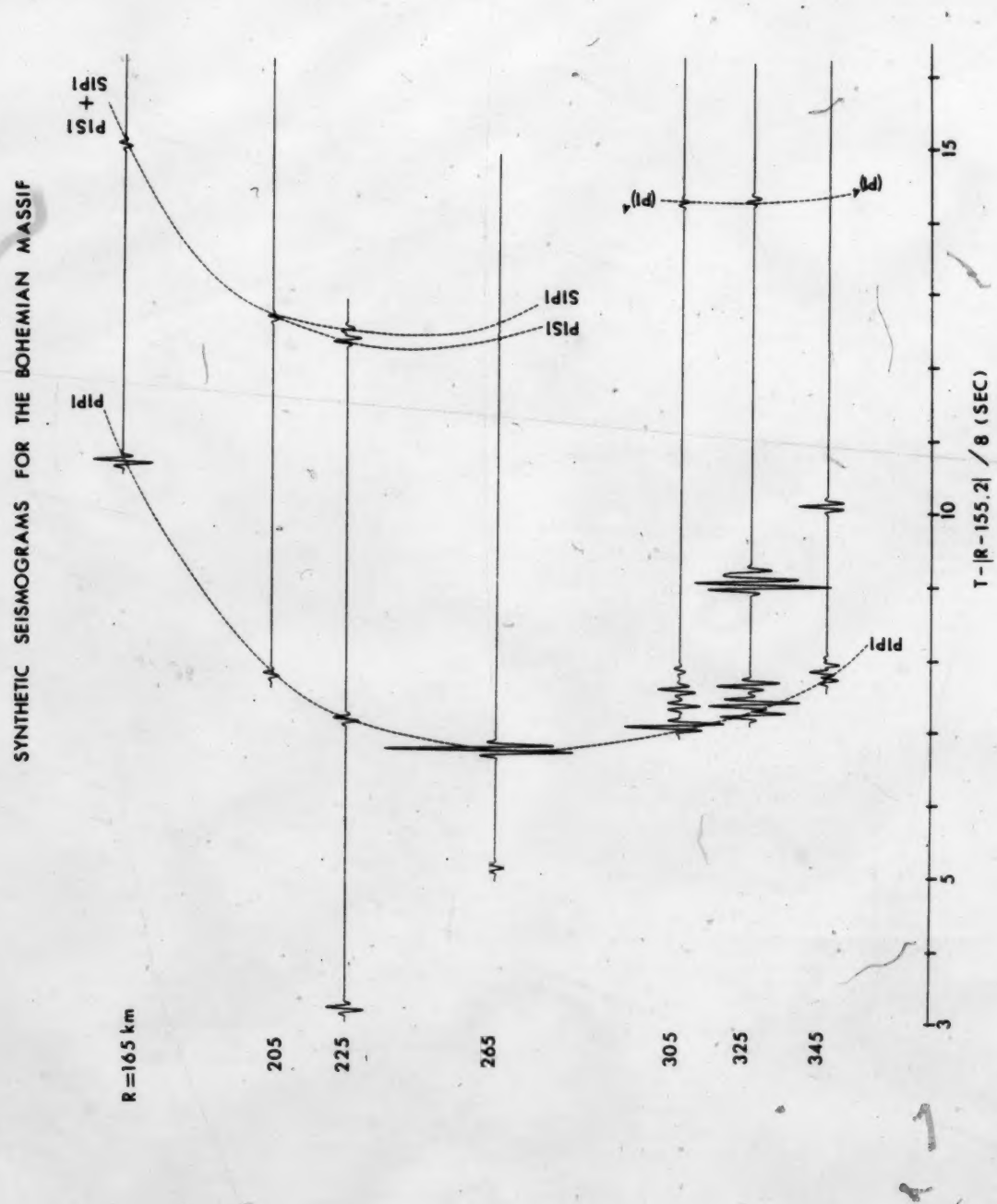

These factors all lead to the variegated nature of the synthetic traces. The phase shift of $n\pi/2$ where n is the number of internal caustics (Choi 1978), is also noticeable in these seismograms.

7.6 Conclusions

While the previous chapter established the accuracy of tracing rays and computing amplitudes by the circular approximation, this chapter has dealt with applications to theoretical and realistic models of the earth's crust. The numerical results presented support the value of the general modelling process described in Figure 7.2. Clearly, asymptotic ray theory, if properly employed, will play a key role in efficient approximate reconstruction of geological structures from field data.

REFERENCES

Abramowitz, M. and Stegun, I., 1965, Handbook of mathematical functions: New York, Dover Publications.

Ahlberg, J., Nilson, E. and Walsh, J., 1967, The theory of splines and their applications: New York, Academic Press.

Alexseev, A. and Gel'chinskiy, B., 1959, On the ray method of computation of wave fields for inhomogeneous media with curved interfaces:Problems in the dynamic theory of propagation of seismic waves, Leningrad University, v. 3, p. 107-160.

Alexseev, A., Babich V. and Gel'chinskiy, B., 1961, Ray method for the computation of the intensity of wave fronts: Problems in the dynamic theory of propagation of seismic waves, Leningrad University, v. 5, p. 3-24.

Aric, K. and Gutdeutsch, R., 1978, Travel times and ways of elastic waves in a medium of two-dimensional velocity distribution: submitted to Pure and Applied Geophysics.

Babich V. and Alexseev, A., 1958, A ray method of computing wave front intensities: Izvestiya, Academy of Sciences, USSR, Geophysics series, v. 1, p. 9-15.

Barnes, A. and Solomon, L. P., 1971, Some curious analytical ray paths for some interesting profiles in geometrical acoustics: J. Acoust. Soc. Am., v. 53, p. 147-155.

Brekhovskikh, L., 1960, Waves in layered media: New York, Academic Press.

Bremmer, H., 1949, The W.K.B. approximation as the first term of a geometrical-optics series, in, The theory of electromagnetic waves: New York, Dover Publications.

Cerveny, V., 1962, On the length of the interference zone of a reflected and head wave beyond the critical point and on the amplitude of head waves: Studia Geophysica and Geodaetica, v. 6, p. 49-64.

Cerveny, V., 1965, The dynamic properties of reflected and head waves around the critical point: Geofysikalni Sbornik, v. 221, p. 135-245.

Cerveny, V., 1967, The theory of reflected and head waves in the case of a layered overburden: Geofysikalni Sbornik, v. 269, p. 133-180.

Cerveny, V. and Ravindra, R., 1971, Theory of seismic head waves: Toronto, University of Toronto Press.

Cerveny, V. and Zahradnik, J., 1972, Amplitude-distance curves of seismic body waves in the neighborhood of critical points and caustics - a comparison: Zeitschrift fur Geophysik, v. 38, p. 499-516.

Cerveny, V., Langer, J.and Psencik, I., 1974, Computation of geometric spreading of seismic body waves in laterally inhomogeneous media with curved interfaces: Geophys. J. R. astr. Soc., v. 38, p. 9-19.

Cerveny, V., Molotkov, I.and Psencik, I., 1977, Ray method in seismology: Prague, Charles University Press.

Cerveny, V. and Pretlova, V., 1977, Computation of ray amplitudes of seismic body waves in vertically inhomogeneous media: Studia Geofisica et Geodaetica, v. 21, p. 248-255.

Cerveny, V. and Hron, F., 1979, The ray series method and dynamic ray tracing system for three dimensional inhomogeneous media: submitted to B.S.S.A..

Chander, R., 1975, On tracing seismic rays with specified end points: J. Geophys., v. 41, p. 173-177.

Chapman, C., 1976, Exact and approximate generalized ray theory in vertically inhomogeneous media: Geoph. J. R. astr. Soc., v. 46, p. 201-233.

Chapman, C., 1978, A new method for computing synthetic seismograms: Geoph. J. R. astr. Soc., v. 54, p 481-518.

Chapman, C., 1979, On impulsive wave propagation in a spherically symmetric model: Geoph. J. R. astr. Soc., v. 58, p. 229-234.

Chen, K. and Ludwig, D., 1972, Calculation of wave amplitudes by ray tracing: J. Acoust. Soc. Am., v. 54, p. 431-436.

Choi, A., 1978, Rays and caustics in vertically inhomogeneous elastic media: M.Sc. Thesis, University of Alberta.

Choy, G. and Richards, P., 1975, Pulse distortion and Hilbert transformation in multiply reflected and refracted body waves: BSSA, v. 65, p. 55-70.

Cumming, G. and Kanasewich, E., 1966, Crustal structure in Western Canada, in, Final report for Advanced Research Projects Agency, Project VELA Uniform, Contract AF 19(628)-2835, Project 8652, Task 865202.

Daley, Patrick Francis and Hron, F., 1979, SH waves in transversely isotropic media: Can. J. Earth Sciences, v. 16, p. 1998-2008.

Dantz, D., 1978, Approximation of arbitrary two-dimensiona isotropic models by polygons and computation of ways and travel times of rays within such models: Presented at the Workshop Meeting on Seismic Waves in Laterally Inhomogeneous Media, Liblice, Czechoslovakia.

de Boor, C., 1971, CADRE: An algorithm for numerical quadrature, in, Mathematical Software: New York, Academic Press.

Eliseevnin, V., 1964, Calculation of rays propagating in an inhomogeneous medium: Acoustical Journal of the Soviet Academy of Science, v.10, p. 284-288.

Ewing, W., Jardetzky, W. and Press, F., 1957, Elastic waves in layered media: New York, McGraw-Hill.

Gardner, G., Gardner, L. and Gregory, A., 1974, Formation velocity and density: The diagnostic basis for stratigraphic traps: Geophysics, v. 39, p. 770-780.

Gazaryan, Yu., 1960, On the geometrical acoustics field in the vicinity of a caustic, in, Problems of the dynamic theory of seismic wave propagation: Leningrad University Press, v. 6.

Gebrande, H., 1976, A seismic ray tracing method for two-dimensional inhomogeneous media, in, Explosion seismology in central Europe: Berlin, Springer Verlag.

Grant, F. and West, G., 1965, Interpretation theory in applied geophysics: New York, Mcgraw-Hill.

Green, A., 1976, Ray paths and relative intensities in one- and two-dimensional models: B.S.S.A., v. 66, p. 1581-1607.

Henrici, P., 1962, Discrete variable methods in ordinary differential equations: New York, Wiley and Sons.

Hron, F., 1972, Numerical methods of ray generation in multilayered media: Methods in computational physics, v. 12, p. 1-34.

Hron, F., 1973, A numerical ray generation and its application to the computation of synthetic seismograms for complex layered media: Geophys. J. R. astr. Soc., v. 35, p. 345-349.

Hron, F., Daley, P. and Marks, L., 1977, Numerical modelling of seismic body waves in oil exploration and crustal seismology, in, Computing methods in geophysical mechanics, Am. Soc. Mech. Eng., AMD, v. 25, p. 21-42.

Hron, F. and Kanasewich, E., 1971, Synthetic seismograms for deep seismic sounding using asymptotic ray theory: BSSA, v. 61, p. 1169-1200.

Julian, B. and Gubbins, D., 1977, Three-dimensional ray tracing: J. Geophysics, v. 43, p. 95-113.

Karal, F. and Keller, J., 1959, Elastic wave propagation in homogeneous and inhomogeneous media: J. Acoust. Soc. Am, v. 31, p. 694-705.

Kline, M. and Kay, I., 1965, Electromagnetic theory and geometrical optics: New York, Interscience Publishers.

Knott, C., 1899, Reflection and refraction of seismic waves with seismological applications: Phil. Mag., v. 48, p. 64-97.

Ludwig, D., 1966, Uniform asymptotic expansions at a caustic: Comm. Pure Appl. Math., v. 19, p. 215-250.

Magnus, W. and Oberhettinger, F., 1949, Formulas and theorems for the special functions of mathematical physics: New York, Chelsea Publishing.

Marcinovskaya, N. and Krasavin, V., 1968, Algorithm for the calculation of reflected waves in media with curvilinear interfaces: Problems in the dynamic theory of propagation of seismic waves, Leningrad University, v. 9, p. 135-144.

Marks, L., 1976, Dynamic properties of head waves near the critical point: M.Sc. Thesis, University of Alberta.

Marks, L. and Hron, F., 1977, Weber function computation in the interference reflected-head wave amplitude: Geophys. Res. Letters, v. 4, p. 255-258.

Marks, L. and Hron, F., 1978, Reviews of true amplitude computation in plane layered structures: J. Can. Soc. Expl. Geophys., v. 14, p. 5-20.

Marks, L. and Hron F., 1978a, Ray tracing in complex media: Presented at the Workshop Meeting on Seismic Waves in Laterally Inhomogeneous Media, Liblice, Czechoslovakia.

Marks, L. and Hron, F., 1979a, Dynamic properties of reflected and head waves near the critical points: Can. J. Earth Sciences, v. 16, p. 1388-1401.

Marks, L. and Hron, F., 1979b, Calculation of synthetic seismograms in laterally inhomogeneous media: Paper S-3 presented to the 49-th Annual meeting of the Society of Exploration Geophysicists, New Orleans, Louisiana.

Nettleton, L., 1940, Geophysical prospecting for oil: New York, McGraw-Hill.

Pod"yapol'skiy, G., 1966, A ray series expansion for reflected and transmitted waves: Izvestiya, Academy of Sciences, USSR, Earth Physics, v. 6 p. 347-363.

Popov, M. and Psencik, I., 1978, Computation of ray amplitudes in inhomogeneous media with curved interfaces: Studia Geoph. et Geod., v. 22, p. 248-258.

Psencik, I., 1972, Kinematics of refracted and reflected waves in inhomogeneous media with non-planar interfaces: Studia Geoph. et Geod., v. 16, p. 126-152.

Sato, R., 1969, Amplitude of body waves in a heterogeneous sphere. Comparison of wave theory and ray theory: Geophys. J. R. astr. Soc., v. 17, p. 527-544.

Simmons, G. F., 1973, Differential equations: New York, McGraw-Hill.

Sorrells, G., Crowley, J. and Veith, K., 1971, Methods for computing ray paths in complex geological structures: BSSA, v. 61, p. 27-53.

Spiegel, M., 1959, Vector analysis: New York, McGraw-Hill.

Wesson, R., 1970, A time integration method for computation of the intensities of seismic rays: BSSA, v. 60, p. 307-316.

Wesson, R., 1971, Travel-time inversion for laterally inhomogeneous crustal velocity models: BSSA, v. 61, p. 729-746.

White, D., 1978, Ray theory for a wide class of sound speed profiles with two-dimensional variation: J. Acoust. Soc. Am., v. 63, p. 405-419.

Will, M., 1976, Calculation of travel times and ray paths for lateral inhomogeneous media, in, Explosion seismology in central Europe: Berlin, Springer Verlag.

Woodhouse, J., 1974, Some problems in mathematical geophysics: Ph.D. Thesis, Cambridge University.

Yanovskaya, T., 1964, Determination of the solution to the elastodynamic equation near a caustic: Problems in the dynamic theory of propagation of seismic waves, Leningrad University, v.7, p. 61-76.

Zahradnik, J., 1970, The kinematic and dynamic properties of seismic waves in the neighborhood of caustics: Acta Universitatis Carolinae, Mathematica et Physica, v. 11, p. 77-106.

Zoeppritz, K., 1919, Uber Erdbebenwellen: Gottingen Nachrichten, v. 7b, p. 66-84.

APPENDIX A

EQUATIONS FOR RAY INTERSECTION POINTS

In this appendix we shall derive explicit equations for the location of intersection points between the normal to the central ray and a nearby auxiliary ray.

Let the equation of the central ray be

$$(x-a)^2 + (z-b)^2 = \rho^2 \qquad (A.1)$$

where

$a = v_0 \cot\theta_0 / k$

$b = v_0 / k$

$\rho = v_0 / k \sin\theta_0$

v_0 = velocity at the beginning of the ray segment,

k = velocity gradient in the current layer,

θ_0 = take-off angle at the beginning of the ray segment.

Equation A.1 is given in a Cartesian coordinate system with its origin at the point where the current ray segment begins (see Figure A.1).

Let an auxiliary ray be given in these coordinates by

$$(x-(A+x_S))^2 + (z-B)^2 = R^2 \qquad (A.2)$$

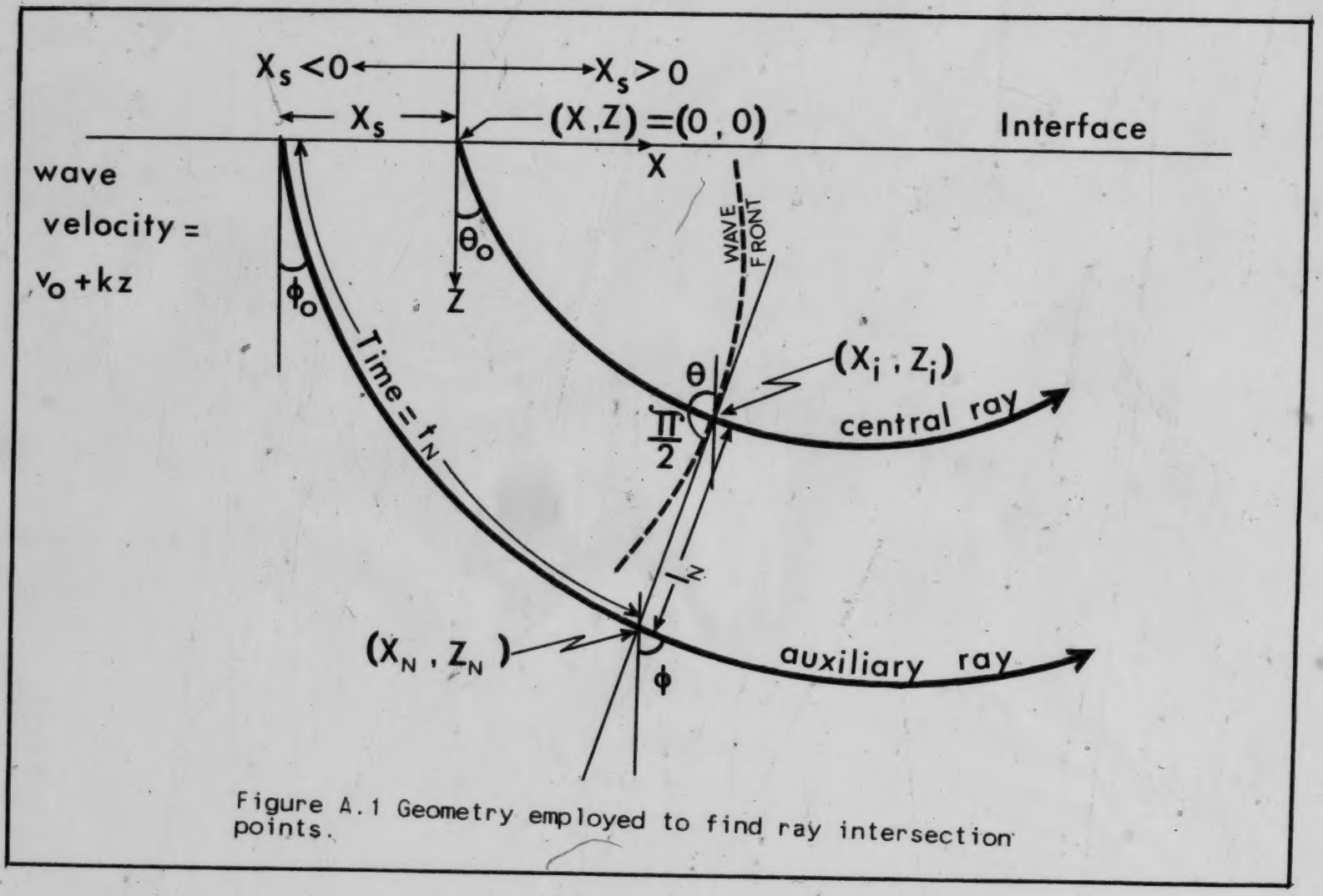

Figure A.1 Geometry employed to find ray intersection points.

where

$$A = v_0 \cot\phi_0 / k$$

$$B = v_0/k = b$$

$$R = v_0/k \sin\phi_0$$

x_S = lateral separation between starting points of the central and the auxiliary ray. If the ray segment under consideration is the first one emanating from the source, then $x_S = 0$.

We seek the values of the intersection, (x_N, z_N), of the auxiliary ray (equation A.2) and the line M normal to the central ray, namely,

$$z = mx - mx_i + z_i \qquad (A.3)$$

where

$$m = (b-z_i)/(a-x_i)$$

Substitution of equation A.3 into A.2 and introduction of

$$S = (1+m^2)$$

$$T = 2(m(z_i - mx_i - B) - A - x_S)$$

$$U = (A+x_S)^2 + (mx_i + z_i - B)^2 - R^2$$

yields

$$Sx_N^2 + Tx_N + U = 0$$

the solutions of which are

$$x_N = (-T \pm (T^2 - 4SU)^{1/2})/2S \qquad (A.4)$$

The ± sign is taken according to which solution gives an intersection nearest the interface in the direction of ray propagation. By substitution, we have

$$z_N = mx_N - mx_i + z_i \tag{A.5}$$

It is also valuable to know certain additional quantities concerning the auxiliary ray's intersection with the line normal to the central ray. The travel time along the auxiliary ray from $(x_S, 0)$ to (x_N, z_N) is

$$t_N = \frac{1}{k} \cosh^{-1} \left[\frac{k^2 (z_N^2 + (x_N - x_S)^2)^2}{2v_0 (v_0 + kz_N)} + 1 \right] \tag{A.6}$$

The length, ℓ_N, from (x_N, z_N) to the central ray as measured along the normal is

$$\ell_N = \left((x_N - x_i)^2 + (z_N - z_i)^2 \right)^{1/2} \tag{A.7}$$

The angle ϕ that the auxiliary ray makes with the vertical at (x_N, z_N) is

$$\phi = 2\tan^{-1} \left(e^{kt_N} \tan\phi_0/2 \right) \tag{A.8}$$

The degeneration of equations A.4-A.8 for cases of homogeneous layers (k = 0) or vertical incidence ($\theta_0 = 0, \pi$) is obtained by taking the limiting values of these expressions.

APPENDIX B

THE WEBER FUNCTION APPROACH FOR AMPLITUDE COMPUTATION

The integral representing the vertical displacement due to a harmonic wave of angular frequency ω which has penetrated L layers, being reflected M times from the L+1-th interface, and arrives at the free surface at an epicentral distance r is written as

$$A(r) = \frac{ike^{-i\omega t}}{2} \int_{-\infty}^{\infty} R^M(q)\sigma(q)\, H_0^1(krq)\, e^{ikB(q)}\, q\, dq \qquad (B.1)$$

where we have used the following notation

$i = \sqrt{-1}$

$k = \omega/a_1$

R ... plane wave reflection coefficient for the L+1 interface,

σ ... product of all other plane wave coefficients corresponding to the wave's traverse of the medium,

B ... phase function of the wave,

H_0^1 ... Hankel function of the first kind and zeroth order.

After suitably deforming the contour of integration (Cerveny 1965, Cerveny and Ravindra 1971) and expanding the Hankel function for high frequencies, approximations may be applied

to the integral when integrating along a portion of the steepest descent contour given by

$$(1-q^2)^{\frac{1}{2}} = (1-x^2)^{\frac{1}{2}} + pe^{-i\pi/4}, \qquad -\infty<p<\infty \tag{B.2}$$

The saddle point, x, is given by

$$\left(\frac{dB}{dq}\right)_{q=x} = r \tag{B.3}$$

Physically, x is closely related to the constant C in Snell's Law by the relation $x = a_1 C = \sin\theta_1$ where θ_1 is the angle of incidence of a P wave on the first interface. For computational purposes, $x=\sin\theta_1$ has been chosen as a parameter for the ray in this thesis. Ray parameters corresponding to critical refraction along the L+1 interface can be written as $x_i^* = a_i/v_{L+1}$, i=1,...,L, where v_{L+1} is the velocity of the refracted segment of the head wave.

Due to the singularity of R at $q = x_L^*$, corresponding to the critical point in terms of the ray parameters, x, the reflection coefficient R can be conveniently decomposed as

$$R(x_L) = E(x_L) - D(x_L)S(x_L)$$

$$S = (x_L^{*2} - x_L^2)^{\frac{1}{2}} \tag{B.4}$$

where D and E depend only on even powers of S.

Performing these operations on equation B.1 yields an expression for the displacement contribution of the reflected wave near the critical point:

$$A_R(r) = e^{-i\omega(t-t_R)} \frac{\sigma(x_L)}{Q} \left\{ R^M(x_L) - ME^{M-1}(x_L)D(x_L) \right.$$

$$\left. c\left(x_L^{*2} - x_L^2\right)^{\frac{1}{2}} \left(\frac{g_1(\beta)}{\beta^{\frac{1}{2}}} - 1 \right) \right\} \qquad (B.5)$$

where the following notation has been employed

t_R = time of arrival of the reflected wave

Q = geometrical spreading of the reflected wave,

$$C = \begin{cases} 1 & \text{for P type head waves} \\ \dfrac{b_{L+1}}{a_{L+1}} & \text{for S type head waves} \end{cases}$$

$x_i = a_1 x/a_i, \quad i=1,\ldots,L$

$$\beta = \left(\frac{k(r-\tilde{r})}{2x^3} \right)^{\frac{1}{2}} \left((1-x_1^{*2})^{\frac{1}{2}} - (1-x^2)^{\frac{1}{2}} \right)$$

$$g_1(\beta) = \pi^{-\frac{1}{2}} \int_{-\infty}^{\infty} \left(\beta - pe^{-i\pi/4} \right)^{\frac{1}{2}} e^{-p^2}\, dp$$

N_{Pi}, N_{Si} number of P and S ray segments in the i-th layer,

h_i thickness of the i-th layer.

$$\tilde{r} = x^3 \sum_{i=1}^{L} \frac{N_{Pi} h_i (a_1^2/a_i^2 - 1)}{(a_1^2/a_i^2 - x^2)^{3/2}} + \sum_{i=1}^{L} \frac{N_{Si} h_i (a_1^2/b_i^2 - 1)}{(a_1^2/b_i^2 - x^2)^{3/2}}$$

For regions beyond the critical distance,

r^*, the integral in equation B.1 has contributions from a circumvention of the branch cut given parametrically by

$$(1-q^2)^{\frac{1}{2}} = (1-x_1^{*2})^{\frac{1}{2}} + pe^{-i\pi/4}, \quad 0 \le p < \infty \tag{B.6}$$

Physically, this may be interpreted as the head wave contribution to the displacement on the surface. Mathematically, the omission of the integration along this path would prohibit a transformation of integration contours since we would end up on a Riemann sheet different from that at the beginning of the contour. Evaluating equation B.1 along contour B.6 and remembering that the maximum value of the integrand occurs near p=0, gives a head wave contribution

$$A_H(r) = Me^{-i\omega(t-t_H)} \sigma(x_L^*)\, \Gamma\, E^{M-1}(x_1^*)c \frac{x_1^*\,(1-x_1^{*2})^{\frac{1}{4}}}{8kr^2(r-\tilde{r}^*)^3}\, g_2(y^*) \tag{B.7}$$

where

t_H = head wave arrival time,

Γ = head wave coefficient = $D(x_L^*)x_L^*$

$\tilde{r}^* = \tilde{r}$ with x_1^* substituted for x

$$y^* = \left(\frac{kx_1^*\,(1-x_1^{*2})}{2(r-\tilde{r}^*)}\right)^{\frac{1}{2}} (r-r^*)$$

$$g_2(y^*) = \pi^{-\frac{1}{2}}\, 2^{5/2}\, e^{7i\pi/8} \int_0^\infty p^{\frac{1}{2}} \exp(-p^2 - 2e^{i\pi/4} py^*)\, dp$$

Near the critical point we must consider the summed total response due to the head wave interfering with the reflected wave. Adding equations B.5 and B.7 and making approximations which are legitimate within the interference zone, gives the displacement of the interference reflected-head wave

$$A(r) = e^{-i\omega(t-t_R)} \frac{\sigma(x_L)}{Q} R^M(x_1) - M\Gamma c \frac{(1-x^{*2}_1)^{\frac{1}{4}}}{x^*_1 k(r-\tilde{r}^*)}$$

$$E^{M-1}(x^*_1)\ i2^{3/4}(g_1(\beta)-\beta^{\frac{1}{2}}) - 2^{-3/4} e^{-iy^2} g_2(y^*) \qquad (B.8)$$

where $y = (\omega(t_R-t_H))^{\frac{1}{2}}$. A new function, G, is introduced as

$$G = i2^{3/4}(g_1(\beta)-\beta^{\frac{1}{2}}) - 2^{-3/4}\ e^{-iy^2} g_2(y^*) \qquad (B.9)$$

Numerical investigation has shown that for realistic seismological models, the three parameters β, y and y* are nearly equal within the interference zone. They can be assigned a common definition as

$$y = \begin{cases} \beta & \text{for } r<r^* \\ (\omega(t_R-t_H))^{\frac{1}{2}} & \text{for } r>r^* \end{cases}$$

With the introduction of

$\gamma = p - ye^{i\pi/4}$ in $g_1(y)$, G(y) can be recast as

$$G(y) = -2^{3/4}\,\pi^{-\frac{1}{2}}\exp(7i\pi/8 - iy^2)\int_{-\infty}^{\infty}\gamma^{\frac{1}{2}}\cdot$$

$$\exp(-\gamma^2 - 2y\gamma e^{i\pi/4})\,d\gamma - i2^{3/4}y^{\frac{1}{2}} \qquad (B.10)$$

This expression for G can be rewritten with the help of the integral form of the Weber function D (Magnus and Oberhettinger 1949),

$$D_{\frac{1}{2}}(y(i-1)) = \pi^{-\frac{1}{2}}\,2^{\frac{1}{4}}\exp\left(-\frac{iy^2}{2} - \frac{i\pi}{4}\right)\cdot$$

$$\int_{-\infty}^{\infty}\gamma^{\frac{1}{2}}\exp(-\gamma^2 2y\gamma e^{i\pi/4})\,d\gamma$$

Near the critical point $S \simeq 0$ in equation B.4 and thus formula B.8 may be simplified further by setting $E^{M-1}(x_L^*) = R^{M-1}(x_L^*)$. With these changes and the use of a pretabulated Weber function file, equation B.8 lends itself to rapid evaluation on a digital computer.

APPENDIX C

APPROXIMATION OF INTERFACES BY PIECEWISE CONTINUOUS PARABOLAE

A method of piecewise approximation of curvilinear boundaries by a group of smoothly linked parabolae was first suggested by Marcinovskaya and Krasavin (1968). Due to the inaccessibility of this paper, the method is presented here in the modified form devised by Hron (personal communication) and used in his programs since 1973. .

Suppose that a set of M discrete points, specified by their two-dimensional Cartesian coordinates $N_m = [\xi_m, \zeta_m]$, $m=1,\ldots,M$, are given as points lying on a curvilinear boundary. We may approximate this boundary with the help of I parabolae .

$$z(x) = (a_i x + b_i)x + c_i, \quad i=1,\ldots,I \tag{C.1}$$

each of them being defined over the interval

$$x \in [X_i, X_{i+1}]$$

As continuity conditions we impose

$$z_i(X_{i+1}) = z_{i+1}(X_{i+1})$$

$$\left.\frac{dz_i}{dx}\right|_{X_{i+1}} = \left.\frac{dz_{i+1}}{dx}\right|_{X_{i+1}}$$

The continuity of the curve that passes through all M points could be realized by solving the following linear system for the (i+1)-th parabola given the i-th one:

$$\begin{bmatrix} X_{i+1}^2 & X_{i+1} & 1 & 0 \\ \xi_m^2 & \xi_m & 1 & 0 \\ 2X_{i+1} & 1 & 0 & -1 \end{bmatrix} \begin{bmatrix} a_{i+1} \\ b_{i+1} \\ c_{i+1} \end{bmatrix} = \begin{bmatrix} z_i(X_{i+1}) \\ \zeta_m \\ -2a_iX_{i+1} + b_iX_{i+1} \end{bmatrix} \qquad (C.2)$$

where $[\xi_m, \zeta_m]$ are coordinates of the closest input point for which $X_{i+2} = \xi_m > X_{i+1}$. However, if this system were solved for all M-1 pairs of adjacent points, considerable CPU time would be consumed and the surface would have a corrugated nature for some types of input data. The problem of time reduction can be vanquished by allowing the curve to fall short of some input points by an arbitrarily specified distance. For this purpose, equation C.2 may be solved for some more distant point (iteratively, beginning with point M) and the i+1-th parabola will be accepted if for any ε

$$\left| \frac{(a_{i+1}\xi_j + b_{i+1})\xi_j + c_{i+1} - \zeta_j}{\text{Max}(\zeta_j) - \text{Min}(\zeta_j)} \right| \leq \varepsilon$$

for,

$$X_{i+1} < \xi_j < \xi_m$$

This method is defeated if the ζ_i are scattered over a large interval compared to the

ξ_i interval. This will bring about the undesirable corrugated surface. In order to avoid this, we must modify the approach. First, a parabola is found that passes through $N_\ell, N_{\ell+1}, N_{\ell+2}$ by solving the usual set of three linear equations for the coefficients $a_{\ell+1}, b_{\ell+1}, c_{\ell+1}$. Then the two predetermined parabolae $(a_{\ell\pm1}, b_{\ell\pm1}, c_{\ell\pm1})$ will be united by an inserted parabola (a_ℓ, b_ℓ, c_ℓ). The right bound of the interval of definition of the l-th parabola is termed $X_{\ell+1}$ and its left bound is $X_\ell = \xi_\ell - \Delta x$. The quantity Δx is selected iteratively to cause the relation

$$X_\ell < \xi_\ell < X_{\ell+1} < \xi_{\ell+1}$$

to hold. The coefficients

$$a = \frac{-2a_{\ell-1}X_\ell + 2a_{\ell+1}X_{\ell+1} - b_{\ell-1} + b_{\ell+1}}{2(X_{\ell+1} - X_\ell)}$$

$$b_\ell = 2(a_{\ell+1} - a_\ell)X_{\ell+1} + b_{\ell+1}$$

$$c_\ell = (a_\ell - a_{\ell+1})X_{\ell+1}^2 + c_{\ell+1} \qquad \text{(C.3)}$$

and the right bound

$$X_{\ell+1} = \frac{2(c_{\ell+1} - c_{\ell-1}) + (b_{\ell+1} - b_{\ell-1})X_\ell}{2(a_{\ell-1} - a_{\ell+1})X_\ell + (b_{\ell-1} - b_{\ell+1})} \qquad \text{(C.4)}$$

are the solutions of the following systems of algebraic equations (with

x_ℓ as a parameter)

$$a_{\ell-1}x_\ell^2 + b_{\ell-1}x_\ell + c_{\ell-1} = a_\ell x_\ell^2 + b_\ell x_\ell + c_\ell$$

$$2a_{\ell-1}x_\ell + b_{\ell-1} = 2a_\ell x_\ell + b_\ell$$

$$a_\ell x_{\ell+1}^2 + b_\ell x_{\ell+1} + c_\ell = a_{\ell+1}x_{\ell+1}^2 + b_{\ell+1}x_{\ell+1} + c_{\ell+1}$$

$$2a_\ell x_{\ell+1} + b_\ell = 2a_{\ell+1}x_{\ell+1} + b_{\ell+1}$$

APPENDIX D

RAY AMPLITUDE IN THE VICINITY OF A CAUSTIC

Asymptotic ray theory, despite its wide degree of relevance, is severly limited in the neighborhood of any point where the rays cross each other. Such a point is termed a caustic. In this appendix the elastodynamic equation of motion will be solved for an arbitrary ray in a laterally inhomogeneous medium. The works of previous researchers (Bremmer 1949, Brekhovskikh 1960, Ludwig 1966, Sato 1969, Zahradnik 1970, Chapman 1976, 1978, 1979, Choi 1978, for example) have focused attention on generally homogeneous or vertically imhomogeneous media. Gazaryan (1960) has presented the solution to the wave equation in the vicinity of a caustic by a modification of the ray method. Yanovskaya (1964) considered the problem of a solution to the elastodynamic equation in the vicinity of a caustic. Since these last two papers are inaccessible to most readers, a brief derivation of these results, with modifications suitable to the geometry used for this thesis, will be presented.

Consider the elastodynamic equation of motion for displacement

$$\vec{L}(\vec{u}) = \rho \frac{\partial^2 \vec{u}}{\partial t^2} \qquad (D.1)$$

where

$$\vec{L}(\vec{u}) = (\lambda+\mu)\nabla(\nabla\cdot\vec{u}) + \mu\nabla^2\vec{u} + (\nabla\cdot\vec{u})\nabla\lambda +$$

$$\nabla\mu\times\nabla\times\vec{u} + 2(\nabla\mu\cdot\nabla)\vec{u}$$

in Cartesian coordinates $x_1=x$, $x_2=y$, $x_3=z$. Let us impose a time dependence $e^{-i\omega t}$. Following the basic geometry of the ray method, ray coordinates (q_1, q_2, τ) are introduced as

q_1 ... take-off angle at source measured from vertical,

q_2 ... azimuthal take off angle at source,

τ ... phase function along ray.

We seek a solution of D.1 in the form

$$\vec{u} = \vec{u}(q_1, q_2, \tau)e^{-i\omega(t-\tau)} \qquad (D.2)$$

Asymptotic ray theory states that the following are solutions to equation D.1 (to zeroth order)

$$\vec{u}_{0P} = \frac{\phi(q_1, q_2)\hat{e}_\tau}{(H_1H_2\rho a)^{\frac{1}{2}}} \qquad \text{(for P waves)}$$

$$\vec{u}_{0S} = \frac{\psi(q_1, q_2)}{(H_1H_2\rho b)^{\frac{1}{2}}}\ \hat{e}_{q_1}\cos\zeta + \hat{e}_{q_2}\sin\zeta \qquad \text{(for S waves)}$$

where

ϕ,ψ ... solve the elastodynamic equation and boundary conditions at each interface,

ρ ... volume density

a,b ... velocities of propagation of P and S waves

H_1, H_2 ... scale factors (Riemann metrics)

$$H_1 = \left|\frac{\partial \vec{x}}{\partial q_1}\right| , \quad H_2 = \left|\frac{\partial \vec{x}}{\partial q_2}\right| , \quad H_3 = \left|\frac{\partial \vec{x}}{\partial \tau}\right|$$

$\hat{e}_\tau, \hat{e}_{q_1}, \hat{e}_{q_2}$ ... unit vectors at any point along the ray,

ς ... angle between the plane of incidence and the direction $\hat{e}_{q_1}$.

At a caustic $H_1 H_2 = 0$. We assume that $H_1 = 0$, $H_2 \neq 0$ at this point. Physically, this excludes rays which focus at a point. Furthermore, we presume that the rays propagate in the (q_1, τ) plane implying

$$\vec{u}(q_1,\tau) = u_1 \hat{e}_{q_1} + u_3 \hat{e}_\tau$$

Substituting equation D.2 into D.1 yields

$$\vec{N}(\vec{u})(i\omega)^2 + \vec{M}(\vec{u}) i\omega + \vec{L}(\vec{u}) = 0 \qquad (D.3)$$

where

$$\vec{N}(\vec{u}) = (\lambda+\mu)(\vec{u}\cdot\nabla\tau)\nabla\tau + \mu\vec{u}(\nabla\tau)^2 - \rho\vec{u}$$

$$\vec{M}(\vec{u}) = (\lambda+\mu)(\nabla\tau(\nabla\cdot\vec{u}) + \nabla(\vec{u}\cdot\nabla\tau)) +$$

$$\Delta\lambda(\vec{u}\cdot\nabla\tau) + (\nabla\mu\cdot\vec{u})\nabla\tau + (\nabla\mu\cdot\nabla\tau)\vec{u}$$

$$+ \mu(\vec{u}\nabla^2\tau + \frac{2\partial\vec{u}}{\partial\tau}(\nabla\tau)^2)$$

We shall only consider here the case when the last ray segment is propagating in the compressional (or P) mode. Similar analysis for an S wave is possible. For a P wave, the eikonal equation is $(\nabla\tau)^2 = a^{-2}$. In what follows, components along q_1 will be indexed 1, and along τ labelled 3. Thus $N_3(\vec{u}) = 0$, $N_1(\vec{u}) = -\rho(1-\gamma^2)u_1$, $\gamma=b/a$ and equation D.3 has the form

$$L_3(\vec{u}) + i\omega M_3(\vec{u}) = 0 \tag{D.4}$$

$$L_1(\vec{u}) + i\omega M_1(\vec{u}) - i\omega\rho(1-\gamma^2)u_1 = 0 \tag{D.5}$$

Let us introduce a quantity $\eta = H_1H_2\rho a$. Then using the definition of vector operators in curvilinear coordinates (Spiegel 1959), we have .

$$L_1(\vec{u}) = \frac{\rho a^2}{H_1}\frac{\partial}{\partial q_1}\frac{\rho}{\eta}\frac{\partial}{\partial q_1}(H_2 a u_1) + \frac{\rho}{\eta}\frac{\partial}{\partial\tau}\frac{\eta}{\rho a}u_3 -$$

$$- \frac{\rho b^2}{H_2 a}\left[\frac{\partial}{\partial\tau}\frac{H_2}{H_1 a}\frac{\partial}{\partial q_1}(a u_3) - \frac{\partial}{\partial\tau}\frac{H_2}{H_1 a}\frac{\partial}{\partial\tau}(u_1 H_1)\right] +$$

$$+ \frac{\partial\lambda}{\partial q_1}\frac{\rho}{H_1\eta}\left[\frac{\partial(H_2 a u_1)}{\partial q_1} + \frac{\partial}{\partial\tau}\frac{\eta u_3}{\rho a}\right] +$$

$$+ \frac{1}{H_1}\frac{\partial\mu}{\partial q_1}\left[\frac{1}{H_1}\frac{\partial u_1}{\partial q_1} + \frac{u_3}{a H_1}\frac{\partial H_1}{\partial\tau}\right] +$$

$$+ \frac{1}{a}\frac{\partial\mu}{\partial\tau}\left[\frac{H_1}{a}\frac{\partial}{\partial\tau}\frac{u_1}{H_1} + \frac{a}{H_1}\frac{\partial}{\partial q_1}\frac{u_3}{a}\right]$$

(D.6)

$$L_3(\vec{u}) = \rho a \frac{\partial}{\partial\tau}\left[\frac{\rho}{\eta}\frac{\partial}{\partial q_1}(H_2 a u_1) + \frac{\rho}{\eta}\frac{\partial}{\partial\tau}\frac{\eta u_3}{\rho a}\right] -$$

$$- \frac{\rho^2 b^2 a}{\eta}\left[\frac{\partial}{\partial q_1}\frac{H_2}{H_1 a}\frac{\partial}{\partial\tau}(H_1 u_1) - \frac{\partial}{\partial q_1}\frac{H_2}{a H_1}\frac{\partial}{\partial q_1}(a u_3)\right] +$$

$$+ \frac{\partial\lambda}{\partial\tau}\frac{\rho}{a\eta}\left[\frac{\partial}{\partial q_1}(H_2 a u_1) + \frac{\partial}{\partial\tau}\frac{\eta u_3}{\rho a}\right] +$$

$$+ \frac{1}{H_1}\frac{\partial\mu}{\partial q_1}\left[\frac{a}{H_1}\frac{\partial}{\partial q_1}\frac{u_3}{a} + \frac{H_1}{a}\frac{\partial}{\partial\tau}\frac{u_1}{H_1}\right] +$$

$$+ \frac{1}{a^2}\frac{\partial\mu}{\partial\tau}\left[\frac{\partial u_3}{\partial\tau} + \frac{u_1}{H_1}\frac{\partial a}{\partial q_1}\right]$$

(D.7)

$$M_1(\vec{u}) = \rho(1-\gamma^2)\frac{a}{H_1}\frac{\partial u_3}{\partial q_1} + \rho b^2\left[\frac{u_1\rho}{\eta}\frac{\partial}{\partial\tau}\left(\frac{\eta}{\rho a^2}\right) + \frac{2}{a^2}\frac{\partial u_1}{\partial\tau}\right] -$$

$$-\rho(1+\gamma^2)\frac{u_3}{H_1}\frac{\partial a}{\partial q_1} + \frac{u_3}{H_1 a}\frac{\partial\lambda}{\partial q_1} + \frac{\partial\mu}{\partial\tau}\frac{u_1}{a^2}$$

(D.8)

$$M_3(\vec{u}) = \rho\left[\frac{2\partial u_3}{\partial\tau} + \frac{\dot{u_3}}{\eta}\frac{\partial\eta}{\partial\tau}\right] + \frac{(\lambda+\mu)\rho}{a\eta}\frac{\partial}{\partial q_1}(H_2 a u_1) +$$

$$+ \frac{u_1}{H_1 a}\left[\frac{2\mu}{a}\frac{\partial a}{\partial q_1} + \frac{\partial\mu}{\partial q_1}\right]$$

(D.9)

Set $\tau = \tilde{\tau}(q_1)$ as the equation of the caustic surface. It is also assumed that on the caustic $H_2 \neq 0$, $\partial H_1/\partial\tau \neq 0$. Then

$$\eta(q_1,\tau) = \frac{\partial\eta}{\partial\tau}_{\tau=\tilde{\tau}} (\tau - \tilde{\tau}(q_1)) + \ldots$$

and therefore

$$\frac{\partial\eta}{\partial q_1} \simeq - \frac{\partial\eta}{\partial\tau}_{\tau=\tilde{\tau}} \frac{\partial\tilde{\tau}}{\partial q_1} \qquad (D.10)$$

We seek a solution to equations D.4 and D.5 in the form

$$u_1 = V(q_1)\ \Phi_1(\eta)$$

$$u_3 = V(q_1)\ \Phi_3(\eta) \qquad (D.11)$$

Equations D.11 can be substituted into equations D.6 to D.9 and subsequently into D.4 and D.5. Terms like $\nabla\lambda, \nabla\mu, \nabla a$ are of a highly insignificant order of η and can be neglected. On the caustic $\eta=0$ and the chief terms of Φ_1, Φ_3 may be determined only if we retain the dominant terms. Clearly, $\Phi, \eta\Phi'$ and $\eta^2\Phi''$ have the same order in η. Introducing

$$M = \frac{\partial\eta}{\partial\tau}\left(\rho b a H_2 \frac{\partial\tilde{\tau}}{\partial q_1}\right)^2$$

$$N = \rho H_2 \frac{\partial\tilde{\tau}}{\partial q_1}\left(a \frac{\partial\eta}{\partial\tau}\right)^2 \qquad (D.12)$$

and three operators of the same order in η.

$$P(\Phi) = \Phi + 2\eta\Phi'$$

$$Q(\Phi) = \eta\Phi' - \eta^2\Phi''$$

$$R(\Phi) = \Phi - \eta\Phi' - \eta^2\Phi'' \qquad (D.13)$$

we have for equations D.4 and D.5

$$-\frac{M}{i\omega\eta^3}\left[Q(\Phi_3) + R(\Phi_1) - \frac{Q(\Phi_1)}{\gamma^2}\left(\frac{\partial\eta}{\partial\tau}\right)^2\frac{\eta}{N}\right]$$

$$+ P(\Phi_3) - N(1-\gamma^2)\Phi_1'/(\partial\eta/\partial\tau)^2 = 0 \qquad (D.14)$$

$$-\frac{M}{i\omega\gamma^2\eta^3}\left[Q(\Phi_1) - (R(\Phi_3) - \gamma^2 Q(\Phi_3))\frac{\eta}{N}\left(\frac{\partial\eta}{\partial\tau}\right)^2\right]$$

$$+ \gamma^2 P(\Phi_1) - N(1-\gamma^2)\Phi_3'/(\partial\eta/\partial\tau)^2$$

$$-i\omega\eta(1-\gamma^2)\Phi_1/(\partial\eta/\partial\tau) = 0 \qquad (D.15)$$

It is asssumed that $\omega >> 1$. Thus, in equation D.15 we may disregard $\gamma^2 P(\Phi_1)$ since for small η it will be small compared with $MQ(\Phi_1)/i\omega\gamma^2\eta^3$ and for large η it will be small compared with

$i\omega\eta(1-\gamma^2)\Phi_1/(\partial\eta/\partial\tau)$. Equation D.14 will be solved for $Q(\Phi_3)$ and substituted into D.15. In the resulting expression

$$\left(\frac{\partial\eta}{\partial\tau}\right)^4 \left(\frac{\gamma\eta}{N}\right)^2 \left[R(\Phi_1) - \frac{Q(\Phi_1)}{\gamma^2}\right]$$

is neglected with respect to $Q(\Phi_1)$,

$$\left(\frac{\partial\eta}{\partial\tau}\right)^2 \frac{\eta}{N} P(\Phi_3)$$

is neglected with respect to $N(1-\gamma^2)\Phi_3'/(\partial\eta/\partial\tau)^2$, and finally $(1-\gamma^2)\eta\Phi_1'$

is neglected for the same reasons as $\gamma^2 P(\Phi_1)$. After these processes we are left with

$$-\frac{M}{i\omega\gamma^2\eta^3}\left[Q(\Phi_1) - \left(\frac{\partial\eta}{\partial\tau}\right)^2 \eta \frac{R(\Phi_3)}{N}\right]$$
$$-\frac{N(1-\gamma^2)\Phi_3'}{(\partial\eta/\partial\tau)^2} - \frac{i\omega\eta(1-\gamma^2)\Phi_1}{(\partial\eta/\partial\tau)} = 0 \qquad \text{(D.16)}$$

In equation D.16 the $R(\Phi_3)$ term is neglected with respect to $Q(\Phi_1)$. Thus, the system D.14-D.15 reduces to

$$-\frac{M}{i\omega\gamma^3}\left[Q(\Phi_3) + \left(\frac{\partial\eta}{\partial\tau}\right)^2 \frac{\eta}{N}\{R(\Phi_1) - Q(\Phi_1)/\gamma^2\}\right]$$

$$+ P(\Phi_3) - N(1-\gamma^2)\Phi_1'/(\partial\eta/\partial\tau)^2 = 0 \qquad \text{(D.17)}$$

$$\frac{M}{i\omega\gamma^2\eta^3}\,Q(\Phi_1) + \frac{N(1-\gamma^2)}{(\partial\eta/\partial\tau)^2}\,\Phi_3' + \frac{i\omega\eta(1-\gamma^2)\Phi_1}{(\partial\eta/\partial\tau)} = 0 \qquad (D.18)$$

These last two equations can be expressed equivalently as

$$-\frac{M}{i\omega\eta^3}\,Q(\Phi_3) + P(\Phi_3) - \frac{N(1-\gamma^2)\Phi_1'}{(\partial\eta/\partial\tau)^2} = 0 \qquad (D.19)$$

$$\frac{N(1-\gamma^2)\Phi_3'}{(\partial\eta/\partial\tau)^2} + \frac{i\omega\eta(1-\gamma^2)\Phi_1}{(\partial\eta/\partial\tau)} = 0 \qquad (D.20)$$

From D.20 we find that

$$\frac{Q(\Phi_3)}{i\omega\eta^3} = \left(\frac{\partial\eta}{\partial\tau}\,\frac{\Phi_1'}{N}\right. \qquad (D.21)$$

Substitution into D.19 yields

$$-\frac{M}{i\omega\gamma^2\eta^3}\,Q(\Phi_3) + P(\Phi_3) = 0 \qquad (D.22)$$

For rays approaching the caustic $M<0$, while for rays leaving the caustic $M>0$. These two cases must be considered separately when solving equation D.22. We define

$$\xi^3 = \alpha|\eta|^3 \qquad (D.23)$$

where $\alpha = \omega\gamma^2/3|M|$. Then equation D.22 may be recast as

$$\eta\Phi_3'' - \Phi_3' (1 \mp 6i\alpha\eta^3) \pm 3\alpha\eta^2\Phi_3 = 0$$

where the upper (lower) sign is for the ray approaching (leaving) the caustic. Substituting

$$\Phi_3 = \eta^{\frac{1}{2}}\exp(3i\alpha\eta^3)C(\eta)$$

yields an equation which is a solution in the form of the Hankel functions. By increasing the frequency ω we can make the argument of the Hankel function large in spite of η being small. If one employs the asymptotic expansion for the Hankel functions (Abramowitz and Stegun 1965), the zeroth order asymptotic ray theory result must be found, viz. $\Phi_3 = \eta^{-\frac{1}{2}}$. This allows us to choose suitable normalizing factors. Such a process as this also enables us to define $V(q_1)$ in order to make equation D.11 consistent with the zeroth order theory. Finally, we have

$$\Phi_3^{ap}(\eta) = \left(\frac{\pi\xi^3}{2|\eta|}\right)^{\frac{1}{2}} \exp(i(\xi^3-5\pi/12))\ H_{1/3}^{(2)}(\xi^3) \qquad (D.24)$$

$$\Phi_3^{le}(\eta) = \left(\frac{\pi\xi^3}{2|\eta|}\right)^{\frac{1}{2}} \exp(i(-\xi^3-\pi/12))\ H_{1/3}^{(1)}(\xi^3) \qquad (D.25)$$

$$V(q_1) = (v_0\rho_0)^{\frac{1}{2}} \prod_{j=1}^{K} \left(\frac{\tilde{v}\ \tilde{\rho}\ \cos\tilde{\theta}}{v\ \rho\ \cos\theta}\right)_j R_j \qquad (D.26)$$

where the superscripts "ap" and "le" denote rays approching and leaving the caustic. v_0, ρ_0 are wave velocity and density at the source, K is the total number of ray segments, R_j is the appropriate plane wave interface coefficient which ends the j-th ray segment $\tilde{v}, \tilde{\rho}, \tilde{\theta}$ are the wave velocity, density and acute angle with the interface normal on the non-incident side of any interface. The corresponding properties on the incident side of the interface are given by v, ρ, θ .

The functions Φ_1^{ap}, , Φ_1^{le} may be found by equation D.20. They are

$$\Phi_1^{ap}(\eta) = \left(\frac{\pi\alpha}{2}\right)^{\frac{1}{2}} \left(\frac{\partial\eta}{\partial\tau}\right)^2 \frac{\eta^2}{N} \exp(i(\xi^3 - 5\pi/12)) \cdot$$

$$\left(H_{1/3}^{(2)}(\xi^3) - i\, H_{-2/3}^{(2)}(\xi^3)\right) \qquad (D.27)$$

$$\Phi_1^{le}(\eta) = \left(\frac{\pi\alpha}{2}\right)^{\frac{1}{2}} \left(\frac{\partial\eta}{\partial\tau}\right)^2 \frac{\eta^2}{N} \exp(i(\xi^3 - \pi/12)) \cdot$$

$$\left(- H_{1/3}^{(1)}(\xi^3) - iH_{-2/3}^{(1)}(\xi^3)\right) \qquad (D.28)$$

Due to the presence of the frequency factor,

Φ_1 is smaller than Φ_3. This is related to the fact that Φ_1 describes the transverse component of the P wave, which is zero in zeroth ray theory.

The equations developed so far have been written in the curvilinear ray coordinates. The computations are performed in Cartesian coordinates and to this end the appropriate conversions must be made.

Consider the point O where the caustic surface intersects the surface on which the receiver lies. Place at O the origin of a Cartesian coordinate system (x,y,z), where x points normal to the caustic and z points tangent to the caustic and into the earth. Let M be a point at a distance ν from O measured along the x axis and $\nu>0$ on the lit side of the caustic. Gazaryan (1960) has demonstrated that

$$q_1(M) = q_1(0) \pm \left(\frac{2H_2 \rho a \nu}{\frac{\partial \eta}{\partial \tau} \frac{\partial \tilde{\tau}}{\partial q_1}} \right)^{\frac{1}{2}} \qquad (D.29)$$

$$\tau(M) = \tau(0) \mp \frac{2}{3a^2} \left(\frac{2\nu^3 \left| \frac{\partial \eta}{\partial \tau} \right|}{H_2 \rho a \frac{\partial \tilde{\tau}}{\partial q_1}} \right)^{\frac{1}{2}} \qquad (D.30)$$

where the upper (lower) sign is for the ray approaching (leaving) the caustic. Since

$$\eta(M) = \eta(0) + \left(\frac{\partial \eta}{\partial q_1}\right)_0 (\alpha_1(M) - \alpha_1(0)) + \ldots$$

and $\eta(0)=0$, it follows that

$$|\eta| = \left(2H_2\rho a \left|\frac{\partial \eta}{\partial \tau}\right| \frac{\partial \tilde{\tau}\nu}{\partial q_1}\right)^{\frac{1}{2}} \qquad (D.31)$$

We must express the unit vectors $\hat{e}_x, \hat{e}_z$ in terms of $\hat{e}_1$, $\hat{e}_3$. Expand $\hat{e}_3(M)$ as

$$\hat{e}_3(M) = \hat{e}_3(0) + \left(\frac{\partial \hat{e}_3}{\partial q_1}\right)_0 (q_1(M) - q_2(0)) + \ldots$$

Taking D.29 into account and also that $\hat{e}_3(0) = -\hat{e}_z$ we have

$$\left(\frac{\partial \hat{e}_3}{\partial q_1}\right)_0 = \frac{\partial H_1}{\partial \tau} \frac{\hat{e}_1(0)}{a} = \frac{\partial \eta}{\partial \tau} \frac{\hat{e}_x}{H_2 \rho a^2}$$

from which

$$\hat{e}_3(M) = -\hat{e}_z \pm \left|\frac{\partial \eta}{\partial \tau}\right| \left(\frac{2H_2\rho a\nu}{\left|\frac{\partial \upsilon}{\partial \tau}\right| \frac{\partial \tilde{\tau}}{\partial q_1}}\right)^{\frac{1}{2}} \frac{\hat{e}_x}{H_2 \rho a^2} \qquad (D.32)$$

Analogously,

$$\hat{e}_1(M) = \hat{e}_x \mp \left|\frac{\partial \eta}{\partial \tau}\right| \left(\frac{2H_2\rho a\nu}{\left|\frac{\partial \eta}{\partial \tau}\right| \frac{\partial \tilde{\tau}}{\partial q_1}}\right)^{\frac{1}{2}} \frac{\hat{e}_z}{H_2 \rho a^2} \qquad (D.33)$$

The upper (lower) sign in these equations corresponds to the

ray approaching and leaving the caustic. Components of displacement in the x and z coordinates can be written as

$$u_x = V(q_1)e^{-i\omega t}\ \Phi_1^{ap}\ e^{i\omega\tau_{ap}} + \Phi_1^{le}\ e^{i\omega\tau_{le}} +$$

$$+ \frac{1}{H_2\rho a^2}\left|\frac{\partial\eta}{\partial\tau}\right|\left(\frac{2H_2\rho a\nu}{\left|\frac{\partial\eta}{\partial\tau}\right|\frac{\partial\tilde{\tau}}{\partial q_1}}\right)^{1/2}\Phi_3^{ap}\ e^{i\omega\tau_{ap}} - \Phi_3^{le}\ e^{i\omega\tau_{le}} \qquad (D.34)$$

$$u_z = V(q_1)e^{-i\omega t}\ -\Phi_3^{ap}\ e^{i\omega\tau_{ap}} - \Phi_3^{le}\ e^{i\omega\tau_{le}} +$$

$$+ \frac{1}{H_2\rho a^2}\left|\frac{\partial\eta}{\partial\tau}\right|\left(\frac{2H_2\rho a\nu}{\left|\frac{\partial\eta}{\partial\tau}\right|\frac{\partial\tilde{\tau}}{\partial q_1}}\right)^{1/2}\left[-\Phi_1^{ap}\ e^{i\omega\tau_{ap}} + \Phi_1^{le}\ e^{i\omega\tau_{le}}\right] \qquad (D.35)$$

In equation D.35 the term involving Φ_1 decreases rapidly with increasing ν compared to the Φ_3 term and can thus be neglected. Expand the variables η and τ in equations D.34 and D.35 and make use of the definition of the Airy function in terms of Hankel functions to arrive at

$$u_x = 2V(q_1)\left(\frac{3\alpha}{2\pi^3}\right)^{-1/6}\exp(-i\omega(t-\tilde{\tau}) + i\pi/4)\cdot$$

$$\cdot\frac{Ai'(-C\omega^{2/3}\nu)}{H_2\rho a^2\frac{\partial\tilde{\tau}}{\partial q_1}} \qquad (D.36)$$

$$u_z = 2V(q_1)\left(\frac{3\pi^3\alpha}{2}\right)^{1/6}\exp(-i\omega(t-\tilde{\tau},+3i\pi/4)Ai(-C\omega^{2/3}\nu) \qquad (D.37)$$

where

$$C = \frac{2\left|\frac{\partial \eta}{\partial \tau}\right|}{H_2 \rho a^5 \frac{\partial \tilde{\tau}}{\partial q_1}}^{1/3}$$

In order that these equations can be employed in the ray programs proposed by this thesis, x and z must be oriented in the standard direction, viz., z pointing vertically downward and x pointing to the right of our profile. This is a simple conversion since the angle Θ, the caustic makes with the standard z direction is found by tracing a ray which ends up on the receiver surface at the point of intersection between that surface and the caustic. For computational purposes we shall neglect the transverse component u_x due to the $\omega^{-1/6}$ dependence as compared to the compressional component which varies as $\omega^{1/6}$.

Finally, after further simplifications, the displacement for P waves arriving at a receiver in the vicinity of a caustic can be written as

$$u(\vec{x}) = V(q_1)\exp(-i\omega(t-\tilde{\tau})+3i\pi/4)\ \frac{(32\omega)^{1/6}}{(H_2 a\rho)^{\frac{1}{2}}}\ \frac{\pi^3 \partial H_1}{\partial \tau}^{1/6} \cdot$$

$$\cdot\ \mathrm{Ai}(-C\omega^{2/3}\nu)\ \ a\left|\frac{\partial^2 \vec{x}}{\partial q_1^2}\right|^{-1/3} \qquad \text{(D.38)}$$

where

$\nu = \pm|\vec{x}-\vec{x}^*|\cos\Theta$

ν = plus (minus) in lit (shadow) zone,

$\vec{x}^*$ = location where caustic intersects receiver surface,

$$C = \frac{2}{a^4}\left(\frac{\partial H_1}{\partial \tau}\right)^2 \left|\frac{\partial^2 \vec{x}}{\partial q_1^2}\right|^{-1\ 1/3}$$

Similarly, for S waves arriving at the receiver, we obtain

$$u(\vec{x}) = V(q_1)\exp(-i\omega(t-\tilde{\tau})+3i\pi/4)\ \frac{(32\omega)^{1/6}}{(H_2 a\rho)^{\frac{1}{2}}}\left(\frac{\pi^3 \partial H_1}{\partial \tau}\right)^{1/6}$$

$$Ai(-D\omega^{2/3}\nu)\ b\left|\frac{\partial^2 \vec{x}}{\partial q_1^2}\right|^{-1/3} \qquad (D.39)$$

where

$$D = \left(\frac{2}{b^4}\right)\left(\frac{\partial H_1}{\partial \tau}\right)^2 \left|\frac{\partial^2 \vec{x}}{\partial q_1^2}\right|^{-1\ 1/3}$$

a,b,ρ = P wave velocity, S wave velocity and volume density at the point $\vec{x}^*$.

All quantities in equations D.38 and D.39 are easy to evaluate by the circular approximation method of ray tracing, which renders the expressions very useful in computing amplitude-distance curves or synthetic seismograms. As pointed out by Choi (1978) or Choy and Richards (1975) a $\pi/2$ phase shift is attributed to the seismic pulse each time the ray passes through an internal caustic. Circular approximation ray tracing as developed in Chapter 5 is well suited to determining the location and number of these caustics. By simultaneously tracing two rays which are separated by a small amount in takeoff angle, one locates all intersection points of the various circular arcs comprising the ray paths. Within each triangular region of the model that the rays traverse, analytical expressions can be written for the intersection of the two circular

segments. If such a point or points is contained within the bounds of the triangular region, then the rays have passed through an internal caustic. Otherwise, this side-by-side ray tracing process continues into the next triangular region.